

ULTRASONIC PROPAGATION PROPERTIES OF CANINE MYOCARDIUM
AND BOVINE ARTICULAR CARTILAGE AT 100 MHZ

BY

DIANE H. AGEMURA

B.S., University of Illinois, 1986

THESIS

Submitted in partial fulfillment of the requirements
for the degree of Master of Science in Electrical Engineering
in the Graduate College of the
University of Illinois at Urbana-Champaign, 1988

Urbana, Illinois

UNIVERSITY OF ILLINOIS AT URBANA-CHAMPAIGN

THE GRADUATE COLLEGE

JULY 1988

WE HEREBY RECOMMEND THAT THE THESIS BY

DIANE H. AGEMURA

ENTITLED ULTRASONIC PROPAGATION PROPERTIES OF CANINE

MYOCARDIUM AND BOVINE ARTICULAR CARTILAGE AT 100 MHz

BE ACCEPTED IN PARTIAL FULFILLMENT OF THE REQUIREMENTS FOR

THE DEGREE OF MASTER OF SCIENCE

W. H. O'Brien

Director of Thesis Research

Timothy A. Erick

Head of Department

Committee on Final Examination†

Chairperson

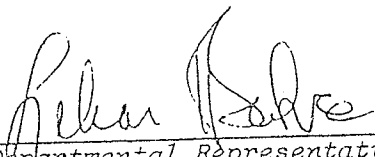
† Required for doctor's degree but not for master's.

University of Illinois at Urbana-Champaign

DEPARTMENTAL FORMAT APPROVAL

THIS IS TO CERTIFY THAT THE FORMAT AND QUALITY OF PRESENTATION OF THE
THESIS SUBMITTED BY DIANE H. AGEMURA AS ONE OF
THE REQUIREMENTS FOR THE DEGREE OF MASTER OF SCIENCE
IS ACCEPTABLE TO THE DEPARTMENT OF ELECTRICAL AND COMPUTER ENGINEERING
(Full Name of Department, Division or Unit)

21 July 1988
Date of Approval


Departmental Representative

ACKNOWLEDGEMENTS

I would like to thank my advisor, Professor William D. O'Brien Jr., for his endless encouragement, support and funding throughout these projects and also for his never-ending faith in my abilities.

Dr. Kiran Sagar, Dr. Lorie Pelc and Jeanne Howard from the Medical College of Wisconsin and Dr. John Olerud from the University of Washington provided much needed assistance.

I would also like to acknowledge Wanda Elliot for her invaluable assistance and advice, not only in the preparation of this thesis but for the past two years. Special thanks to Nadine Smith, Lenora Louie and Carol Nakamura for their constant encouragement.

I dedicate this thesis to my family, without whom this goal would not have been possible.

TABLE OF CONTENT

CHAPTER	PAGE
1 INTRODUCTION	1
2 SYSTEM DESCRIPTIONS	15
3 METHODS	31
4 MYOCARDIUM RESULTS AND DISCUSSION	41
5 ARTICULAR CARTILAGE RESULTS AND DISCUSSION.	55
APPENDIX I: THE SLAM ATTENUATION COEFFICIENT, ULTRASONIC SPEED AND HETEROGENEITY INDEX FOR CANINE MYOCARDIUM	69
APPENDIX II: THE IBr5 AND WATER CONCENTRATION FOR CANINE MYOCARDIUM	71
APPENDIX III: THE SLAM ATTENUATION COEFFICIENT AND ULTRASONIC SPEED FOR BOVINE ARTICULAR CARTILAGE	72
APPENDIX IV: STATGRAPHICS ANALYSIS OF CANINE MYOCARDIUM.	74
APPENDIX V: STATGRAPHICS ANALYSIS OF BOVINE ARTICULAR CARTILAGE	88
REFERENCES	106

CHAPTER 1

INTRODUCTION

1.1. Introduction

Ultrasound is a currently available, noninvasive modality used to investigate a variety of tissues. In the past decade, important developments have occurred in the use of ultrasound for detecting and identifying diseases of abdominal organs. The results of studies in the early 1970's have been incorporated into commercially available scanners which has prompted the large growth and widespread availability of clinical ultrasound instruments. Conventional systems for imaging abdominal organs use ultrasonic energy at frequencies ranging from 2-10 MHz. Higher frequency experimental ultrasonic systems (25-50 MHz) have been developed for interrogating skin [Dines et al., 1984; Forster et al., 1983]. Increased image resolution is one advantage for increasing the frequency range.

The backscatter of ultrasound energy creates clinical ultrasonic images from discontinuities wherever ultrasonic propagation properties are sufficiently different. Ultrasonic properties such as attenuation coefficient, speed, backscatter characteristics and heterogeneity are used to assess material properties of tissues. These measurements of material properties contain information regarding tissue composition, structure and mechanical characteristics.

The use of clinical systems requires sufficient knowledge of the interaction of ultrasound with tissue. Reported herein are two separate experiments which use a 100 MHz scanning laser acoustic microscope (SLAM) to study the relationship between ultrasonic propagation properties and biochemical changes in tissue. The first experiment studies the effect of normal and ischemic canine myocardia analyzed by the SLAM and a clinical integrated backscatter technique. The second experiment studies the effect of a sequential enzyme extraction procedure on bovine articular cartilage analyzed only by the SLAM. The SLAM and the ultrasonic backscatter instrumentation are described in Chapter 2. Tissue preparation of canine myocardium and bovine articular cartilage for SLAM evaluation are described in Chapter 3. Segmental contractile function and water concentration are determined for the myocardium samples.

The results of the canine myocardium experiments are presented and discussed in Chapter 4. The specific objectives of these experiments are

1. To determine the attenuation coefficient, ultrasonic speed, heterogeneity index and integrated backscatter (IBR5) of normal and ischemic myocardium.
2. To determine if the ultrasonic propagation properties are statistically correlated with water concentration and segment shortening.
3. To determine if the SLAM ultrasonic properties are statistically correlated with IBR5.

The results of the bovine articular cartilage experiments are presented and discussed in Chapter 5. The specific objectives of these experiments are

1. To assess the contribution of individual matrix components to ultrasonic propagation properties i.e., attenuation coefficient and ultrasonic speed.
2. To determine the influence of collagen fibril orientation and collagen cross-linking.

1.2. Background

The use of ultrasound in medicine requires an understanding of the tissue properties responsible for or associated with the propagation of sound in tissue. Nearly 30 years ago, a relationship between the tissue molecular constituents and the attenuation of ultrasound was noted [Dussik et al., 1958]. A more recent study has shown that the ultrasonic propagation properties of tissue are determined largely at the macromolecular level [Pohlhammer et al., 1980]. Carstensen, Li and Schwan [1953] found that protein content determines the ultrasonic absorption in blood and speed in albumen solutions. They also found that attenuation coefficient is directly proportional to protein concentration. Further research shows that a small fraction of the attenuation in blood arises due to its cellular organization [Carstensen et al., 1959]. Early studies on liver tissue show that approximately two thirds of its attenuation occurs at the macromolecular level, with the remaining one third attributed to microscopic structure [Pauly et al., 1971].

A study on the ultrasonic attenuation coefficient and mean backscatter amplitude in various tissues as a function of time after excision shows that the attenuation coefficient does not change significantly while the mean backscatter amplitude decreases substantially [Bamber et al., 1977]. The results suggest that backscatter signals are associated with large parenchymal structures, which are the first to disintegrate. Attenuation, on the other hand, is associated with the macromolecular structure which degrades more slowly, hence supporting the hypothesis that ultrasonic absorption occurs at the macromolecular level in biological materials.

These and additional studies strongly support the idea that tissue constituents determine the ultrasonic propagation properties in most tissues. The three tissue constituents under consideration are water, protein and fat, since they account for most of the tissue.

A compilation of the attenuation coefficient, speed, protein and water concentration in various tissues indicates that the speed and attenuation coefficient in tissue increase as the protein concentration increases and as the water decreases [Dunn, 1983; O'Brien, 1977a]. Tendon has a low water concentration (68%) and a very high protein content (35-40%). Both the attenuation coefficient and speed in tendon are among the highest for any tissue except bone. Conversely, testis, which is almost entirely water (80%) and only about 12% protein, show the lowest absorption for any tissue. Tissues with

intermediate water and protein concentration also have intermediate attenuation coefficient and speed values.

Water probably contributes little to the absorption properties of tissue [Goss et al., 1980]. Its overall effect is to dilute the concentration of macromolecules; therefore, it does not directly affect the acoustic properties of tissue. The attenuation coefficient in infant brain is lower than in adult brain tissue. Infant brain has a 10 to 15% higher water concentration than adult brain. In adults, edematose (water-filled) brain tissue has a lower attenuation coefficient than normal brain tissue. In infant brain, the ultrasonic speed also increases as water concentration decreases.

Fat is an almost water-free tissue. Total body water is largely inversely dependent upon the total amount of body fat. Recent studies of orotic acid-treated rat liver [O'Brien et al., 1988] have shown that as water concentration increases, the speed increases. This result contradicts previous results in which speed decreases as water concentration increases. This discrepancy is explained by the almost one-to-one replacement of water with fat, which causes the decrease in speed.

There are two distinct types of proteins: one provides structural features to the body and the other provides necessary metabolic functions. The structural protein, collagen, plays an important role in the acoustical properties of tissues. Collagen, a high tensile strength insoluble fiber, is the most abundant protein in the human body, which exhibits widely different acoustic properties from those of other common tissue

constituents [Fields et al., 1973; Goss et al., 1979]. Collagenous fibers exhibit a static elastic modulus (Young's modulus) approximately 1000 times greater than that of other soft tissue components [Fields et al., 1973]. Since ultrasonic speed is proportional to the square root of the elastic modulus, this suggests that the ultrasonic speed would be greater for collagen than for other constituents. Ultrasonic speed measurements in tendon threads support this concept [Goss et al., 1979].

The higher speed in collagen implies that collagen has a higher characteristic acoustic impedance. Because of the large impedance mismatch between collagen and the surrounding tissue, collagen containing tissues are expected to exhibit greater acoustic reflectivity and scattering. Skin and cartilage, which contain large amounts of collagen, have attenuation coefficients much greater than low collagen content tissues [Dussik et al., 1958; O'Brien, 1977b]. Similar observations have been made concerning the speed in tissues with high collagen contents [Johnston et al., 1979].

1.2.1. Canine myocardium

The diagnosis of cardiac disease is a promising application of ultrasound. Sufficient knowledge of the ultrasonic characterization of myocardium must be developed so that it can be used to detect acute myocardial infarction (death of heart tissue), quantify infarct size and ultimately follow structural and functional recovery after interventions used to reduce infarct size.

Ultrasonic exploration with normal and abnormal myocardium began in 1957 when Wild [Wild et al., 1957] studied excised human hearts with 15 MHz ultrasound to diagnose infarction. Early methods of tissue characterization utilized standard echocardiographic displays of acoustically abnormal tissue. Regions of "brightness," "speckling" and changes in grey scale were seen in patients with old myocardial infarction [Rasmussen et al., 1978], amyloid heart disease (accumulation of a starchlike glycoprotein in the heart tissue) [Bhandari et al., 1983; Chianamider et al., 1980] and idiopathic hypertrophic cardiomyopathy (unknown increase in the size of the heart) [Martin et al., 1979]. These methods were highly dependent on the observer's recognition of slight changes in grey scale of the images.

To avoid the subjective problems, computer analysis of regional average echo amplitude and spatial distribution (texture) of amplitude were introduced. These techniques succeeded in differentiating normal, ischemic and post-ischemic reperfused myocardium [Skorton et al., 1983a; Skorton et al., 1983b; Haendchen et al., 1985]. The major disadvantage of this technique was its sensitivity to individual adjustments of the instrument.

A more promising method of myocardial tissue characterization utilizes the "raw" radio frequency ultrasound signals and measures changes in ultrasound attenuation and backscatter. Lele and Namery [1974] are among the first to show alterations in acoustic properties associated with changes in

structure. They have found that infarcted myocardium exhibits a lower acoustic impedance than normal myocardium.

Mimbs and coworkers [1977] study attenuation in vitro using "through" transmission ultrasound. This involves two ultrasonic transducers (one transmitting and one receiving) on either side of the tissue or a single transducer with a perfect reflector for double passage through the tissue. Their results demonstrate that early after myocardial infarction attenuation decreases followed by periods of increased attenuation.

Since this technique could not be applied to the intact heart, O'Donnell, Mimbs and Miller developed an index of ultrasonic backscatter to distinguish normal from abnormal myocardium [O'Donnell et al., 1979a; O'Donnell et al., 1979b], and created the term Integrated Backscatter (IB). Their research demonstrated that IB increased significantly after myocardial infarction in vitro and in vivo [Mimbs et al, 1981]. In addition, the IB increase correlated with changes in coronary blood flow and alterations in myocardial water content.

Rhyme and coworkers [1986a] studied the absolute myocardial backscatter as a function of the frequency and phase of the cardiac cycle. They discovered a first-order model in which the scattering from the myocardium was Rayleigh scattering with a cardiac cycle variation in the scattering cross section. The data suggested a periodic modulation in the physical size of the scatterers (such as myofilaments) with a minimum effective scattering area presented in systole and maximal area presented in diastole.

This research led to the introduction of a new integrated backscatter parameter called the Integrated Backscatter Rayleigh 5 MHz corrected (IBR5), which was an absolute measure of the backscatter per cm independent of the instrumentation and diffraction [Rhyne et al., 1986b]. The IBR5 measurement, the maximum likelihood estimate of the backscatter, was a refinement of the IB measurement developed by O'Donnell, Mimbs and Miller. The theoretical difference was that IBR5 achieved minimum variance and zero bias, and permitted a maximum likelihood estimate of the amplitude variation.

Sagar and associates [1987] studied the effects of coronary occlusion and reperfusion on integrated backscatter. They demonstrated that cardiac cycle-dependent modulation is directly related to myocardial contraction. Changes in amplitude modulation with the cardiac cycle followed changes in segmental shortening during ischemia and reperfusion. The results showed that integrated backscatter detected not only the pathological abnormalities, but also functional changes in myocardium during acute ischemia and reperfusion.

The above studies indicate that the mechanisms of ultrasonic interaction with myocardium arise from the myocardial microstructure seen by the ultrasonic waves. A direct approach to studying the mechanisms of myocardial backscatter is to image the myocardium at very high frequencies, i.e., using the SLAM at 100 MHz. These techniques offer the opportunity to directly study the ultrasonic myocardial microstructure and to correlate alterations in backscatter with pathophysiological changes.

1.2.2. Bovine articular cartilage

Classical methods for assessing wound healing (tensile strength, burst strength, biochemistry, histology and ultrastructure) have been extensively employed in animal studies [Peacock et al., 1970a; Viljanto, 1971]. The disadvantage is that each method requires excision or disruption of the wound in some manner and thus has a limited potential for evaluating wounds in humans. Development of ultrasound techniques capable of measuring material properties in wound tissue would provide a clinical method for evaluating human wounds in a noninvasive fashion.

Studies on wound healing [Steiger, 1986] have shown that changes in the mechanical properties (tensile strength) and in the collagen concentration during wound maturation are highly correlated with the acoustic parameters of the SLAM. The results indicate that ultrasonic speed may be a better indicator of the changing mechanical properties of the wound, while the attenuation coefficient may better reflect the changes in wound collagen content. The results also suggest that the relationships between the acoustic properties and tissue water content may be an indirect result of the strong correlation which exists between tissue water and total collagen content.

Studies of other connective tissue models can provide valuable information regarding the influence of glycosaminoglycans (GAG), elastin, collagen type, degree of collagen cross-linking, as well as the effect of pyridinoline cross-links on ultrasonic propagation properties of soft tissue.

These models are of interest in the clinical use of ultrasound, since the composition and configuration of connective tissues change during disease states such as cirrhosis of the liver and degenerative joint disease as well as physiological processes such as wound healing.

Presently, there are no studies available on the role of glycosaminoglycans or elastin in the ultrasonic propagation properties in soft tissues. O'Brien [1975] has studied chondroitin sulfate in aqueous solutions and showed an increase in absorption and velocity as a function of temperature, pH and ultrasonic frequency. Researchers have shown differences in acoustic properties of large bovine blood vessels as a function of distance from the heart but did not quantify collagen and elastin separately. Similarly, there are no studies relating the collagen type or degree of cross-linking to ultrasonic propagation properties in tissues.

Pyridinoline is an amino acid which forms a mature collagen cross-link found in most load bearing tissue other than skin [Eyre et al., 1984]. The absence of this cross-link in skin collagen may be related to its ring structure, which is unstable in the presence of ultraviolet light. Pyridinoline cross-links are suspected to provide a lateral rigidity in collagen fibrils which would be expected to alter mechanical and ultrasonic properties.

In the later stages of the wound healing process, structural changes occur involving pyridinoline cross-links. As the tissue collagen becomes more and more cross-linked, it

becomes less and less soluble [Peacock et al., 1970b]. Intermolecular collagen cross-linking begins to occur soon after the collagen is synthesized, but the solubility is not affected. Once intramolecular cross-links (between collagen molecules) are established, strong acid solutions must be used to dissolve the collagen. As more and more cross-links are formed, the collagen will finally become insoluble. Thus, the acid solubility of tissue collagen can be used as an indicator of the degree of cross-linking present and therefore, provide a valuable index of wound maturity, since they are not present in surrounding normal skin.

Using articular cartilage, which is a relatively homogeneous, avascular connective tissue, the present experiment has begun to study the effect of tissue constituents by selectively degrading components of the extracellular matrix.

The molecular type of collagen throughout hyaline articular cartilage is primarily genetic type II. Ultrastructural studies of adult cartilage, however, show that the preferential orientation of the collagen fibers is quite different for the tangential zone near the articular surface (approximately 200 μm) compared to the intermediate (transitional) and deep (radial) zones (Figure 1). In the tangential zone the collagen is more densely packed and oriented approximately parallel to the surface, while in the deeper, radial zone the collagen is more loosely packed and oriented approximately perpendicular to the articular surface [Hukins et al., 1984; Hukins et al., 1985]. In the transitional zone the orientation is more random and, as the

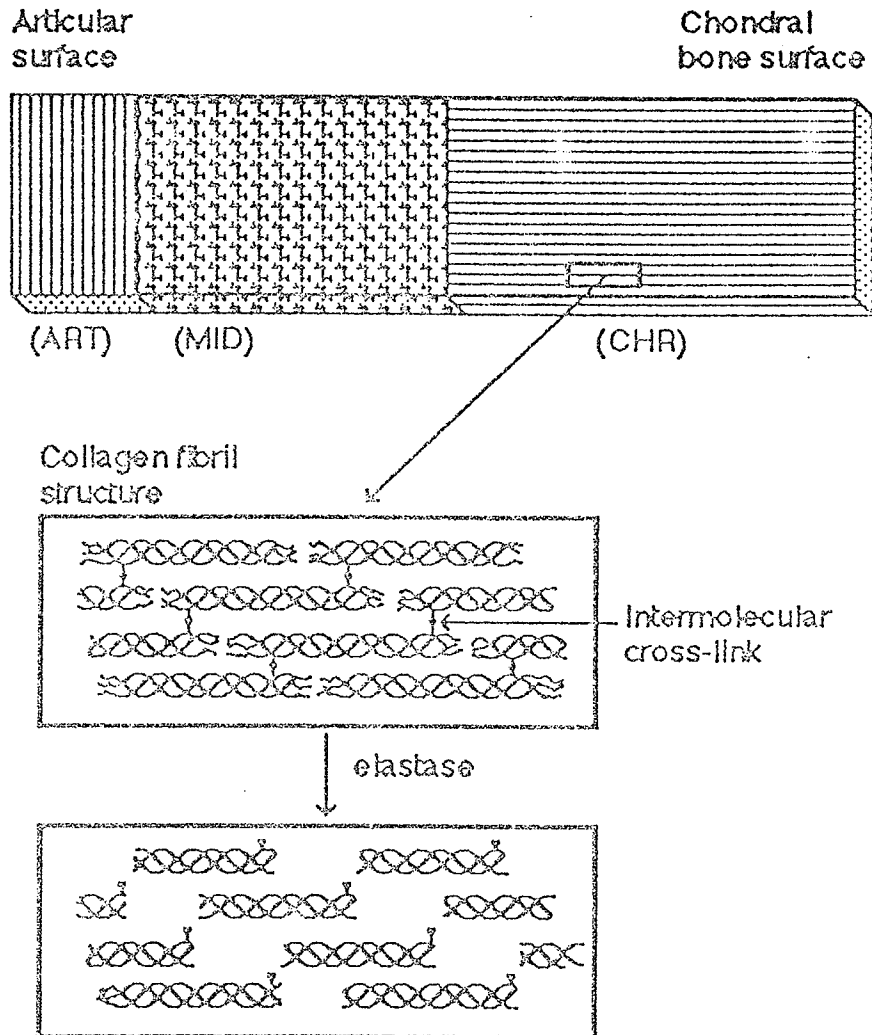


Figure 1 - Diagram of the predominant orientations of collagen fibrils in different zones of articular cartilage. The lower panels illustrate the head-to-tail positions of cross-links between collagen molecules packed in fibrils and how these are disrupted by the telopeptidase activity of pancreatic elastase.

name suggests, represents a gradual transition from one preferred orientation to the other. Hence, several questions can be addressed using this cartilage model, including the effect of collagen orientation on the ultrasonic propagation properties, and the effects of removing individual glycosaminoglycans and proteoglycans and destroying cross-links in the collagen framework.

CHAPTER 2

SYSTEM DESCRIPTIONS

2.1. Scanning Laser Acoustic Microscope

A scanning laser acoustic microscope (Sonomicroscope 100^R, Sonoscan, Inc., Bensenville, IL 60106), operating at a frequency of 100 MHz is used to determine the attenuation coefficient, speed and heterogeneity index of ultrasonic propagation. The operating techniques of this instrument have been reported in detail [Tervola et al., 1985a; Tervola et al., 1985b] and will be summarized in this section.

A block diagram of the SLAM is shown in Figure 2. A piezoelectric transducer produces sound at a frequency of 100 MHz which propagates through a fused silica stage. The specimen is placed on the sonically activated stage supported by a 25 μm sheet of mylar along with a thin layer of normal saline and covered with a semireflective coverslip. A focused scanning laser beam probe detects a dynamic ripple (surface displacement) by reflection from the coverslip surface whose amplitude is proportional to the transmitted acoustic pressure. The laser light transmitted through the specimen and coverslip is processed by the SLAM, producing a two-dimensional image of the specimen on a standard television monitor representing an area approximately 3 mm horizontally by 2 mm vertically.

The laser light reflection angle depends on the changing amplitude of the dynamic ripple at that position. A knife edge, placed in the path of the reflected light, blocks a portion of

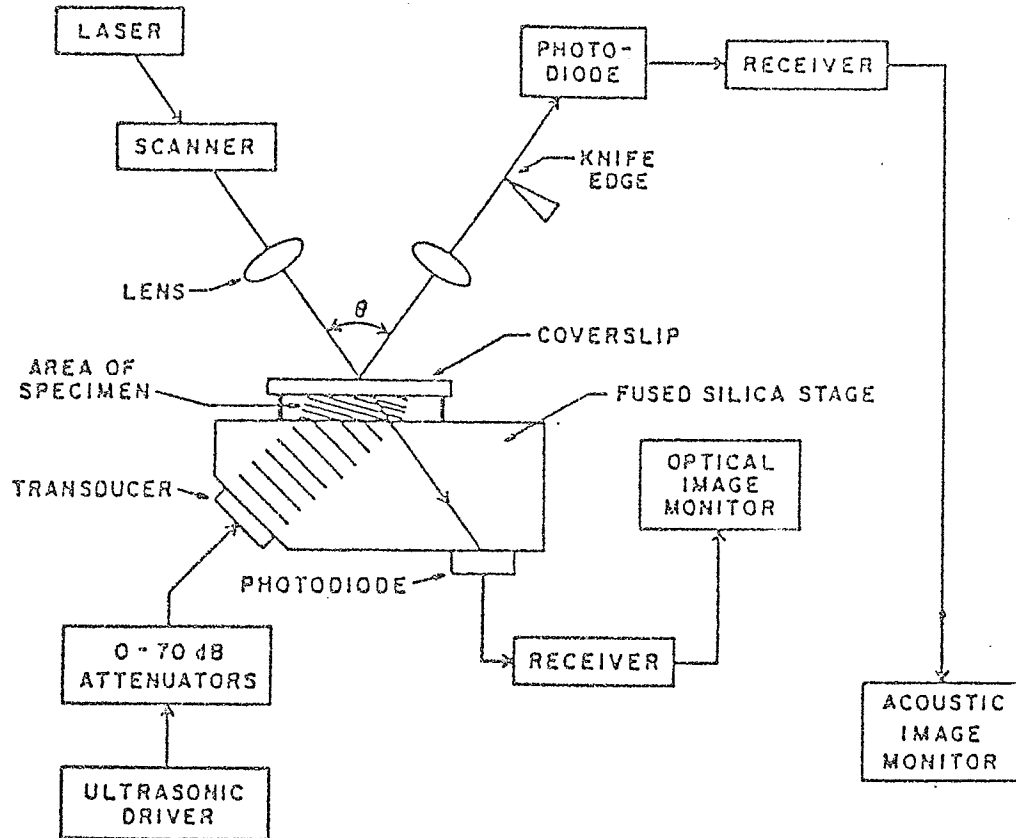


Figure 2 - Block diagram of the SLAM

the light falling on the photodiode. The amount of light blocked depends on the angle of the reflected laser light which allows the angular modulation to be converted to light intensity modulation then to an electrical signal proportional to the ripple amplitude. The SLAM processes the electrical signal to yield either the acoustic amplitude image or the interference-mode image.

The acoustic amplitude image displays the spatial amplitude of the acoustic field after passing through the specimen and is used to determine the attenuation coefficient. Brighter areas on the television monitor represent areas of higher ultrasonic energy, while darker areas correspond to areas of low ultrasonic energy. The acoustic wavelength and laser beam size, which is approximately $20\ \mu\text{m}$, limits the spatial resolution.

Adding a reference signal to the received signal, phase coherent with the transmitted acoustic wave, produces the interference-mode image. The interference-mode image consists of alternating light and dark vertical bands or fringes which correspond to equal phase wavefronts of the ultrasonic field. A change in the ultrasonic speed causes the fringes to bend to the right if the speed is increasing or to the left if the speed is decreasing.

The semitransparent coverslip allows a fraction of the laser beam to penetrate through the sample. A separate photodiode collects the transmitted light and a second TV monitor displays the processed signal as the optical image. The

optical image is useful in positioning the specimen on the microscope stage and identifying transparent structures.

The function of the stage is to couple acoustic energy to the specimen at the desired angle of illumination and support mechanically the specimen parallel and close to the faceplate. The stage is constructed so that the gold-plated surface of the coverslip is in the near field of the sound image. The specimen is placed on the stage with a thin layer of water. The sound beam strikes the quartz surface at an angle of 45° and refracts into the water at 10° .

Described in the next section the data acquisition system developed to allow quantitative measurement of the ultrasonic propagation properties. This system has been described previously [Steiger, 1986] and will only be summarized.

2.1.1. The SLAM data acquisition system

Computer acquisition and analysis of the SLAM's acoustic image data and interference-mode image data provide quantitative determination of the attenuation coefficient and the ultrasonic speed. Figure 3 shows a block diagram of the data acquisition system. This system was developed for a series of studies on wound healing [Steiger, 1986].

The Z-80 microprocessor controlled system includes two serial ports, one communicating with a VAX 11/730 and one connecting to a terminal for data entry and program control. The 12 K EPROM includes the system monitor and a BASIC interpreter program.

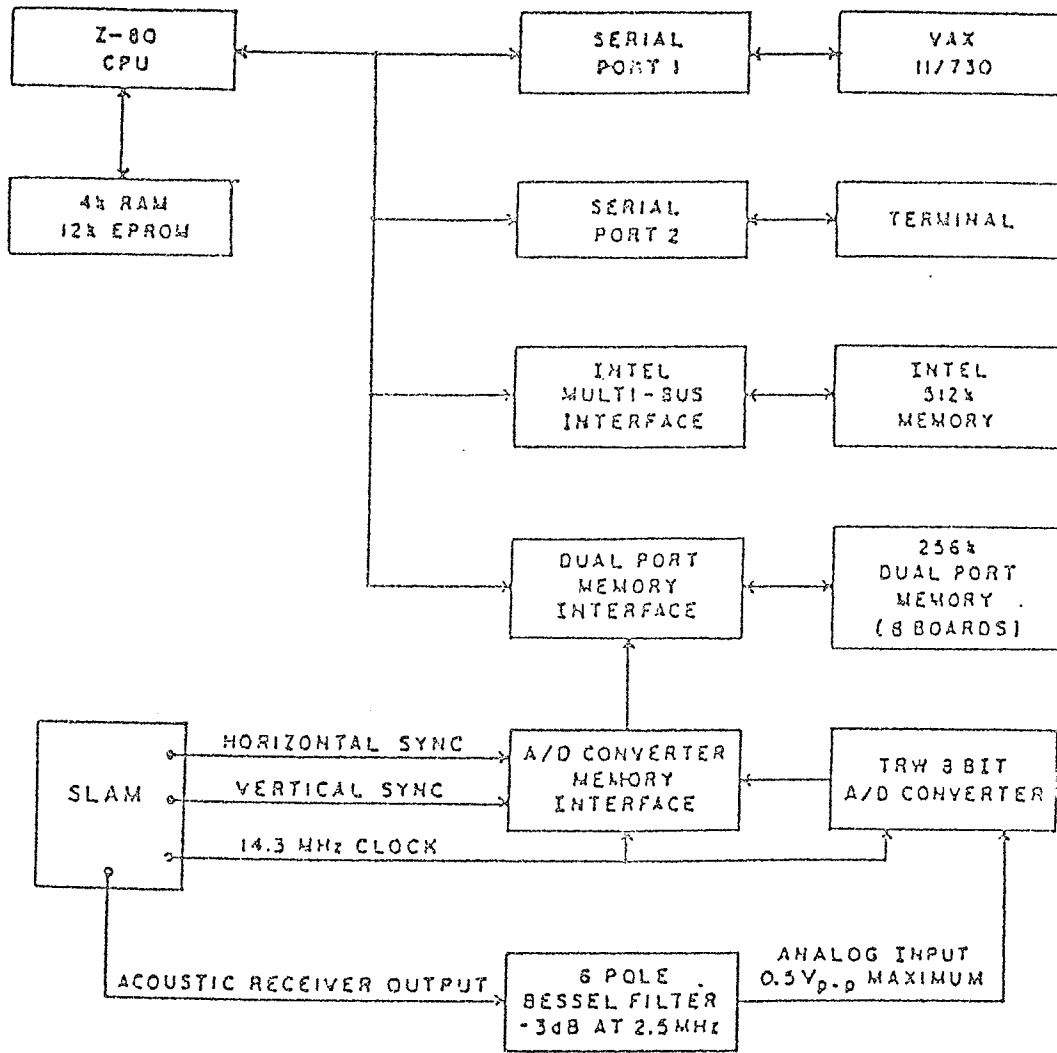


Figure 3 - Block diagram of the SLAM data acquisition system.

The high speed dual port memory allows for storage of up to 256 K bytes of data. The dual port memory can be accessed either by the analog-to-digital (A/D) converter for storage of SLAM image data, or by the Z-80 microprocessor for data analysis. A more detailed description of this system can be found elsewhere [Embree, 1985a]. An additional 512 K bytes of Intel MULTIBUS memory is available for data storage and allows for frame averaging.

A TRW TDC1007PCB 30 MHz, 8-bit A/D converter digitizes the SLAM data. The A/D converter 14.3 MHz clock signal, the frame horizontal and vertical synchronization signals are taken directly from the SLAM. A single frame from the SLAM image is digitized in 768 points horizontally and 255 points vertically.

2.1.2. Ultrasonic attenuation coefficient

The attenuation coefficient represents the normalized decrease in ultrasonic energy after passing through a specimen. The attenuation coefficient is determined by an insertion loss procedure [Tervola et al., 1985a] which compares the received signal amplitude of a specimen of known thickness in the sound path with that of the reference medium, normal saline.

The Z-80 microprocessor system utilizes a BASIC program for data acquisition and for data processing. A subimage area of approximately $400 \mu\text{m} \times 250 \mu\text{m}$ near the center of the acoustic image (the brightest, most uniform area) is used. To insure that the acoustic subimage remains at the same location as the detectors, the specimen is placed on a sheet of mylar ($25 \mu\text{m}$

thick) that is coupled to the acoustic wave from the SLAM stage with distilled water. The subimage area is digitized to yield an average amplitude value (V). The average of these subimage area averages is calculated, converted to decibels (dB), and displayed on the terminal screen. Equation (1) mathematically describes this procedure.

$$V = 10 \log \left\{ \frac{1}{n} \sum_{i=1}^n \left[(1/3072) \sum_{i=y}^{y+31} \sum_{j=x}^{x+95} (v_{ij} - r_i) \right] \right\} \quad (1)$$

where V = the average of the image area averages expressed in dB,

n = the number of times the imaging area is averaged,

i = image row index,

j = image column index,

y = starting row number of the imaging area,

x = starting column number of the imaging area,

v_{ij} = digitized value of the pixel at the i^{th} row and j^{th} column, and

r_i = average reference level of the i^{th} row (raster line).

Using the saline, the SLAM is adjusted to optimize the imaging area for brightness and uniformity. Several values of V are recorded for normal saline and for the specimen. Insertion loss (IL) is represented as a logarithmic function of the ratio of these two signal amplitudes and provides a quantitative index in decibels of the energy loss through the specimen. An IL value, in dB, is calculated using Equation (2)

$$IL = V_s - V_r \quad (2)$$

where V_r is the average of V recorded for the saline and V_s is the value of V recorded for the specimen.

The attenuation coefficient is determined by measuring the IL for three or four different thicknesses. Three to five separate IL values from different areas of the specimen are obtained for each thickness. The slope of the linear least squares fit line for an IL versus thickness plot yields the attenuation coefficient.

2.1.3. Ultrasonic speed

Ultrasonic speed [Tervola et al., 1985b] is determined from the interference-mode image of the SLAM. The field of view (3 mm x 2 mm) contains approximately 39 vertical interference lines equally spaced about 85 μm apart and covers the specimen and the reference medium of known ultrasonic speed. The speed of sound is determined by the horizontal shift in the fringe lines between the reference medium and the specimen according to Equation (3) [Goss et al., 1979].

$$C_x = (C_o / \sin \theta_o) \sin \left\{ \arctan \left[\frac{1}{\left(\frac{1}{\tan \theta_o} \right) - (N \lambda_o / T \sin \theta_o)} \right] \right\} \quad (3)$$

where C_x = speed of sound in the specimen of interest,

C_o = speed of sound in the reference medium,

θ_0 = angle of sound from the normal in the reference medium,

N = normalized fringe shift,

λ_0 = wavelength of sound in the reference medium, and

T = specimen thickness.

The λ_0 can be calculated from $\lambda_0 = C_0/f$ where $f = 100$ MHz. The θ_0 can be determined using Snell's Law (4)

$$\theta_0 = \sin^{-1} \left[\frac{C_0}{C_s} \sin \theta_s \right] \quad (4)$$

where C_s (= 5968 m/s) is the speed of sound in the fused-silica stage, θ_s (= 45°) is the angle at which the sound waves are traveling through the stage and C_0 (= 1520 m/s) is the speed of sound in saline at 30°C. Inserting these values into Equation (4) yields $\theta_0 = 10.4^\circ$. The only parameter which needs to be determined is N , the normalized fringe shift, which refers to the amount of lateral fringe shift relative to the fringe spacing.

Several techniques have been developed to quantitate N . The first involves manually measuring the fringe shift and fringe spacing using a ruler on the TV monitor or a photograph of the monitor. This method is time-consuming and relies on the operator's experience and judgment yielding only a few speed estimates per sample. The second method utilizes the automated data acquisition system and the spatial domain technique (SDT) [Foster, 1981; Embree et al., 1984; Embree et al., 1985b]. Using this technique, a fringe shift of 0.03 can be detected compared

to 0.1 for the manual method. The degree of accuracy allows statistical parameters: standard deviation, mean, mode, median, skewness and kurtosis to be calculated. The SDT works well on homogeneous specimens like rat liver but often fails for heterogeneous specimens like canine skin. The present method, the spatial frequency domain technique (SFDT) [Tervola et al., 1985b], allows the analysis of heterogeneous specimens.

The SFDT determines the normalized fringe shift, N , in the frequency domain rather than in the spacial domain. The Fourier transform of a horizontal raster line is its plane wave spectrum or spacial frequency spectrum. If the phase components of the Fourier transforms of two raster signals, one shifted relative to the other, are evaluated at the frequency at which the spectrum is a maximum, the phase difference, $\Delta\phi(\xi_0)$, is given by Equation (5)

$$\Delta\phi(\xi_0) = 2\pi y_0 / \lambda_y = 2\pi N \quad (5)$$

where ξ_0 = spatial frequency at which the spectrum is a maximum,
 y_0 = amount of horizontal shift in the signal,
 λ_y = fringe line spacing, and
 N = normalized fringe shift.

Therefore, the change in phase between two raster lines is simply related to N . To calculate $\Delta\phi(\xi_0)$, the phase for each raster line in the specimen is subtracted from the average phase determined for the saline reference raster lines (lines 1-50 and 205-255). A running-mean algorithm corrects for a modulo 2π

uncertainty of the phase due to the cyclic nature of the Fourier transform.

The SFDT has several advantages over the previous technique. The SFDT works for heterogeneous specimens where the SDT fails; it is twice as fast and more noise tolerant. Because the SFDT analyzes the SLAM image in the vertical direction rather than horizontally, a contour or speed profile of speed versus data point can be constructed giving an illustration of the change in speed of sound from saline to specimen.

For the wound healing studies [Steiger, 1986], a few modifications of the SFDT were introduced to make the method more adaptable to variations in the SLAM images. The SFDT assumed fringe line spacing (raster signal wavelength) remained constant over the entire image and determined the phase at a fixed frequency. Investigation of the digitized data for several interferograms showed this false. Depending upon the position of the image, saline had maximum frequency components between 700 and 800 kHz. Comparison of the interference-mode image of a heterogeneous specimen to a homogeneous specimen showed variability in the fringe line spacing. Examination of the heterogeneous specimen revealed maximum frequency components between 600 and 800 kHz.

To compensate for this difference, the Fourier transform was computed for a range of frequencies, and the phase for the frequency with the maximum amplitude was used to compute N . To reduce leakage in the Fourier transform, a Discrete Fourier Transform (DFT) was used instead of the Fast Fourier Transform

(FFT), allowing the data window length to be an integer number of wavelengths.

The DFT length, the frequency components, data window length and position on the image are program parameters which can be varied as desired. Typically, a DFT length of 768, 18 frequency components between 600 and 915 kHz, and a window length of 20 data points (the average raster signal wavelength) are used to compute N.

2.1.4. Heterogeneity index (HI)

One advantage of determining the speed of sound in a specimen using the modified SFDT is that many speed values representing a different area of the specimen are obtained. The variation in the spatial speed distribution indicates the acoustic heterogeneity of the specimen. The standard deviation (SD) of the mean speed value is a statistical measure of the variation of the speed values about the mean.

Using the SD as an indication of the heterogeneity, Steiger's [1986] results show that SD is dependent on the number of times the image is averaged, on the thickness of the sample and on the number of speed values averaged.

2.1.5. Comparison of ultrasonic attenuation coefficient and speed

Greater regional differences can be distinguished with the speed analysis as compared to that of the attenuation coefficient analysis. Each speed pixel is approximately 4 μm by

8 μm , and a speed profile (80 μm by 2 mm) along the vertical direction of the section is generated. The advantage of determining the ultrasonic speed using the speed profile is that many speed values, each representative of a different area of the field of view, are obtained. The variation in the spatial speed distribution can then be used as an indication of heterogeneity index of the specimen. In contrast, each insertion loss pixel is 400 μm by 250 μm , and an average IL value per section is generated over a region approximately 1 mm in extent. Further, at least three separate sections are required to calculate the attenuation coefficient.

Uncertainty in the SLAM assessment of wave speed and attenuation coefficient was determined for solutions of known acoustic properties and duplicate samples of skin and healing wound tissue. The details of these measurements were reported elsewhere [Steiger et al., in press]. Using a homogeneous medium, the accuracy (proximity to the true value) was $\pm 2.9\%$ and the precision (reproducibility of successive independent measurements) was $\pm 0.4\%$ for speed and for attenuation coefficient and $\pm 12\%$ and $\pm 15\%$, respectively. Using heterogeneous samples of normal skin and wound tissue, the speed and attenuation coefficient precisions were $\pm 1.7\%$ and $\pm 16\%$, respectively.

2.2 Ultrasonic Backscatter Instrumentation

A portable research instrument, the CTC-II (Marquette Electronics), measures ultrasonic backscatter. The details of

this instrument have been described elsewhere [Sagar et al., 1987; Sagar et al., 1988; Rhyne, 1977; Rhyne et al., 1986a; Rhyne et al., 1986b]. The instrument consists of a computer-automated ultrasonic transmitter-receiver, high-resolution display, control panel, microprocessor circuitry and an ECG monitor constructed in a mobile cart. The transmitted signals consist of 2 μ s duration carrier bursts. The programmed CTC-II performs frequency scans consisting of separate pulse-echo transmissions over frequencies between 4.0 and 6.8 MHz, in 0.1 MHz steps. Using the ECG waveform, the computer selects six frequency scans at evenly spaced intervals over the cardiac cycle.

The transducer is a 6 mm, 5 MHz, unfocused disk fitted with a 2 cm water-filled fixture, closed by a finger cot. The hand-held fixture with the transducer is applied directly to the epicardium (cardiac surface). To encompass the entire myocardial wall, range gates are positioned by observing A-mode echo patterns. At each sampling site, frequency scans over approximately 16 cardiac cycles are automatically performed. The digitized echoes, ECG waveform and various instrument settings are then recorded on floppy disks.

A marking signal, added to the electrocardiogram and coincident with each frequency scan, determines the timing of the frequency scan relative to the cardiac cycle. The repetition rate of the frequency scans adjusts for heart rate. The electrocardiogram is read manually, and phase annotation for each frequency scan is added to the data disks after each experiment.

The data disks containing the frequency scan echoes, instrument settings, and ECG waveform are analyzed with the use of a computer (IBM PC). The magnitude of the echo signals adjusts for 1) transmitter level, 2) receiver gain setting, 3) transducer frequency calibration, 4) diffraction calibration, 5) bulk attenuation (1.0 dB/cm-MHz), and 6) Rayleigh scattering spectrum of the tissue [Sagar et al., 1983]. This scaling results in signals with an absolute reflection magnitude and a perfectly flat frequency content (whitened spectrum). Next, five of the echo signals from each frequency scan, each having a resolution of 2 μ s (0.5 MHz bandwidth), are coherently combined to form a composite echo signal having 0.5 μ s resolution (over 2 MHz bandwidth). The Integrated Backscatter Rayleigh Five MHz is constructed by sampling the corrected high resolution echoes at selected ranges (and for selected scans) and averaging the squared magnitudes. The magnitude expresses (after averaging) in decibels the absolute measure of the backscatter in square centimeters of reflecting material per cubic centimeter of volume [Sagar et al., 1988].

The subendocardial region is analyzed by averaging successive data points from the high resolution echo over a 1 μ s interval (approximately 0.77 mm/ μ s time of flight). Taking into account the 0.5 μ s resolution of the echoes, this represents two samples each 0.39 mm in duration, spaced 0.77 mm apart. (The large epicardial wall echo automatically tracks and positions the subendocardial region to begin 5.4 mm from the epicardial surface.) At each data site, 16 beats are recorded with six

frequency scans per beat. The mean IBR5 represents averaging over all data taken at that site and for the selected range.

CHAPTER 3

METHODS

3.1 Tissue Preparation: Canine Myocardium

Five mongrel dogs of either sex weighing 20-30 kg were anesthetized with sodium pentobarbital (30 mg/kg i.v.) and ventilated with a respirator (Harvard Model 607). Atelectasis (collapse of lung tissue) was prevented by maintaining an end expiratory pressure of 5-7 cm of water with a trap. Body temperature was controlled at 38°C with a heating pad and servomechanical controller. The PO₂, PCO₂ and pH were maintained at physiological levels. Phasic and mean aortic blood pressures were recorded by a catheter inserted into the right femoral artery, advanced to the ascending thoracic aorta and connected to a strain gauge pressure transducer (Statham P50). The right femoral vein was cannulated with a flexible tube for drug administration.

A thoracotomy, an opening into the thoracic cavity, was performed in the left fifth intercostal space (the space between two ribs), the lungs retracted, and the heart suspended in a pericardial cradle. Left ventricular pressures were monitored by inserting a pressure transducer tipped catheter (Millar PC380, 8F) into the left ventricle through the left carotid artery. The left ventricular pressure pulse was electronically differentiated to obtain peak positive dp/dt. The differentiator was calibrated by means of a triangular waveform of known slope. A 1.0 to 1.5 cm segment of the left anterior descending coronary artery

(Figure 4) was isolated and a precalibrated electromagnetic flow probe was positioned around the vessels for measurement of coronary blood flow (Statham 2202). A micrometer-driven, mechanical vascular occluder was placed distal to the flow probe for production of total coronary artery occlusion (blockage). The electrocardiogram (limb lead II) and aortic blood pressure were recorded continuously on a Grass (Model 7) polygraph.

Total occlusion of the left anterior descending coronary artery for five hours (N=5) produced acute myocardial ischemia causing a decrease in the blood supply to the heart tissue. Presence of acute myocardial ischemia was documented by loss of systolic segment shortening and subsequent electronmicroscopic examination of the tissues. The IBRS, systolic segment shortening and systemic hemodynamics were recorded before and after five hours of coronary artery occlusion. At the end of each experiment, the dog was killed and tissue specimen (5 mm x 5 mm) from the subendocardium of the left anterior descending and left circumflex coronary artery perfusion territories were obtained for SLAM study, electron microscopic examination and determination of myocardial water content.

The SLAM samples were mounted on a circular cork (22 mm diameter, 3 mm thickness) with Ames Tissue-Tek OCT^R, frozen in liquid nitrogen, placed in Ziploc^R bags and shipped on dry ice from the Medical College of Wisconsin to the Bioacoustics Research Laboratory at the University of Illinois for storage in a -70°C Revco freezer pending analysis. Specific orientation of the endocardial and epicardial surfaces were carefully marked on

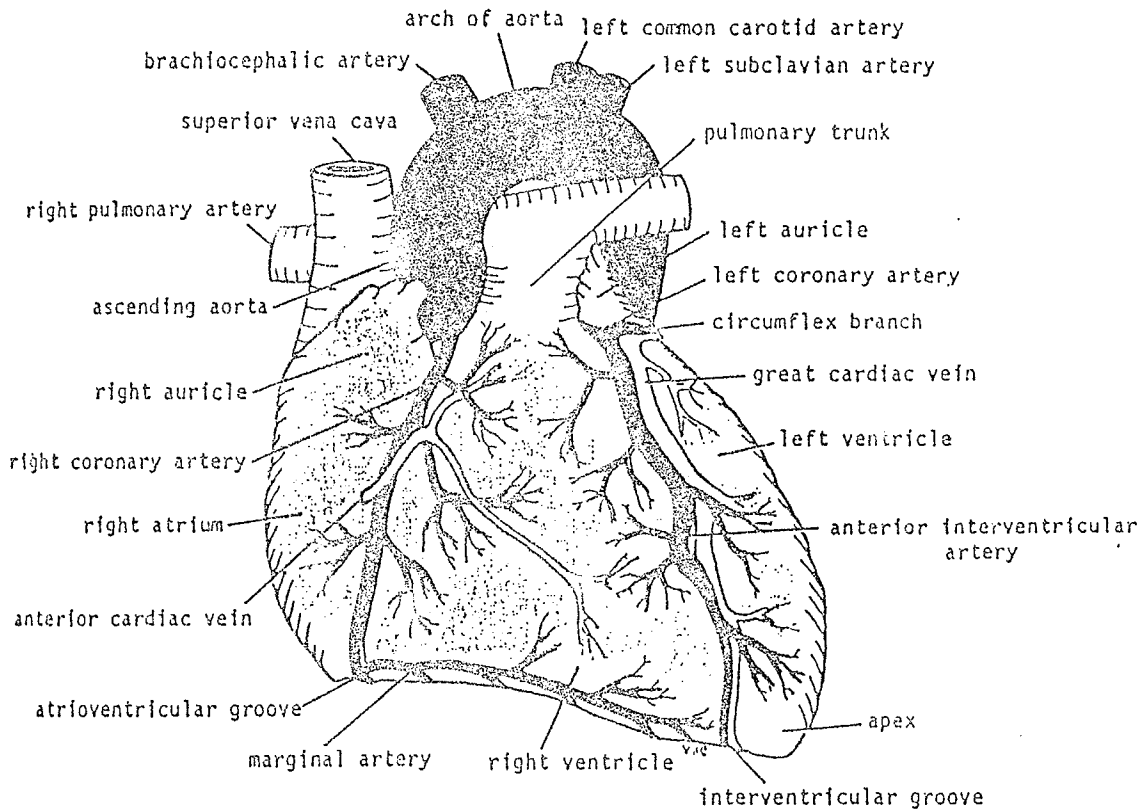


Figure 4 - Anterior view of myocardium showing the locations of the left anterior descending coronary artery and the circumflex branch.

the corks and then coded so that the investigators making ultrasound measurements did not know the sample's tissue type.

Specimens of known thickness (50, 75, 100, 125 and 150 μm) were mounted on a one-square-inch sheet of mylar (25 μm thick) with albumin fixative so that the position of the endocardium was always known.

3.1.1 Segmental contractile function and biochemical determinations

Regional myocardial contractile function (segment shortening) was measured in the perfusion territory of the left anterior descending coronary artery by a pair of piezoelectric crystals. The crystals were inserted approximately 10-15 mm apart and 7-10 mm deep within the left ventricular free wall in a circumferential plane parallel to the expected subendocardial muscle fiber orientation. Next, the crystals were secured with a single suture, and the depth (average of 8.8 ± 1.0 mm) of each was verified at the completion of the experiment. The leads of each crystal were connected to an amplifier that transformed the sound pulse transmitted between the two crystals into an electronic signal proportional to the distance between the crystals. The tracings were monitored on a Soltec oscilloscope (Model 520). Diastolic segment length was determined as the distance between the two crystals at the beginning of the rising phase of positive dP/dt (onset of isovolumetric contraction), and systolic segment length was measured at peak negative dP/dt . The diastolic and systolic segment lengths were normalized to a

control value of 10 for the initial diastolic segment length by the method of Theroux [Theroux et al., 1972]. Percent segment shortening (%SS) was calculated from the equation: $\%SS = (DL - SL) / DL \times 100$, where DL is the diastolic and SL is the systolic segment length. The piezoelectric crystals were disconnected during ultrasonic backscatter data acquisition to avoid any potential interference.

Myocardial tissue water concentration was determined by the wet weight/dry weight ratio. Tissue specimens from normal and ischemic zones were weighed and dried to a constant weight at 95°C in tared vials.

3.1.2. Statistical analysis

All SLAM values and myocardial water concentration values are reported as mean \pm SD. The IBR5 values are reported as mean \pm SEM. Comparisons between normal and ischemic myocardium were performed with Statgraphics, a statistical graphics program. In addition, paired T tests were performed on the IBR5, water concentration and segment shortening data. Changes were considered significant when the probability (p) values were less than 0.05.

3.2 Tissue Preparation: Bovine Articular Cartilage

Articular cartilage was obtained immediately postmortem from the stifle (knee) joint of 1-to 2-year-old adult steers. Full thickness cartilage plugs were excised from the patellar groove with a cylindrical 6 mm-diameter punch and washed in

saline plus protease inhibitors (2 mM phenylmethylsulfonyl fluoride, 10 mM N-ethyl maleimide, 2 mM ethylene diamine tetraacetic acid and 5 mM benzamidine-HCl) prior to enzyme digestion. A sequential enzyme extraction procedure [Chun et al., 1986] was used to deplete cartilage plugs of specific matrix constituents. The enzymatic alteration included the following steps. In step one, control (NORMAL) plugs incubated in buffer alone (0.05 M Tris-HCl, 0.06 M sodium acetate, pH 8.0).

Chondroitinase ABC is added to the intact cartilage plugs in step two (CS-DEPLETED). Chondroitinase ABC removes 85% or more of the chondroitin sulfate, measured as galactosamine, leaving most of the keratan sulfate (85% at the glucosamine) still in the matrix. Studies of cartilage plugs treated for various time periods show that the enzyme steadily digests its way from the surface to the interior rather than diffusing in rapidly and then uniformly depleting throughout the plug [Chun et al., 1986].

In step three the remainder of the noncollagenous matrix is removed using streptomyces hyaluronidase and trypsin digestion (COLLAGEN ONLY). Cartilage treated with trypsin after chondroitinase retains only a trace of chondroitin sulfate (< 1% galactosamine) and less than 5% glucosamine, but loses less than 1% of its hydroxyproline. Treatment with streptomyces hyaluronidase removes the remaining glucosamine along with an equimolar amount of uronic acid. The residual plug is essentially devoid of noncollagenous matrix, but retains the shape, integrity and tensile strength of its collagen network [Chun et al., 1986].

Step four includes the functional disruption of the intermolecular cross-links using porcine pancreatic elastase (CROSS-LINKS CLEAVED) for 24 hours at 25°C in 0.07 M Tris/Cl, pH 8.5. This enzyme specifically degrades the nonhelical terminal peptides of collagen molecules, which are principal cross-linking sites. Denaturant extraction shows that this treatment functionally destroys more than 70% of the intermolecular bonds [Schmidt et al., 1987]. All plugs are washed with distilled, deionized water for 60 minutes at 4°C to remove buffer salts and enzymes before mounting for acoustical measurements.

At the completion of the enzyme digestions the treated cartilage plugs along with the untreated plugs were mounted on cork with Ames Tissue-Tek OCT^R, frozen in liquid nitrogen, placed in Ziploc^R bags and shipped on dry ice from the University of Washington to the Bioacoustics Research Laboratory at the University of Illinois for storage in a -70°C Revco freezer pending analysis. The samples were sent in duplicate and coded so that the investigators making ultrasound measurements did not know how the cartilage samples were treated. Figure 5 shows the specimen orientation for both perpendicular and parallel sections. Each 6 mm disc of cartilage was cut in half. From one half, a 2 mm plug was bored for sectioning parallel to the articular surface. The other half was trimmed and mounted for sections perpendicular to the articular surface (cross-section). Specimens of known thickness (25 μm , 40 μm , 50 μm , and 60 μm for perpendicular samples and 25 μm , 50 μm , and 70 μm for parallel samples) were mounted on glass slides with albumin fixative so

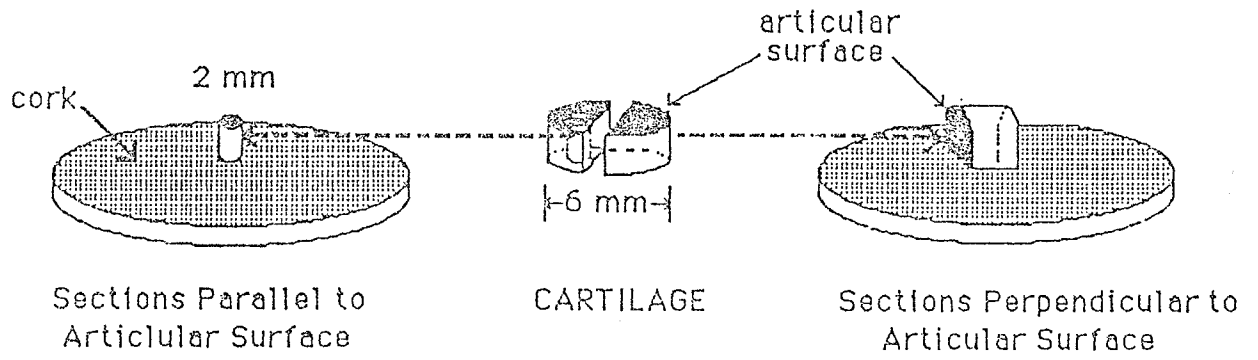


Figure 5 - Diagram of the specific specimen orientation for both perpendicular and parallel sections of articular cartilage.

that the position of the articular surface was always known. A record of depth from the articular surface was kept for the parallel section specimens.

3.2.1 Statistical analysis

Statgraphics was used to determine the significance of both attenuation coefficient and ultrasonic speed versus treatment and fiber orientation. Changes were considered significant when the probability (p) values were less than 0.05.

3.3 Specific Experimental Protocol

Immediately before ultrasonic analysis, each tissue specimen was removed from the freezer, and the corks were mounted on an object disk of a Lipshaw cryostat (maintained at -35°C). Approximately 50-100 μm of the upper surface of the specimen was sectioned and discarded to provide a flat, even surface for subsequent sections.

It has been demonstrated that rapid freezing in liquid nitrogen does not affect the mechanical properties of skin and wound tissue [Marangoni et al., 1966]. Similarly, Geleskie and Shung [1982] observed no differences in ultrasonic impedance among several tissue studies before and after freezing. It was necessary for the myocardia and cartilage specimens to be frozen in these studies both for transporting specimens and sectioning them for the SLAM, but the studies were designed so that all experiments could be accomplished with one freeze-thaw cycle.

For all samples, the thinnest specimen was cut first and the thickest specimen cut last. Each specimen was trimmed to a size 2-3 mm horizontally by 1-1.5 mm vertically in order to fit within the field of view of the SLAM.

CHAPTER 4

MYOCARDIUM RESULTS AND DISCUSSION

The IBR5, systemic hemodynamics and regional segment shortening were measured in each of five dogs. A total of 10 infarcted and 7 normal tissue specimens from the five dogs were analyzed with the SLAM. Myocardial water content was determined from five normal and five infarcted myocardial tissue samples.

4.1 The SLAM Ultrasonic Propagation Results

A complete listing of the SLAM ultrasonic propagation properties for the normal and infarcted regions is given in Appendix I. An analysis of variance (ANOVA) is performed to assess the effects of tissue type and thickness on attenuation coefficient, ultrasonic speed and heterogeneity index. An ANOVA partitions the total variance of a dependent variable into portions due to the independent factors through comparison of group means. The statistical program assumes that the data represent normally distributed variables. The significance of the effect of a factor on the variance of the dependent variable is determined using the F-test, where F is calculated as the ratio of the mean squared variance between the factor category means and the mean squared variance within all the categories of the factor. In other words, the F statistic is a measure of the variation that would result if the variation was due totally to random factors. The factors and categories for each factor included in the ANOVA are listed in Table 1.

Table 1. Factors and categories included in the ANOVA of canine myocardium attenuation coefficient, ultrasonic speed and heterogeneity index.

Factor	Categories				
Thickness (μm)	1)50	2)75	3)100	4)125	5)150
Tissue	1)Normal	2)Ischemic			

An ANOVA was performed on the speed and heterogeneity index data to assess the effect of thickness. Since the determination of the attenuation coefficient yielded only one value per specimen, it was excluded from this ANOVA. The results are shown in Table 2. The table includes tissue type, propagation property, F-ratio and significance level of the factor.

Table 2. The ANOVA results for the effect of thickness on ultrasonic speed and heterogeneity index.

Tissue	Property	F-ratio	Significance
Normal	Speed	4.13	0.018
	HI	1.55	0.237
Ischemic	Speed	1.29	0.303
	HI	1.04	0.409

The results of Table 2 indicate that thickness had an effect on the speed of the normal tissue. Examination of Figure 11 in Appendix IV shows that the data for the 50 μm thickness is significantly higher than the other thicknesses. The difference

in the speed values can be explained by the thickness error. The margin for error due to slicing the specimen is much greater for thinner sections than for thicker sections. Since speed is dependent on the thickness and the fringe shift (described in Section 2.1.3.), the error is compounded. These results suggest that for canine myocardium, thicker sections (75-100 μm) are needed to eliminate this thickness error.

Closer examination of Figures 11-18 in Appendix IV illustrates the dependence of HI upon speed. The HI versus thickness graphs track the speed graphs closely. The current definition of HI, i.e., the standard deviation, is a function of the mean speed value. Ultimately, HI should be an independent measure of the speed variation. With the limited scope of this study it is not possible to determine a solution to this problem. A larger study comparing homogeneous and heterogeneous specimens is needed to find a better indicator of heterogeneity.

The ANOVAs are performed again on the data with the 50 μm values removed. For consistency, the 50 μm values are also removed from the ischemic tissue speed, the normal tissue HI and the ischemic tissue HI. The results are listed in Table 3.

Table 3. The ANOVA results for the effect of thickness on ultrasonic speed and heterogeneity index after removing the 50 μm values.

Tissue	Property	F-ratio	Significance
Normal	Speed	0.13	0.942
	HI	0.20	0.894
Ischemic	Speed	2.78	0.066
	HI	1.47	0.252

The results of Table 3 indicate that there is no variation in speed nor heterogeneity index due to specimen thickness. Therefore, the data for all four thicknesses can be pooled without affecting the results. The significance level of the ischemic tissue speed ($p = 0.066$) decreases compared to that reported in Table 2 ($p = 0.303$). Removal of the 50 μm values explains this decrease. Since the standard deviation of the 50 μm values is so large, removing these values decreases the 95% confidence level, thereby decreasing the overall significance level.

The speed and heterogeneity index data were individually combined and a separate ANOVA was performed to determine the effect of tissue type. Table 4 lists the results of the variance in ultrasonic propagation properties due to tissue type, and Table 5 lists the corresponding mean \pm SD.

Table 4. The ANOVA results for the effect of tissue type on attenuation coefficient, ultrasonic speed and heterogeneity index.

Property	F-ratio	Significance
Attenuation Coefficient	22.1	0.0003
Ultrasonic Speed	3.4	0.0737
Heterogeneity Index	0.7	0.4314

Table 5. The SLAM attenuation coefficient (dB/mm), ultrasonic speed (m/s) and heterogeneity index (m/s) \pm SD for normal and ischemic samples.

Tissue	Attenuation Coefficient	Ultrasonic Speed	Heterogeneity Index
Normal	63.8 \pm 17.2	1602 \pm 26	13 \pm 6
Ischemic	33.8 \pm 4.2	1589 \pm 19	11 \pm 7

Tissue type had a significant effect on the variance in attenuation coefficient but not on ultrasonic speed or heterogeneity index. Ultrasonic speed had a low p value ($p = 0.0737$); therefore, tissue type was having some effect on the speed, not enough to be considered significant, but within the noise range. The attenuation coefficient variation explained by tissue type (22.1) was much higher compared to the others.

This trend was also seen in the mean values. The most dramatic difference between the normal and infarcted myocardium occurred in the attenuation coefficient. Attenuation coefficient in the ischemic tissue (33.8 \pm 4.2 dB/mm) was almost 2 times less than that in the normal tissue (63.8 \pm 17.2 dB/mm). Irreversible

tissue damage appeared to have a smaller effect on the ultrasonic speed and heterogeneity index, but both also demonstrated a consistent reduction. Ultrasonic speed was 1602 ± 26 m/s in the normal and 1589 ± 19 m/s in the infarcted myocardium. Similarly, the heterogeneity index was 13 ± 6 m/s in the normal and 11 ± 7 m/s in the damaged tissue.

4.2 The IBR5, Biochemical and Segment Shortening Results

A complete listing of the IBR5, myocardial water concentration and segment shortening for both normal and infarcted myocardium is given in Appendix II. To determine the effect of tissue type on IBR5, water content and segment shortening, a paired student's T-test was performed. Like the ANOVA, a student's T-test is a comparison of sample means. The T ratio is defined as the deviation divided by a standard deviation, where the difference between the means is the deviation and the standard error of the difference between the means is the standard deviation. The results of the T-test for the normal and ischemic tissue are given in Table 6.

Table 6. Paired T-test for differences in IBR5 (dB), myocardial water content (%) and segment shortening (%) between normal and ischemic tissue.

	Normal (Mean \pm SD)	Ischemic (Mean \pm SD)	Δ	Significance
IBR5	-46.6 \pm 0.6	-37.8 \pm 1.8	8.8	< 0.01
% Water	78.0 \pm 0.2	80.9 \pm 0.6	2.9	< 0.05
Segment Shortening	15 \pm 5	-5 \pm 2	20	< 0.01

The IBR5 in the infarcted zone (-37.8 ± 1.8 dB) was significantly higher than in normal regions (-46.6 ± 0.6 dB). Myocardial water concentration was also increased in damaged tissue ($80.9 \pm 0.6\%$) as compared to normal ($78 \pm 0.2\%$). Segment shortening was measured in the territory of LAD coronary artery before and after the total occlusion. Segment shortening in the left anterior descending region ($15 \pm 5\%$) was replaced by aneurysmal bulging ($-5 \pm 2\%$) during total coronary artery occlusion.

Light microscopic features of the ischemic and the normal myocardium were identical after five hours of ischemia. As shown in Figure 6, changes at the ultrastructural level were apparent in the ischemic myocardium. Myofibrils swelled and interstitial tissue increased. There was also loss of mitochondrial cristae and mitochondrial swelling, along with an absence of intermyofibril glycogen. In contrast, the control tissue shown in Figure 7 showed no swelling of myofibrils. The myofibrils

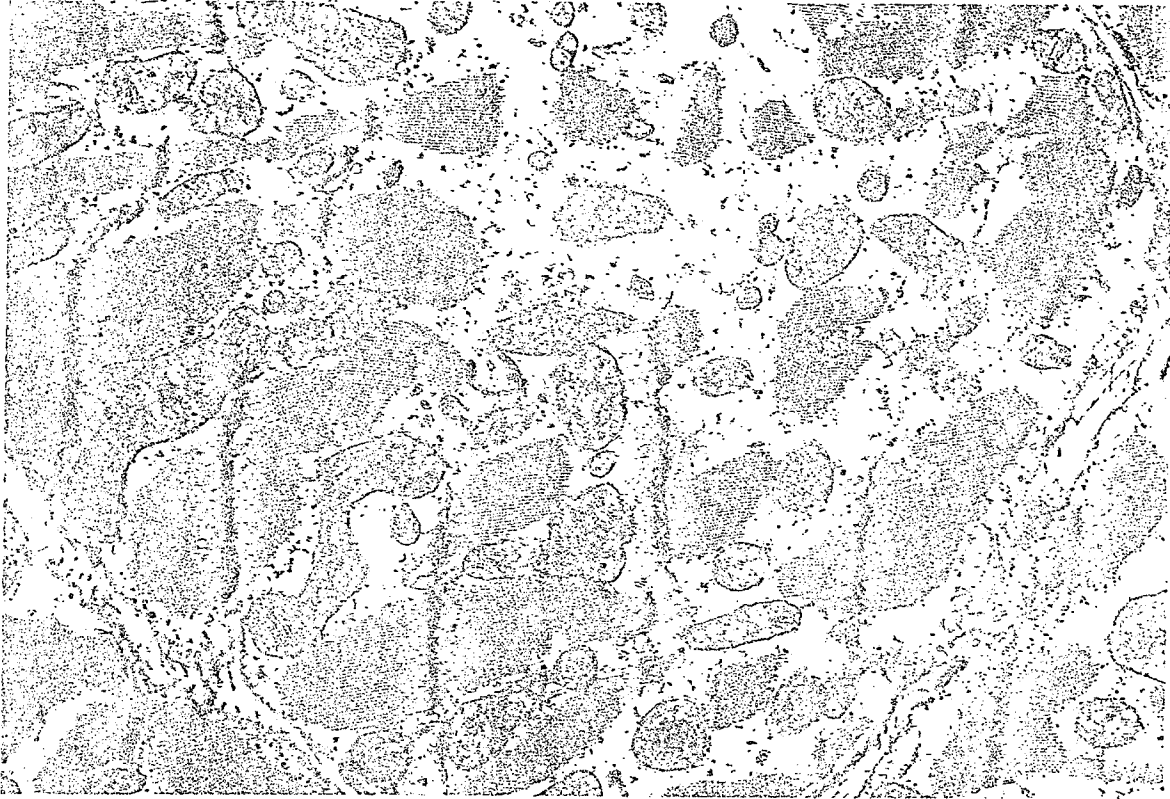


Figure 6 - Electronmicroscopic examination of canine myocardium after five hours of ischemia shows swelling of myofibrils, mitochondria and depletion of glycogen (X 12,000).

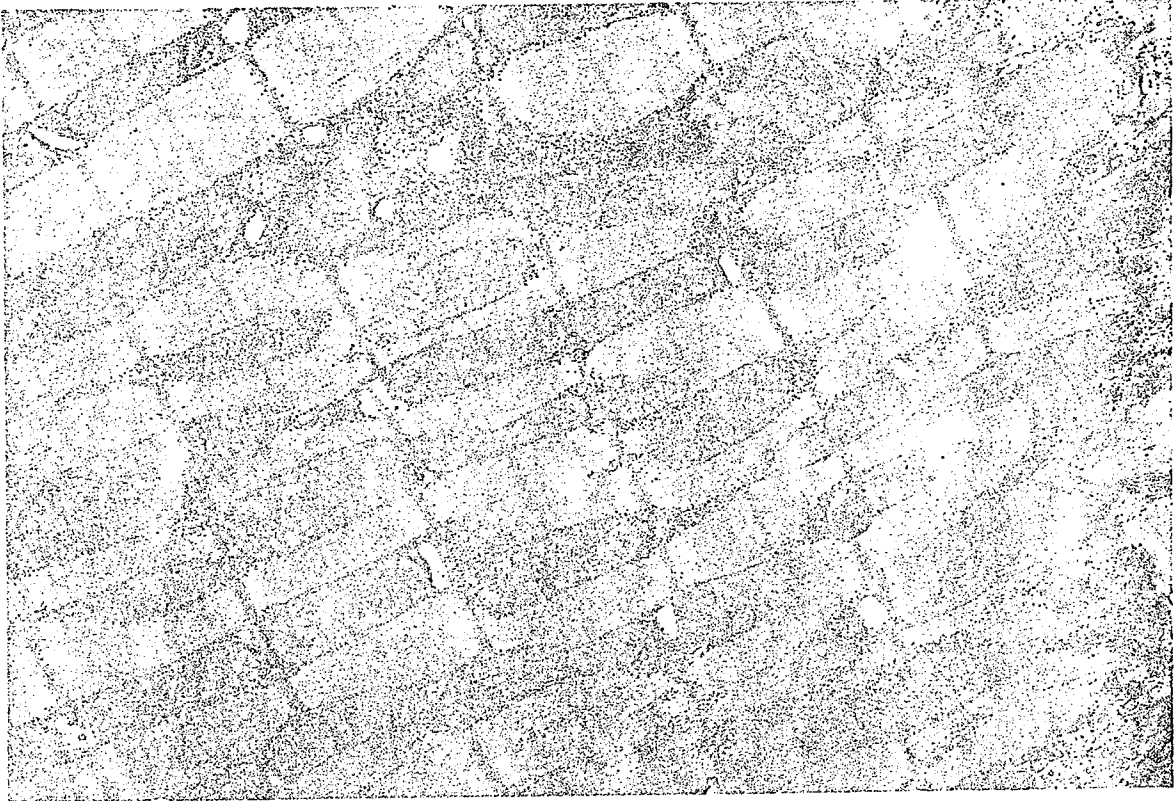


Figure 7 - Electronmicroscopic examination of normal canine myocardium shows intact myofibrils, mitochondria and abundant interfibrillar glycogen (X 15,000).

were lined by mitochondria with prominent crystae, and interfibril glycogen was abundant.

Statistical analysis comparing the SLAM acoustic properties to IBR5 and water concentration could not be accomplished since a reliable record of the specimen dates and order could not be determined. A more complete record of the dates and number of specimens is being kept in present studies to avoid this problem.

4.3 Discussion

The present investigation demonstrates that irreversible tissue damage produces a decrease in attenuation coefficient, ultrasonic speed and heterogeneity index as measured by the SLAM, and this is associated with an increase in integrated backscatter and myocardial water concentration.

It has been known for three decades that the ultrasonic propagation properties, particularly the attenuation coefficient, of biological materials are strongly affected at the macromolecular level [Carstensen et al., 1953; Carstensen et al., 1959; Pauly et al., 1971]. A comparison of attenuation coefficient and ultrasonic speed to tissue constituents has suggested that ultrasonic propagation properties of tissue can be modeled as a function of constituent concentrations [O'Brien, 1977b; Pohlhammer et al., 1980]. Four tissue constituents that are of particular importance acoustically are water, protein, collagen and lipid.

Graphic representations of studies have shown statistically significant negative correlations between attenuation coefficient and water concentration for human liver [Bamber et al., 1981], for canine wound tissue [Olerud et al., 1987] and orotic acid treated rat liver [O'Brien et al., 1988]. Similarly, graphic representations of studies [Bamber et al., 1981; Olerud et al., 1987; Sarvazyan et al., in press] have shown significant negative correlations between ultrasonic speed and water concentration.

However, a more complete regression analysis has shown that protein, collagen and lipid concentrations play a more dominant role in the determination of ultrasonic speed and attenuation coefficient and that water plays a secondary role. O'Brien, Erdman and Hebner [1988] have found statistically significant negative interactions between lipid and water concentrations (Δ lipid/ Δ water = -0.82) and between protein and water concentrations (Δ protein/ Δ water = -0.93), i.e., lipid and protein accumulation displaces water and vice versa. Similar results are shown with respect to collagen and water concentration [Olerud et al., submitted].

It had been previously believed that water is the major contributor to differences in ultrasonic propagation properties. Prolonged ischemia has been shown to cause an increase in myocardial water concentration and a decrease in attenuation coefficient [O'Donnell et al., 1979c]. But it is unlikely that water could be responsible for a decrease in attenuation coefficient of almost 50% and a decrease in ultrasonic speed of

1%. Collagen, on the other hand, has been shown to play an important role in the propagation properties of ultrasound [Olerud et al., 1987; Olerud et al., submitted; Wladimiroff et al., 1977]. Chronic infarction results in an increase in collagen concentration and attenuation coefficient [O'Donnell et al., 1979c]. Collagenous fibers exhibit a Young's modulus approximately 1000 times greater than other tissues [Goss et al., 1979; Fields et al., 1973]. Since ultrasonic speed is proportional to the square root of Young's modulus, the ultrasonic speed would be expected to be greater for collagen than for other constituents. Although collagen concentration has not been determined in this study, it is likely that collagen concentration decreases due to an increase in water concentration, leading to the decrease in both attenuation coefficient and ultrasonic speed.

Previous study [Steiger, 1986] on canine skin and wound shows that heterogeneity index negatively correlates with tissue water content and that the relationship between HI and water content is linear and very strong ($r = 58\%$). In addition, significant nonlinear (3.4 power of collagen) correlations between HI and total collagen concentration (both as % wet and DDF weight) are also indicated.

The HI results in this study exhibit a linear relationship between water concentration (3% increase in ischemic compared to normal) and HI (2 m/s decrease in ischemic compared to normal). Even though collagen seems to have a strong nonlinear effect on

heterogeneity, it would be impossible to speculate its effect on ischemic myocardium without knowing its collagen concentration.

The IBR5 data are significantly higher in the area of infarction compared to normal. Previous studies also report similar increases in integrated backscatter [Mimbs et al., 1981; Sagar et al., 1987]. This investigation and previous investigations indicate that the increase in water concentration is the secondary mechanism contributing to the increase in ultrasonic backscatter. The primary mechanism is the altering of the framework of the myocardium, due to increased water concentration, which creates a larger distance between adjacent muscle fibers, thus, explaining the increase in scattering of ischemic tissue.

Studies [Wickline et al., 1985; Wear et al., 1986; Rhyne et al., 1986a] suggest that changes in acoustic properties of scatters depends on not only the changes in elastic properties, but also its geometric configuration. After 60 to 180 minutes of acute occlusion of the coronary artery, intercellular edema is more prominent, mitochondrial dense bodies are numerous and breaks in the sarcolemma are present [Kloner et al., 1980]. Nuclear chromatin clumping, intermyofibrillar swelling and mitochondrial dense bodies may also be a contributing factor in the increase in scattering by altering the size and density of possible scatterers, although the exact nature of scatterers still remains unknown.

Theoretically, a strong correlation should exist between IBR5 and HI. A material containing inhomogeneities, i.e.,

particles or scatterers, loses acoustic energy faster than a homogeneous material. A further effect of inhomogeneities is scattering, whereby acoustic energy is being reflected and refracted away from its initial direction. The difference between these two parameters is due to the fact that integrated backscatter is sensitive to compressibility and density, whereas the SLAM is sensitive to the ratio of compressibility and density.

These findings also corroborate the earlier belief that myocardial tissue is a tight-knit framework of muscle fibers. Increased water concentration in ischemic tissue loosens the framework causing the decrease in HI. On the other hand, the loosening of the framework increases the number of sites for scatterers which in turn causes the increase in IBRS.

In this study, the interaction of ultrasound with normal and ischemic myocardium has been characterized in a unique fashion with the aid of the SLAM. For the first time, the elastic properties of myocardial tissue have been quantified both in vivo and in vitro. Further research will be necessary in order to develop a sufficient understanding of the ultrasonic tissue signature of myocardium and its promising application in the diagnosis of cardiac pathologies, like amyloidosis and hypertrophy.

CHAPTER 5

ARTICULAR CARTILAGE RESULTS AND DISCUSSION

5.1 The SLAM Ultrasonic Propagation Results

A complete listing of the SLAM attenuation coefficient and ultrasonic speed for the articular cartilage is given in Appendix III. Table 7 lists the attenuation coefficient (mean \pm SE) for all 16 cartilage samples, and Figure 8 depicts the same data graphically.

Table 7. The SLAM attenuation coefficient (dB/mm) \pm SE for perpendicular and parallel samples.

Tissue	Sample	Perpendicular	Parallel
NORMAL	A	88 \pm 9	92 \pm 10
	B	105 \pm 11	147 \pm 15
CS-DEPLETED	A	108 \pm 6	40 \pm 4
	B	112 \pm 6	63 \pm 3
COLLAGEN ONLY	A	75 \pm 9	77 \pm 14
	B	85 \pm 5	90 \pm 5
CROSS-LINKS CLEAVED	A	143 \pm 14	166 \pm 14
	B	185 \pm 14	165 \pm 15

The most consistent and striking difference in attenuation coefficient is seen between the COLLAGEN ONLY and the CROSS-LINKS CLEAVED samples. These samples contain essentially the same amount of collagen, but most of the intermolecular cross-links of collagen have been functionally disrupted in the latter as shown

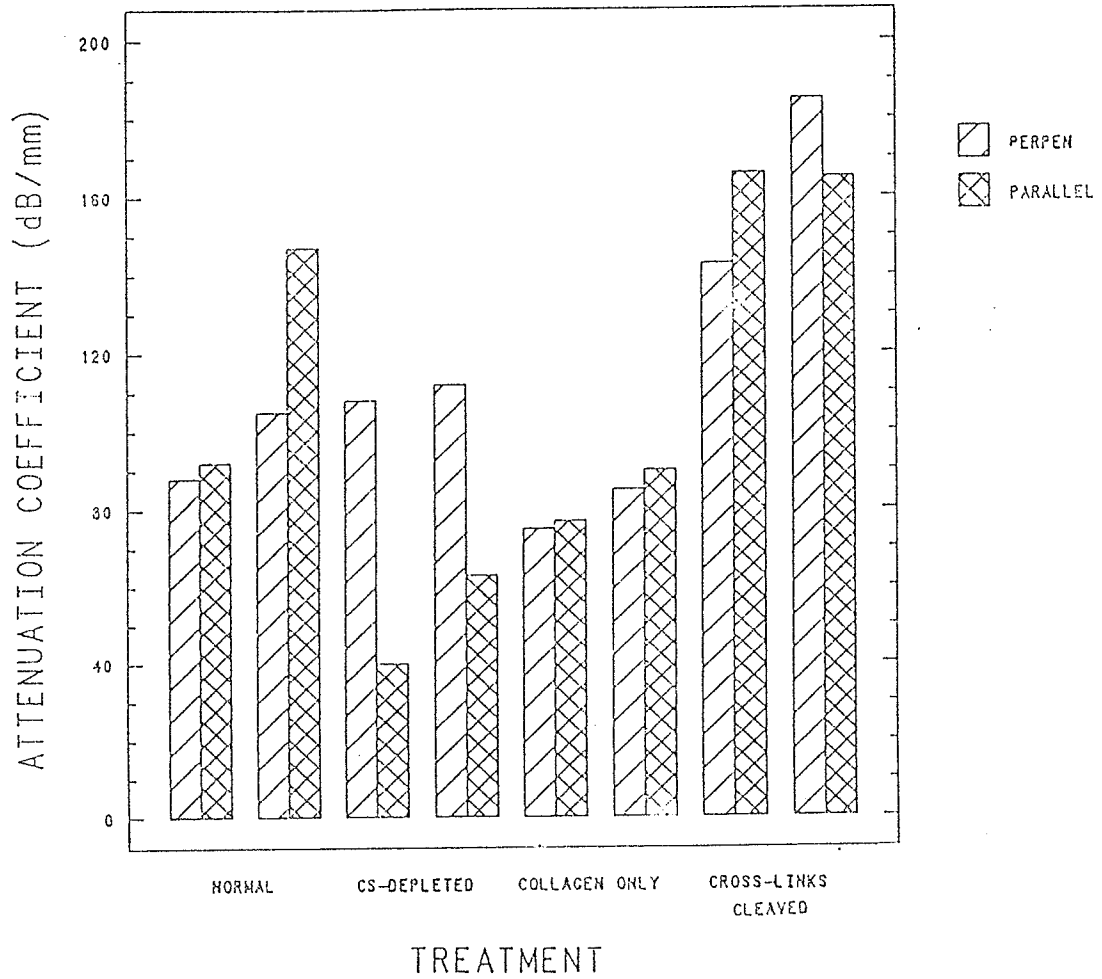


Figure 8 - The SLAM attenuation coefficient vs. treatment for perpendicular and parallel samples of articular cartilage.

diagrammatically in Figure 1. Disrupting intermolecular cross-links doubled the attenuation coefficient of both parallel and perpendicular sections. Removing glycosaminoglycans, proteoglycans and other noncollagenous proteins appeared to have a less predictable effect on attenuation. In perpendicular section, the CS-DEPLETED samples attenuated the ultrasonic energy slightly more than did NORMAL or COLLAGEN ONLY samples, but in parallel sections the CS-DEPLETED samples attenuated much less than NORMAL and COLLAGEN ONLY samples. Also, CS-DEPLETED samples attenuated ultrasonic energy much more in perpendicular section than in parallel whereas, for the other preparations there was little distinction between perpendicular and parallel.

Figure 9 graphically displays the ultrasonic speed data for the 16 cartilage samples while Table 8 lists the mean \pm SD. The most complete speed data came from perpendicular section samples. Because of smaller pixel size, speed data could be obtained for perpendicular sections from three anatomical regions of articular cartilage (tangential, transitional and radial).

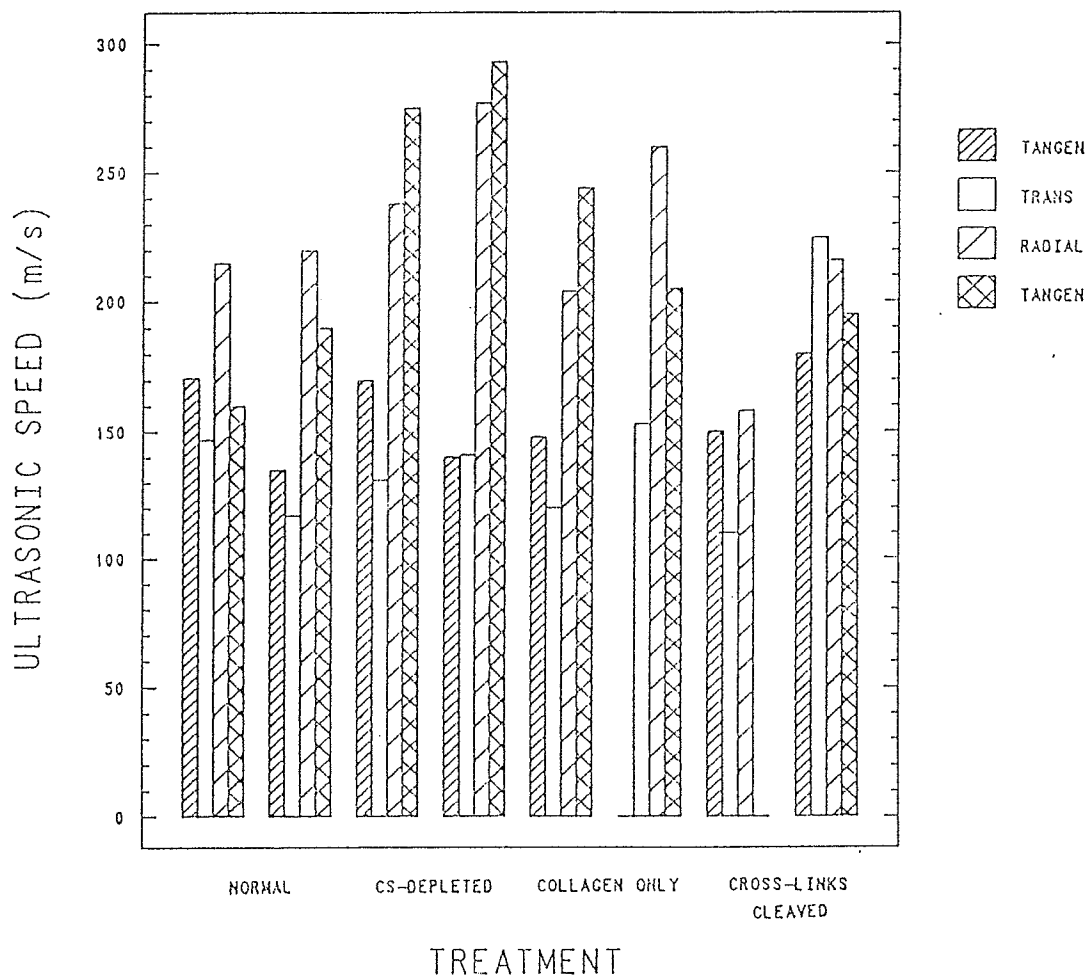


Figure 9 - The SLAM ultrasonic speed vs. treatment for perpendicular and parallel samples of articular cartilage.

Table 8. The SLAM ultrasonic speed (m/s) \pm SD for perpendicular and parallel samples. The data marked with an "a" represent samples from which only one tangential speed value could be calculated. Dashes represent missing data.

Tissue	Sample	Perpendicular			Parallel
		Tangential	Transitional	Radial	Tangential
NORMAL	A	1671 \pm 61	1647 \pm 76	1715 \pm 25	1660 \pm 44
	B	1635 \pm 27	1617 \pm 41	1720 \pm 99	1690 \pm 76
CS-DEPLETED	A	1670a	1631 \pm 27	1738 \pm 51	177 \pm 66
	B	1640 ^a	1641 \pm 56	1777 \pm 114	1793 \pm 25
COLLAGEN ONLY	A	1648 ^a	1620 \pm 38	1704 \pm 106	1744 \pm 87
	B	----	1653 \pm 38	1760 \pm 103	1705 \pm 74
CROSS-LINKS CLEAVED	A	1650 \pm 20	1610 \pm 33	1658 \pm 53	----
	B	1680 ^a	1725 \pm 88	1716 \pm 9	1695 \pm 59

Although actual values varied greatly between individual sections (hence the large SD) the speed profile across a section was consistent. Figure 10 shows a typical speed profile. The highest speed value was seen in the radial zone where the fibrils are oriented mainly perpendicular to the articular surface (sound propagation direction perpendicular to fibrils). Speed dropped significantly in the transitional zone then tended to rise again slightly in the surface, tangential zone where the fibrils lie parallel to the articular surface.

Parallel sections were examined only from the tangential zone (Table 8). The direction of sound in these sections was primarily perpendicular to the fibril orientation. The ultrasonic speed in these samples approached that seen in the

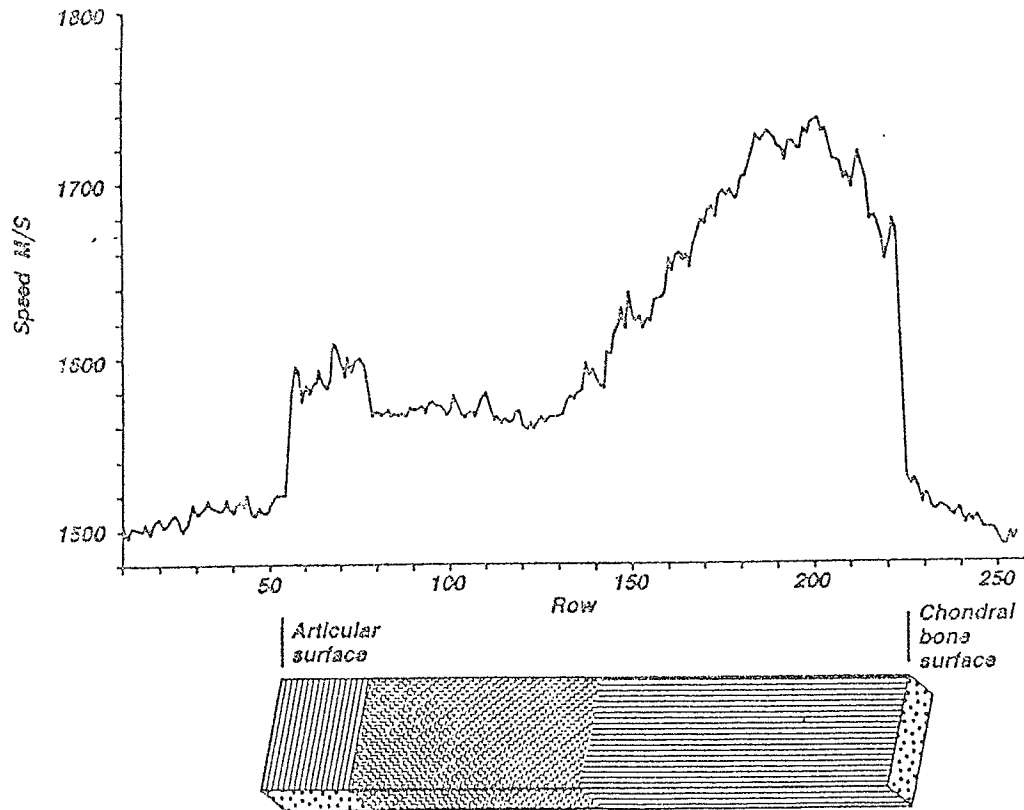


Figure 10 - Profile of wave speed as a function of tissue depth for a slice of normal cartilage cut in perpendicular section. Changes in the predominant orientation of fibrils with depth are depicted below.

radial domain of perpendicular sections. Hence, acoustic waves appear to be propagated more rapidly across the long axes of collagen fibrils than along them.

An analysis of variance is performed to assess the effects of treatment, section and fiber orientation on attenuation coefficient and ultrasonic speed. The factors and categories for each factor included in the ANOVA are listed in Table 9.

Table 9. Factors and categories included in the ANOVA of bovine articular cartilage attenuation coefficient and ultrasonic speed.

Factors	Categories	
Treatment	1) NORMAL 3) COLLAGEN ONLY	2) CS-DEPLETED 4) CROSS-LINKS CLEAVED
Section	1) Perpendicular	2) Parallel
Fiber Orientation	1) Tangential 3) Radial	2) Transitional

The ANOVAs are performed on the attenuation coefficient to assess the effect of treatment and section. Fiber orientation is not a factor for attenuation coefficient since a value for each zone could not be determined. Table 10 lists the ANOVA results of the effect of treatment. The table includes section, F-ratio and significance level of the factor. The results indicate that treatment had a significant effect on the variation in attenuation coefficient. The amount of attenuation coefficient variation explained by treatment is about the same for both perpendicular section (9.76) and parallel section (10.30).

Table 10. The ANOVA results for the effect of treatment on attenuation coefficient.

Section	F-ratio	Significance
Perpendicular	9.76	0.026
Parallel	10.30	0.024

Table 11 lists the ANOVA results of the effect of section. The ANOVA results confirm the observations seen in Figure 8. Only in the CS-DEPLETED samples is section a significant factor whereas, in the other treatments, section has no effect. In addition to the CS-DEPLETED significance level being low, the F-ratio is large indicating that the correlation between attenuation coefficient variation and section is strong.

Table 11. The ANOVA results for the effect of section on attenuation coefficient.

Treatment	F-ratio	Significance
NORMAL	0.64	0.516
CS-DEPLETED	25.12	0.038
COLLAGEN ONLY	0.18	0.715
CROSS-LINKS CLEAVED	0.01	0.950

Similar analysis is performed on the ultrasonic speed data to determine the effects of treatment and fiber orientation. First, the speed values for the perpendicular sections are

analyzed for the effect of treatment. The results are given in Table 12a.

Table 12a. The ANOVA results for the effect of treatment on ultrasonic speed (perpendicular section).

Fiber Orientation	F-ratio	Significance
Tangential	0.16	0.918
Transitional	0.28	0.836
Radial	1.72	0.300

The results of Table 12a show that there is no variation in speed in the three zones due to treatment. Therefore, the data from the three zones can be pooled without affecting the results. Next, the perpendicular section speed data are combined and a separate ANOVA is performed on the perpendicular and parallel sections to determine the effect of treatment. Table 12b lists the ANOVA results.

Table 12b. The ANOVA results for the effect of treatment on ultrasonic speed.

Section	F-ratio	Significance
Perpendicular	0.10	0.961
Parallel	9.35	0.050

Treatment has a significant, but marginal ($p = 0.05$) effect on the ultrasonic speed variation in only the parallel sections.

Comparing the attenuation coefficient results (Table 10) to the speed results, treatment has an equal effect on perpendicular and parallel attenuation coefficients, whereas treatment has no effect on the perpendicular speed. Also, the F-ratio of the parallel speed (9.35) and the parallel attenuation coefficient (10.3) are similar. Overall, the attenuation coefficient results appear to be more significantly related to treatment.

Finally, an ANOVA is performed to determine the effect of fiber orientation on ultrasonic speed. Table 13 lists the results of this ANOVA. Fiber orientation has a significant effect on the ultrasonic speed of the perpendicular samples. The low significance level and high F-ratio support the observations of Figure 10, that there is a profound effect of the "preferred" collagen fibril orientation on acoustic speed.

Table 13. The ANOVA results of the effect of fiber orientation on ultrasonic speed. N/A denotes not applicable.

Factor	F-ratio	Significance
Section:		
Perpendicular	14.52	0.0001
Parallel	N/A	N/A
Treatment:		
NORMAL	6.86	0.0469
CS-DEPLETED	30.41	0.0033
COLLAGEN ONLY	4.66	0.1191
CROSS-LINKS CLEAVED	0.11	0.9467

The NORMAL and CS-DEPLETED samples are statistically significant, while the COLLAGEN ONLY and CROSS-LINKS CLEAVED samples are not. The most striking observation is seen in the change in significance level at the different stages of treatment and the corresponding change in F-ratio. The NORMAL or untreated samples are marginally significant ($p = 0.0469$). Removal of 85% of the chondroitin sulfate decreases the significance level 14 times and increases the amount of speed variation explained by fiber orientation by 6. From the CS-DEPLETED samples to the CROSS-LINKS CLEAVED samples, the significance level gradually increases and the F-ratio decreases, so that at the third stage of the sequential enzyme procedure (CROSS-LINKS CLEAVED), orientation of the collagen fibers no longer has an effect on acoustic wave speed. The ANOVA results show that treatment has a strong effect on the anisotropy of the articular cartilage.

5.2 Discussion

The effects on cartilage composition of the enzyme treatments used here have been established [Chun et al., 1986; Schmidt et al., 1987]. In CS-DEPLETED samples 85% of the chondroitin sulfate is removed. COLLAGEN ONLY samples are essentially devoid of noncollagenous matrix, but retain the shape and tensile strength of the original NORMAL sample [Chun et al., 1986]. From CROSS-LINKS CLEAVED samples about two thirds of the collagen can be extracted as molecular monomers by non-proteolytic solvents [Schmidt et al., 1987], indicating that

most of the intermolecular cross-links have been disrupted, even though under physiological conditions the tissue maintains its original size, shape and collagen content. While the tensile strength of CS-DEPLETED and COLLAGEN ONLY samples is not dramatically altered [Chun et al., 1986; Li et al., 1984], the CROSS-LINKS CLEAVED samples have a 100-fold reduction in tensile strength [Schmidt et al., 1987].

A marked increase in the attenuation coefficient was observed when intermolecular cross-links were disrupted (covalent links broken) in the collagen of the cartilage as compared to the more rigidly interconnected collagen framework of the unaltered tissue. This observation is the most compelling evidence to date that acoustic propagation may be sensitive not only to the amount of collagen present in tissue but also to its configuration (degree of cross-linking). In addition to bonds between type II collagen molecules within individual fibrils, the recent finding that type IX collagen may provide covalent links between fibrils in cartilage matrix [Eyre et al., 1987] could also be relevant since the elastase treatment will also disrupt such bonding.

Removal of chondroitin sulfate and proteoglycans from the cartilage (CS-DEPLETED samples) apparently had some effect on the acoustic measurements but no obvious trend could be deduced from the few samples studied. Sulfated glycosaminoglycans and proteoglycans bind water and inflate collagenous matrices through the osmotic swelling pressure of their high fixed-charge density [Muir, 1980]. Hence, removing these macromolecules may affect

acoustic propagation by perturbing the equilibrium between protein-bound and free water [O'Brien et al., 1972]. The tension put on the collagen framework by this swelling pressure may also influence acoustic propagation.

Acoustic wave speed was seen to be influenced most by collagen fibril orientation. Changes in composition and collagen cross-linking had a greater effect on wave speed than on attenuation coefficient. The anisotropy and dependence on fibril orientation of wave speed in cartilage could be seen from differences in wave speed between tangential and radial zones in perpendicular samples, where the direction of fibril orientation is largely orthogonal between the two zones. In support of this observation is the similarity of wave speed in the tangential zone of parallel sections compared to radial zones of perpendicular sections. In both cases the sound direction was primarily perpendicular to the plane of fibril direction. The differences in predominant fibril orientations between these zones are well established [Hukins et al., 1984; Hukins et al., 1985].

The Brillouin scattering study of the hydration of Li-DNA and Na-DNA films yielded the velocity of phonons propagating perpendicular to the helix axis was greater by 2 to 10% than that propagating parallel to the helix axis [Lee et al., 1987]. This observation is consistent with this study, wherein the speed of the ultrasonic wave propagating perpendicular to the fibril orientation was greater (by about 6%) than the wave propagating parallel to the fibril orientation (see Figure 10).

Although the number of observations in this series of experiments is small, they give valuable clues on the interaction of ultrasonic energy with soft connective tissues at the ultrastructural and molecular levels. Further studies using a larger number of samples and more complete acoustic and morphological correlations are now needed to confirm and extend these conclusions.

APPENDIX I: THE SLAM ATTENUATION COEFFICIENT, ULTRASONIC SPEED
AND HETEROGENEITY INDEX FOR CANINE MYO ARDIUM

For the ultrasonic speed and heterogeneity index, the thinnest section value is listed first and the thickest section last. Dashes represent missing data.

Sample ID	Attenuation Coefficient (dB/mm)	Ultrasonic Speed (m/s)	Heterogeneity Index (m/s)
=====			
NORMAL TISSUE			
1	96.0	1674	10.8
		1557	12.5
		1647	17.0
2	50.3	1654	26.0
		1620	13.9
		1591	14.6
3	57.0	1691	34.5
		1603	16.8
		1596	7.9
4	82.3	1571	19.5
		1616	24.7
		1623	23.2
5	53.0	1603	4.9
		1623	5.6
		1625	6.0
6	44.9	1591	7.5
		1555	15.3
		1561	13.0
7	62.8	1634	8.7
		1613	9.4
		1614	11.4

APPENDIX I, continued

Sample ID	Attenuation Coefficient (dB/mm)	Ultrasonic Speed (m/s)	Heterogeneity Index (m/s)
ISCHEMIC TISSUE			
1	34.7	1599	8.8
		1622	22.8
		1587	8.5
2	36.9	1640	22.5
		1594	9.0
		--	--
3	29.3	1534	8.4
		1566	7.8
		1602	15.2
4	27.4	1541	4.2
		1635	6.7
		1590	7.5
5	36.8	1567	32.0
		1609	10.7
		1556	7.5
6	31.1	1598	10.7
		1558	6.1
		1578	15.9
7	32.8	1600	17.9
		1579	4.0
		1559	8.3
8	32.8	1607	7.2
		1580	10.7
		1580	8.2
9	42.3	1599	18.7
		1610	4.5
		1583	19.6
10	--	1598	4.7
		1585	10.0
		1591	6.6

APPENDIX II: THE IBR5 AND WATER CONCENTRATION FOR CANINE MYOCARDIUM

NORMAL TISSUE

Dog	IBR5 (dB)	Water Concentration (%)
1	-47.9	78.2
2	-46.2	77.6
3	-47.0	77.8
4	-45.8	78.3
5	-46.6	78.2

ISCHEMIC TISSUE

1	-39.9	80.9
2	-38.1	81.0
3	-35.9	80.5
4	-37.8	80.8
5	-36.0	81.5

APPENDIX III: THE SLAM ATTENUATION COEFFICIENT AND ULTRASONIC SPEED FOR BOVINE ARTICULAR CARTILAGE

For both perpendicular and parallel sections, the ultrasonic speed of the thinnest section is listed first and the thickest section last. Dashes represent missing data.

PERPENDICULAR SECTION

	Sample ID	Attenuation Coefficient (dB/mm)	Ultrasonic Speed (m/s)		
			Tangential	Transitional	Radial
NORMAL	A	88	--	1752	--
			1748	1669	--
			1600	1541	1690
			1664	1625	1740
	B	105	1666	1629	1860
			1600	1580	1640
			1638	1580	1660
			--	1680	--
CS- DEPLETED	A	108	--	1587	1664
			--	1660	1804
			--	1645	1759
			1670	1631	1725
	B	112	--	1733	1975
			--	1634	1706
			--	1585	1706
			1640	1610	1721
COLLAGEN ONLY	A	75	--	1593	1863
			1648	1574	1618
			--	1664	1599
			--	1650	1736
	B	85	--	--	1927
			--	1606	1671
			--	1655	1680
			--	1699	1763
CROSS-LINKS CLEAVED	A	143	--	1643	1582
			--	1560	1635
			1670	1635	1710
			1630	1600	1706
	B	185	--	1826	--
			--	1800	1729
			--	1634	1709
			1680	1641	1711

APPENDIX III, continued

PARALLEL SECTION

	Sample ID	Attenuation Coefficient (dB/mm)	Ultrasonic Speed (m/s)
NORMAL	A	92	-- 1720/1619 1640
	B	147	1580/1800 1627/1710 1762/1660
CS- DEPLETED	A	40	1851/1700 1718 1829
	B	63	1772/1826 1802/1775 1821/1761
COLLAGEN ONLY	A	77	1582/1700 1749/1841 1831/1761
	B	90	1838/1693 1608/1703 1684
CROSS-LINKS CLEAVED	A	166	-- -- --
	B	165	1759 1711 1616

APPENDIX IV: STATGRAPHICS ANALYSIS OF CANINE MYOCARDIUM

Files, tables and graphs generated by Statgraphics while performing the ANOVAs. First, the files of factors and categories needed in the analysis are listed. Next, is the table containing the F-ratio and significance level followed by the corresponding graph. The abbreviations used are

TISSUE = Tissue: 1 = Normal and 2 = Ischemic
THICKNES = Thickness (microns)
ATTEN = Attenuation coefficient (dB/mm)
SPEED = Speed (m/s)
HI = Heterogeneity index (m/s)
SPDNORM = Speed (m/s) Normal tissue
SPDISCH = Speed (m/s) Ischemic tissue
HINORM = Heterogeneity index (m/s) Normal tissue
HIISCH = Heterogeneity index (m/s) Ischemic tissue

The speed and heterogeneity index columns containing "2," i.e., SPDNORM2, etc., represent the data after the 50 μm values have been removed.

Table 14. Statgraphics files of factors and categories for canine myocardium.

File DGHRT05A 7/15/88

row	ATTEN	TISSUE
1	96.0	1
2	50.3	1
3	57.0	1
4	82.3	1
5	53.0	1
6	44.9	1
7	62.8	1
8	34.7	2
9	36.9	2
10	29.3	2
11	27.4	2
12	36.8	2
13	31.1	2
14	32.8	2
15	32.8	2
16	42.3	2
17		2

File DGHRT05B 7/15/88

row	TISSUE2	SPEED2	HI2
1	1	1571	20.
2	1	1603	5.
3	1	1591	8.
4	1	1634	9.
5	1	1557	13.
6	1	1620	14.
7	1	1603	17.
8	1	1616	25.
9	1	1623	6.
10	1	1555	15.
11	1	1613	9.
12	1	1647	17.
13	1	1591	15.
14	1	1596	8.
15	1	1623	23.
16	1	1625	5.
17	1	1561	13.
18	1	1614	11.
19	2	1567	32.
20	2	1598	11.
21	2	1600	18.
22	2	1607	7.
23	2	1599	19.
24	2	1598	5.
25	2	1622	23.
26	2	1594	9.
27	2	1566	8.
28	2	1635	7.
29	2	1609	11.
30	2	1558	6.
31	2	1579	4.
32	2	1580	11.
33	2	1610	5.
34	2	1585	10.
35	2	1587	9.
36	2		
37	2	1602	15.
38	2	1590	8.
39	2	1556	8.
40	2	1578	16.
41	2	1559	8.
42	2	1580	8.
43	2	1583	20.
44	2	1591	7.

Table 14, continued

File DGHRT05C 7/14/88

row	THICKNES1	SPDNORM	HINORM	SPDISCH	HIISCH	SPDNORM2	THICKNES3	THICKNES2
1	50	1674	10.8	1599	9.	1557	50	75
2	50	1654	26.0	1640	23.	1620	50	75
3	50	1691	34.5	1534	8.	1603	50	75
4	75	1557	12.5	1541	4.	1647	50	100
5	75	1620	13.9	1622	23.	1591	75	100
6	75	1603	16.8	1594	9.	1596	75	100
7	100	1647	17.0	1566	8.	1571	75	100
8	100	1591	14.6	1635	7.	1603	75	100
9	100	1596	7.9	1567	32.	1591	75	100
10	100	1571	19.5	1587	9.	1634	100	100
11	100	1603	4.9	1602	15.	1616	100	125
12	100	1591	7.5	1590	8.	1623	100	125
13	100	1634	8.7	1609	11.	1555	100	125
14	125	1616	24.7	1598	5.	1613	100	125
15	125	1623	5.6	1598	11.	1623	100	150
16	125	1555	15.3	1600	18.	1625	100	150
17	125	1613	9.4	1607	7.	1561	100	150
18	150	1623	23.2	1599	19.	1614	100	150
19	150	1625	5.0	1585	10.		125	
20	150	1561	13.0	1558	6.		125	
21	150	1614	11.4	1579	4.		125	
22				1580	11.		125	
23				1610	5.		125	
24				1556	8.		150	
25				1591	7.		150	
26				1578	16.		150	
27				1559	8.		150	
28				1580	8.		150	
29				1583	20.		150	

File DGHRT05C 7/14/88

row	THICKNES4	SPDISCH2	HINORM2	HIISCH2
1	75	1622	12.5	23.
2	75	1594	13.9	9.
3	75	1566	16.8	8.
4	75	1635	17.0	7.
5	75	1567	14.6	32.
6	100	1587	7.9	9.
7	100	1602	19.5	15.
8	100	1590	4.9	8.
9	100	1609	7.5	11.
10	100	1598	8.7	5.
11	100	1598	24.7	11.
12	100	1600	5.6	18.
13	100	1607	15.3	7.
14	100	1599	9.4	19.
15	125	1585	23.2	10.
16	125	1558	5.0	6.
17	125	1579	13.0	4.
18	125	1580	11.4	11.
19	125	1610		5.
20	150	1556		8.
21	150	1591		7.
22	150	1578		16.
23	150	1559		8.
24	150	1580		8.
25	150	1583		20.

Table 15. ANOVA results for the effect of thickness on ultrasonic speed of normal tissue.

One-Way Analysis of Variance

Data: DGHRT05C.SPDNORM

Level codes: DGHRT05C.THICKNES1

Labels: 5 3 RESHAPE '050075100125150'

Range test: Conf. Int. Confidence level: 95

Analysis of variance

Source of variation	Sum of Squares	d.f.	Mean square	F-ratio	Sig. level
Between groups	13151.643	4	3287.9107	4.125	.0175
Within groups	12753.595	16	797.0997		
Total (corrected)	25905.238	20			

0 missing value(s) have been excluded.

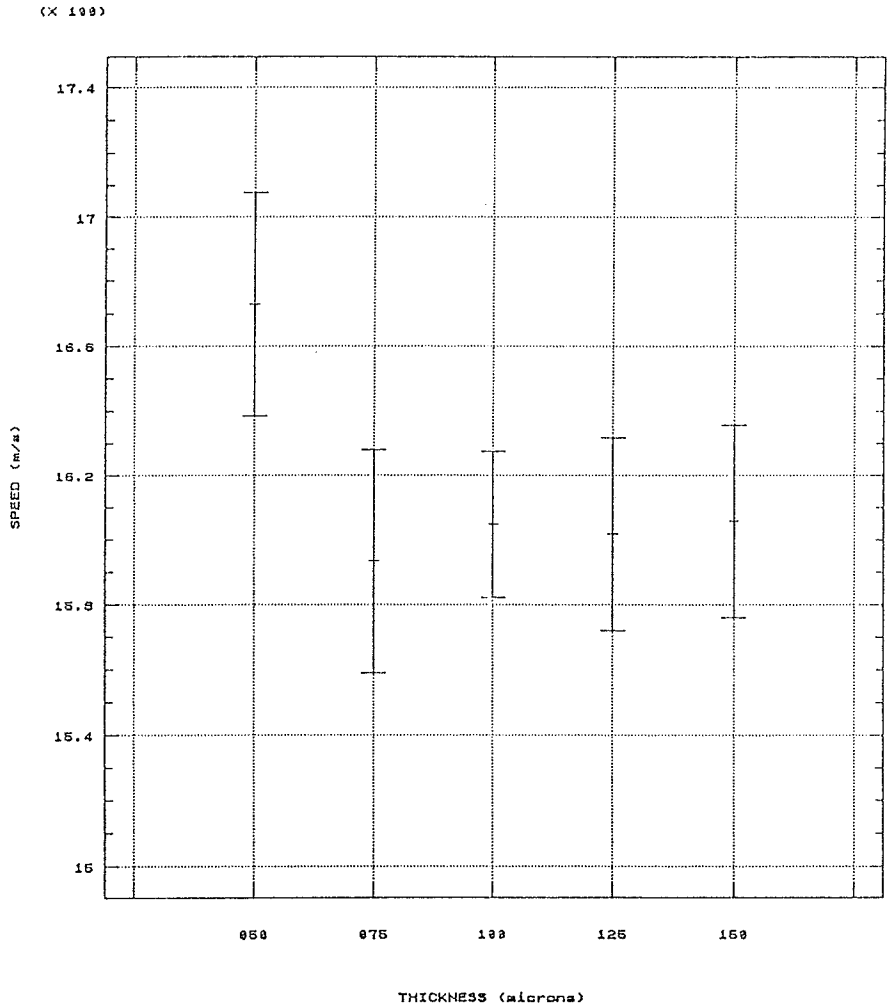


Figure 11. Statgraphics ANOVA: ultrasonic speed of normal tissue vs. thickness.

Table 16. ANOVA results for the effect of thickness on heterogeneity index of normal tissue.

One-Way Analysis of Variance

Data: DGHRT05C.HINORM
 Level codes: DGHRT05C.THICKNES1
 Labels: 5 3 RESHAPE '050075100125150'
 Range test: Conf. Int. Confidence level: 95

Analysis of variance

Source of variation	Sum of Squares	d.f.	Mean square	F-ratio	Sig. level
Between groups	332.35429	4	83.088571	1.545	.2367
Within groups	860.30381	16	53.768988		

Total (corrected)	1192.6581	20			

0 missing value(s) have been excluded.

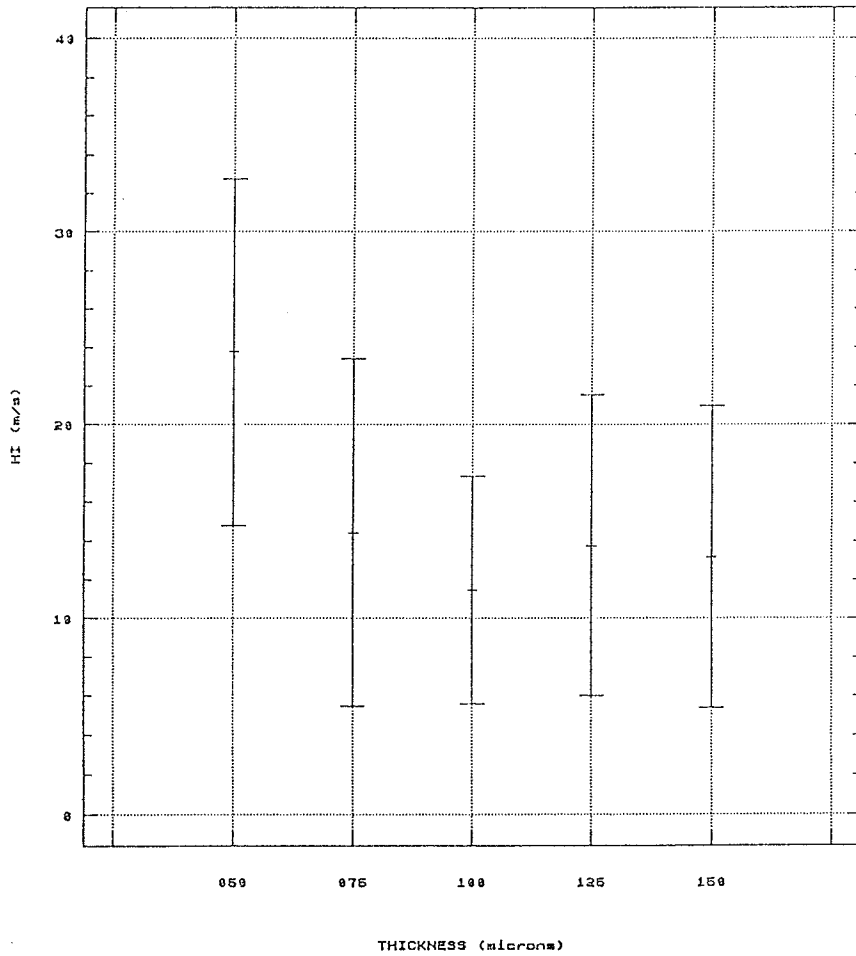


Figure 12. Statgraphics ANOVA: heterogeneity index of normal tissue vs. thickness.

Table 17. ANOVA results for the effect of thickness on ultrasonic speed of ischemic tissue.

One-Way Analysis of Variance

Data: DGHRT05C.SPDISCH

Level codes: DGHRT05C.THICKNES3

Labels: 5 3 RESHAPE '050075100125150'

Range test: Conf. Int. Confidence level: 95

Analysis of variance

Source of variation	Sum of Squares	d.f.	Mean square	F-ratio	Sig. level
Between groups	3064.749	4	766.18726	1.288	.3026
Within groups	14279.389	24	594.97454		

Total (corrected)	17344.138	28			

0 missing value(s) have been excluded.

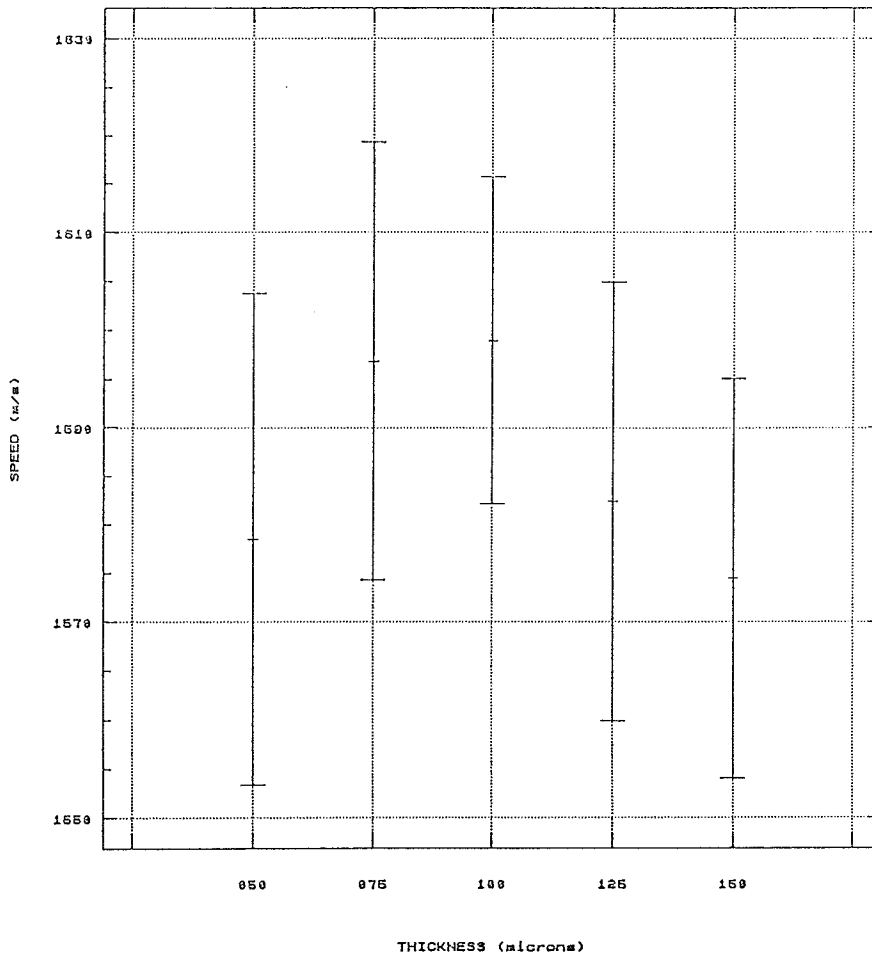


Figure 13. Statgraphics ANOVA: ultrasonic speed of ischemic tissue vs. thickness.

Table 18. ANOVA results for the effect of thickness on heterogeneity index of ischemic tissue.

One-Way Analysis of Variance

Data: DGHRT05C.HIISCH
 Level codes: DGHRT05C.THICKNES3
 Labels: 5 3 RESHAPE '050075100125150'
 Range test: Conf. Int. Confidence level: 95

Analysis of variance

Source of variation	Sum of Squares	d.f.	Mean square	F-ratio	Sig. level
Between groups	185.5698	4	46.392455	1.036	.4092
Within groups	1074.7798	24	44.782493		
Total (corrected)	1260.3497	28			

0 missing value(s) have been excluded.

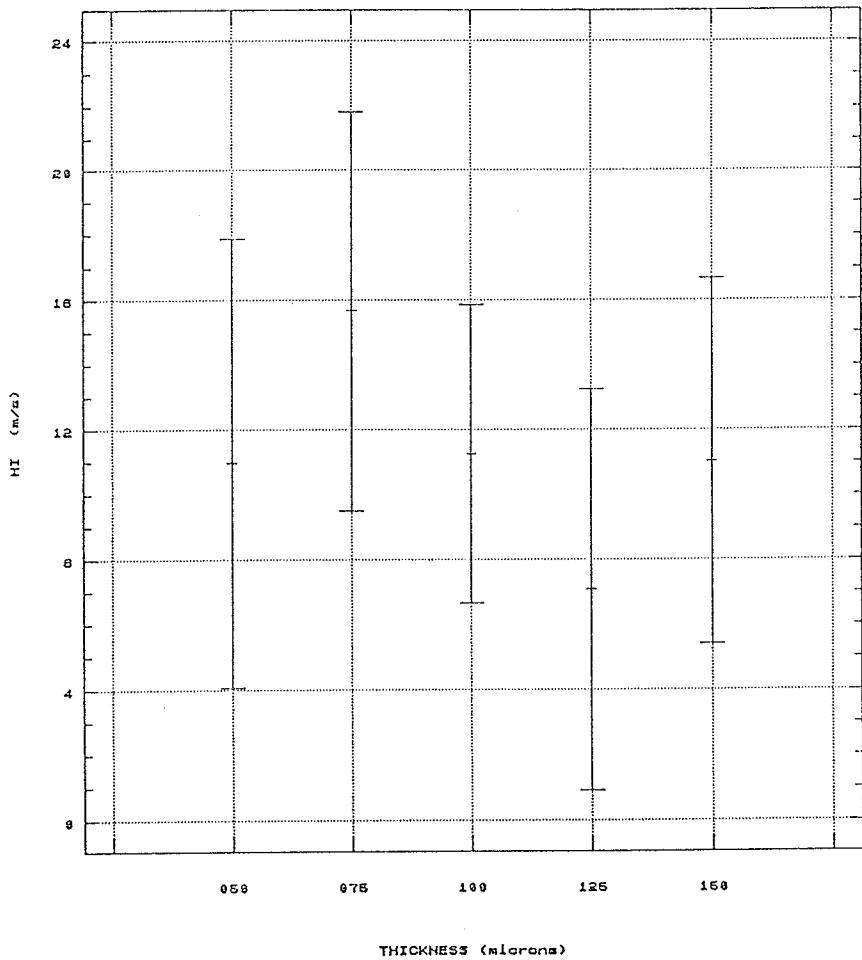


Figure 14. Statgraphics ANOVA: heterogeneity index of ischemic tissue vs. thickness.

Table 19. ANOVA results for the effect of thickness on ultrasonic speed of normal tissue excluding 50 μm values.

One-Way Analysis of Variance

Data: DGHRT05C.SPDNORM2
 Level codes: DGHRT05C.THICKNES2
 Labels: 4 3 RESHAPE '075100125150'
 Range test: Conf. Int. Confidence level: 95

Analysis of variance

Source of variation	Sum of Squares	d.f.	Mean square	F-ratio	Sig. level
Between groups	330.683	3	110.22751	.128	.9420
Within groups	12067.595	14	861.97109		
Total (corrected)	12398.278	17			

0 missing value(s) have been excluded.

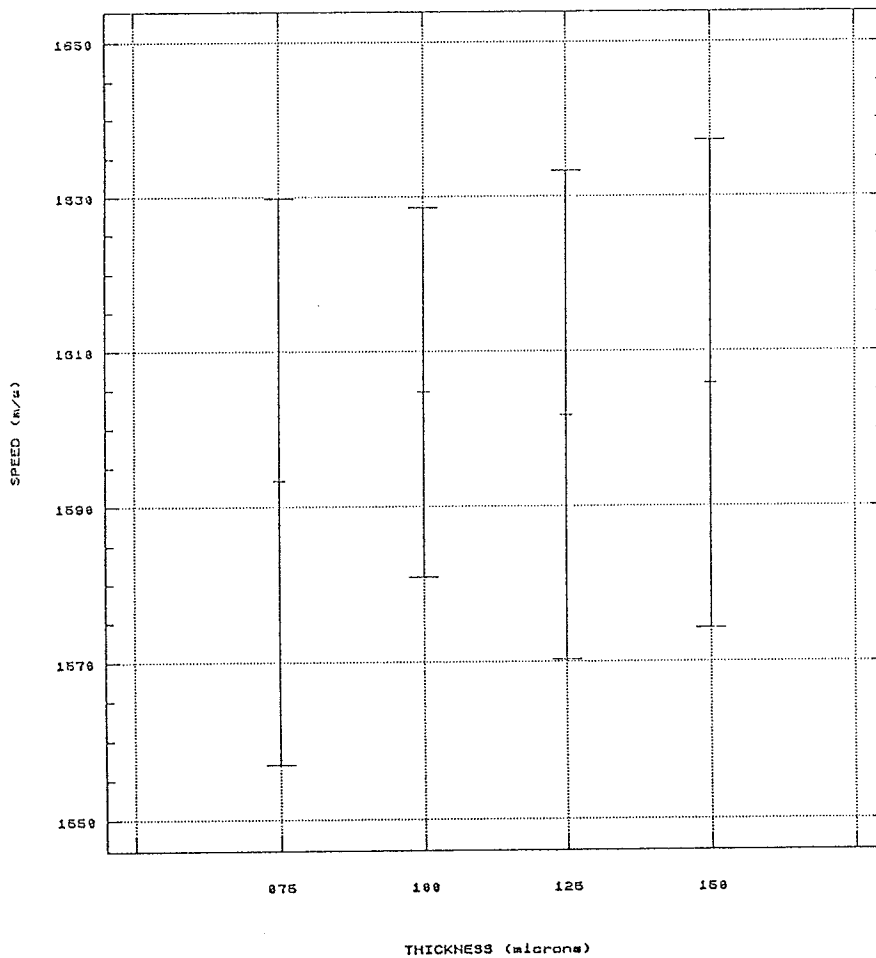


Figure 15. Statgraphics ANOVA: ultrasonic speed of normal tissue vs. thickness excluding 50 μm values.

Table 20. ANOVA results for the effect of thickness on heterogeneity index of normal tissue excluding 50 μm values.

One-Way Analysis of Variance

Data: DGHRT05C.HINORM2
 Level codes: DGHRT05C.THICKNES2
 Labels: 4 3 RESHAPE '075100125150'
 Range test: Conf. Int. Confidence level: 95

Analysis of variance

Source of variation	Sum of Squares	d.f.	Mean square	F-ratio	Sig. level
Between groups	24.65897	3	8.219656	.201	.8938
Within groups	571.97714	14	40.855510		
Total (corrected)	596.63611	17			

0 missing value(s) have been excluded.

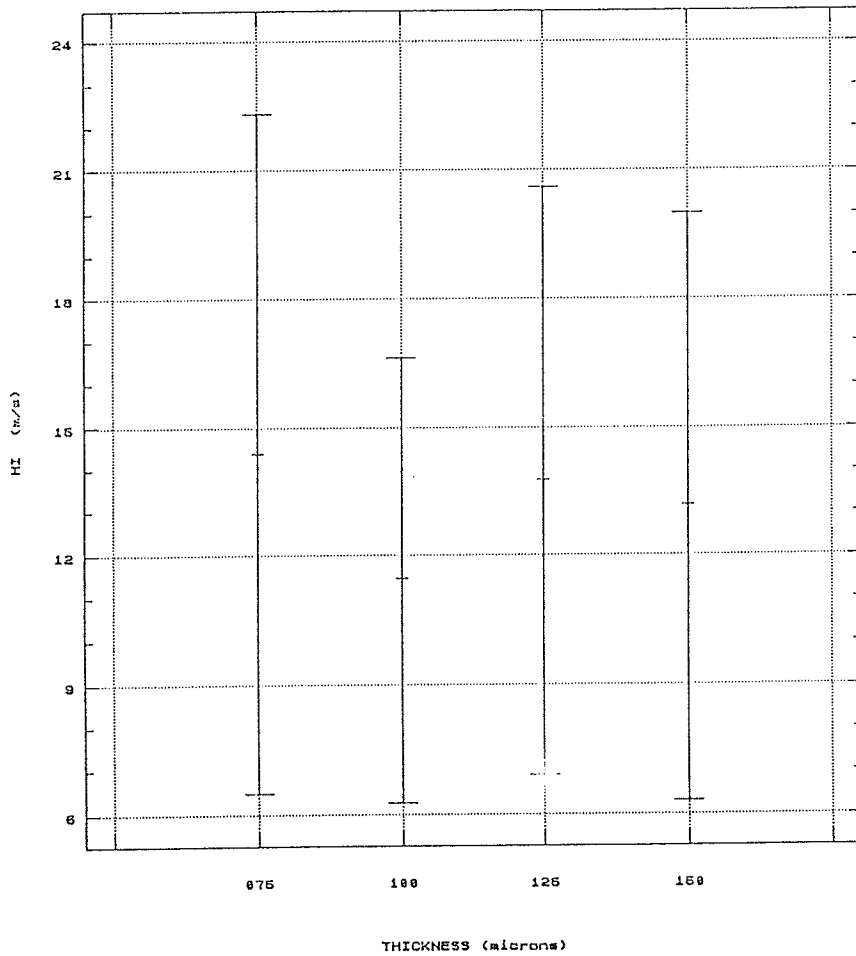


Figure 16. Statgraphics ANOVA: heterogeneity index of normal tissue vs. thickness excluding 50 μm values.

Table 21. ANOVA results for the effect of thickness on ultrasonic speed of ischemic tissue excluding 50 μm values.

One-Way Analysis of Variance

Data: DGHRT05C.SPDISCH2
 Level codes: DGHRT05C.THICKNES4
 Labels: 4 3 RESHAPE '075100125150'
 Range test: Conf. Int. Confidence level: 95

Analysis of variance

Source of variation	Sum of Squares	d.f.	Mean square	F-ratio	Sig. level
Between groups	2661.0511	3	887.01704	2.784	.0660
Within groups	6690.3889	21	318.58995		
Total (corrected)	9351.4400	24			

0 missing value(s) have been excluded.

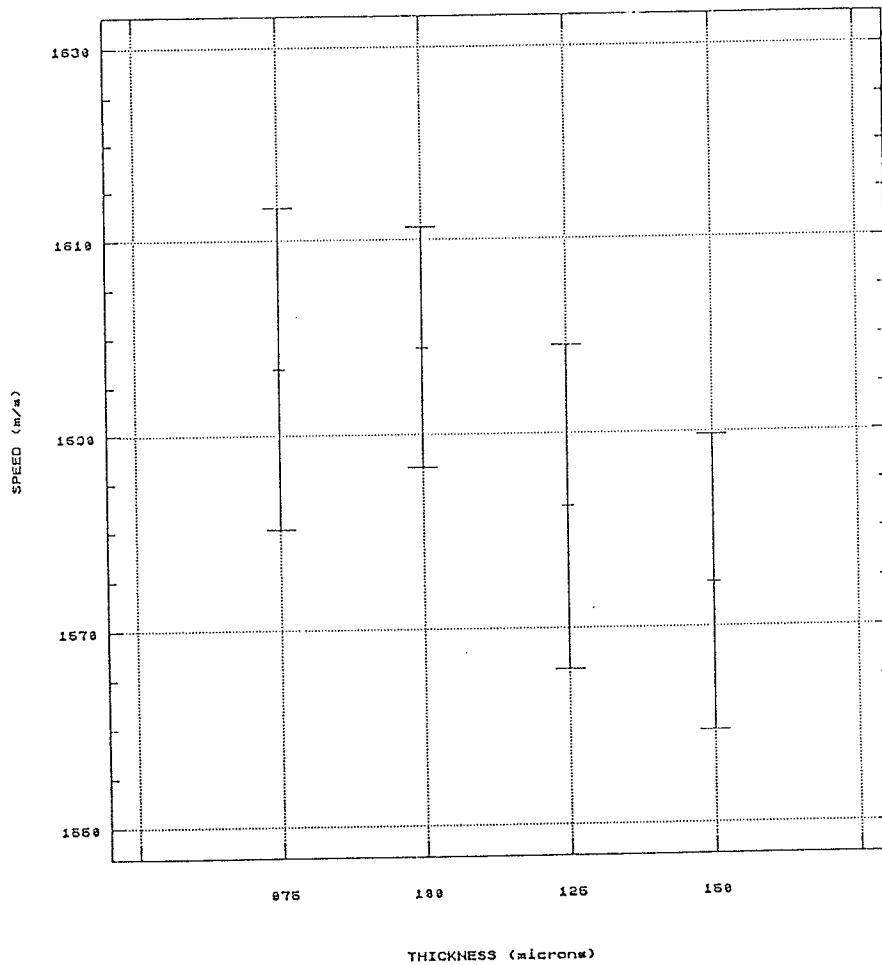


Figure 17. Statgraphics ANOVA: ultrasonic speed of ischemic tissue vs. thickness excluding 50 μm values.

Table 22. ANOVA results for the effect of thickness on heterogeneity index of ischemic tissue excluding 50 μm values.

One-Way Analysis of Variance

Data: DGHRT05C.HIISCH2
 Level codes: DGHRT05C.THICKNES4
 Labels: 4 3 RESHAPE '075100125150'
 Range test: Conf. Int. Confidence level: 95

Analysis of variance

Source of variation	Sum of Squares	d.f.	Mean square	F-ratio	Sig. level
Between groups	185.34207	3	61.780689	1.466	.2523
Within groups	884.69233	21	42.128206		
Total (corrected)	1070.0344	24			

0 missing value(s) have been excluded.

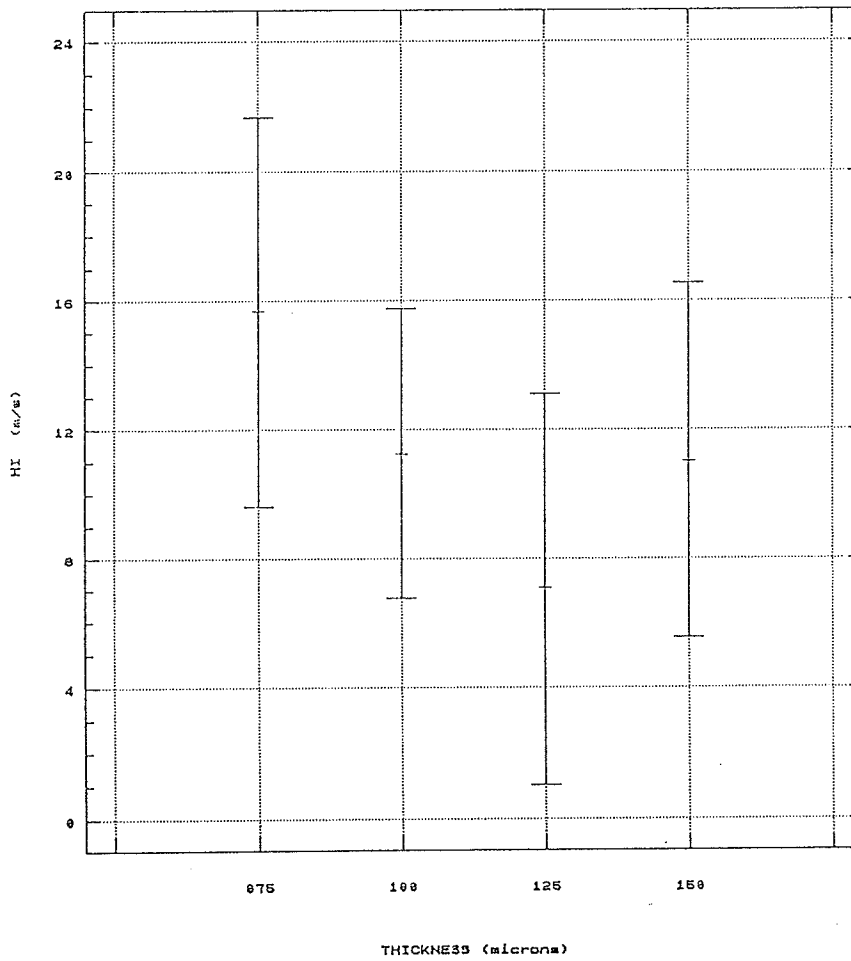


Figure 18. Statgraphics ANOVA: heterogeneity index of ischemic tissue vs. thickness excluding 50 μm values.

Table 23. ANOVA results for the effect of tissue type on attenuation coefficient.

One-Way Analysis of Variance

Data: DGHRT05A.ATTEN
 Level codes: DGHRT05A.TISSUE
 Labels: 2 8 RESHAPE 'NORMAL, ISCHEMIC'
 Range test: Conf. Int. Confidence level: 95

Analysis of variance

Source of variation	Sum of Squares	d.f.	Mean square	F-ratio	Sig. level
Between groups	3536.2540	1	3536.2540	22.056	.0003
Within groups	2244.5860	14	160.3276		
Total (corrected)	5780.8400	15			

1 missing value(s) have been excluded.

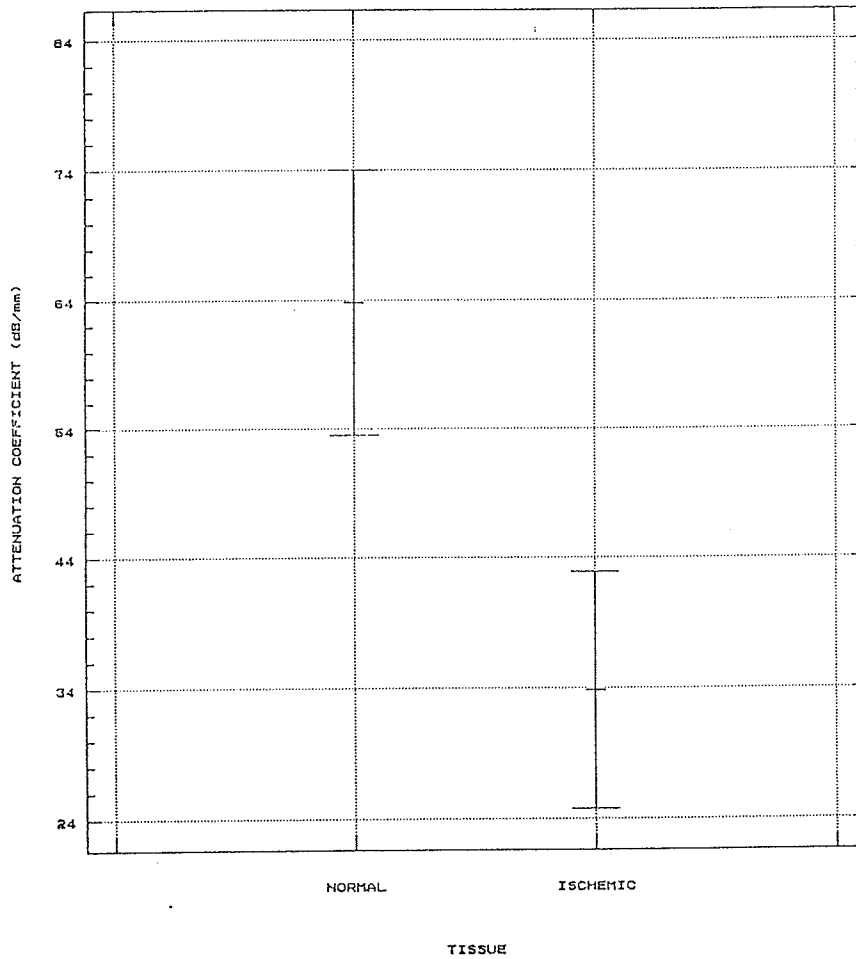


Figure 19. Statgraphics ANOVA: attenuation coefficient vs. tissue type.

Table 24. ANOVA results for the effect of tissue type on ultrasonic speed excluding 50 μm values.

One-Way Analysis of Variance

Data: DGHRT05B.SPEED2
 Level codes: DGHRT05B.TISSUE2
 Labels: 2 8 RESHAPE 'NORMAL ISCHEMIC'
 Range test: Conf. Int. Confidence level: 95

Analysis of variance

Source of variation	Sum of Squares	d.f.	Mean square	F-ratio	Sig. level
Between groups	1787.399	1	1787.3985	3.369	.0737
Within groups	21749.718	41	530.4809		
Total (corrected)	23537.116	42			

1 missing value(s) have been excluded.

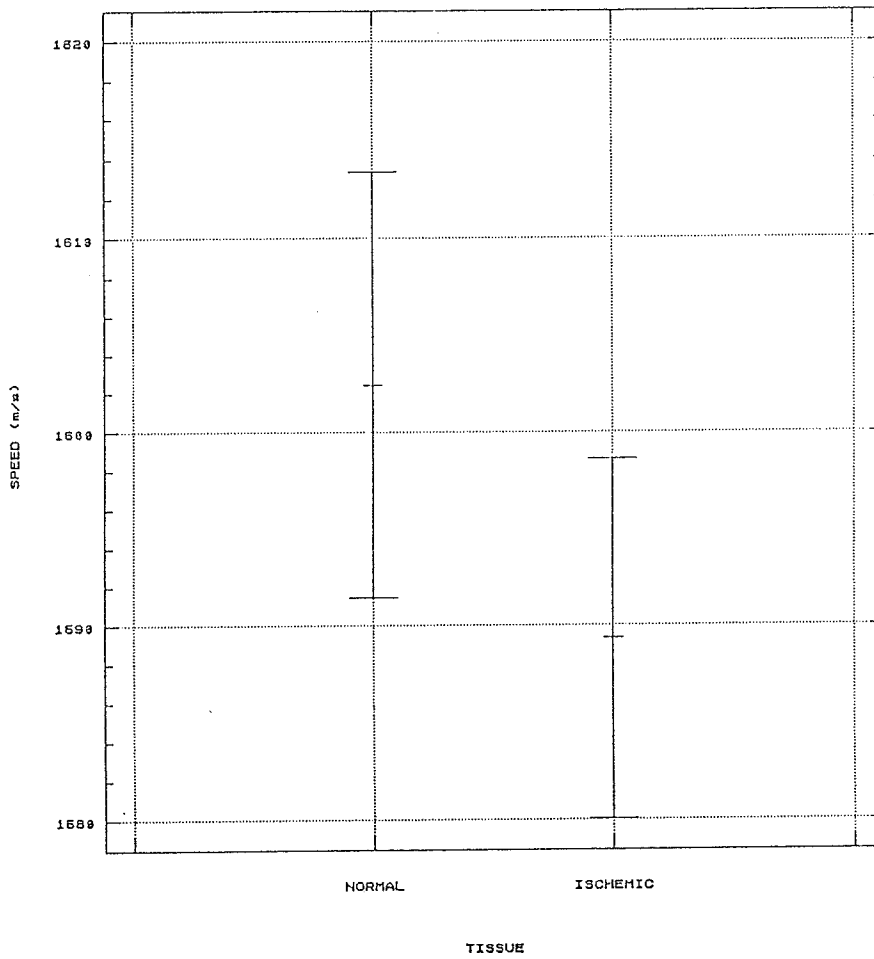


Figure 20. Statgraphics ANOVA: ultrasonic speed vs. tissue type excluding 50 μm values.

Table 25. ANOVA results for the effect of tissue type on heterogeneity index excluding 50 μm values.

One-Way Analysis of Variance

Data: DGHRT05B.HI2
 Level codes: DGHRT05B.TISSUE2
 Labels: 2 8 RESHAPE 'NORMAL ISCHEMIC'
 Range test: Conf. Int. Confidence level: 95

Analysis of variance

Source of variation	Sum of Squares	d.f.	Mean square	F-ratio	Sig. level
Between groups	26.6495	1	26.649489	.656	.4314
Within groups	1666.6705	41	40.650500		
Total (corrected)	1693.3200	42			

1 missing value(s) have been excluded.

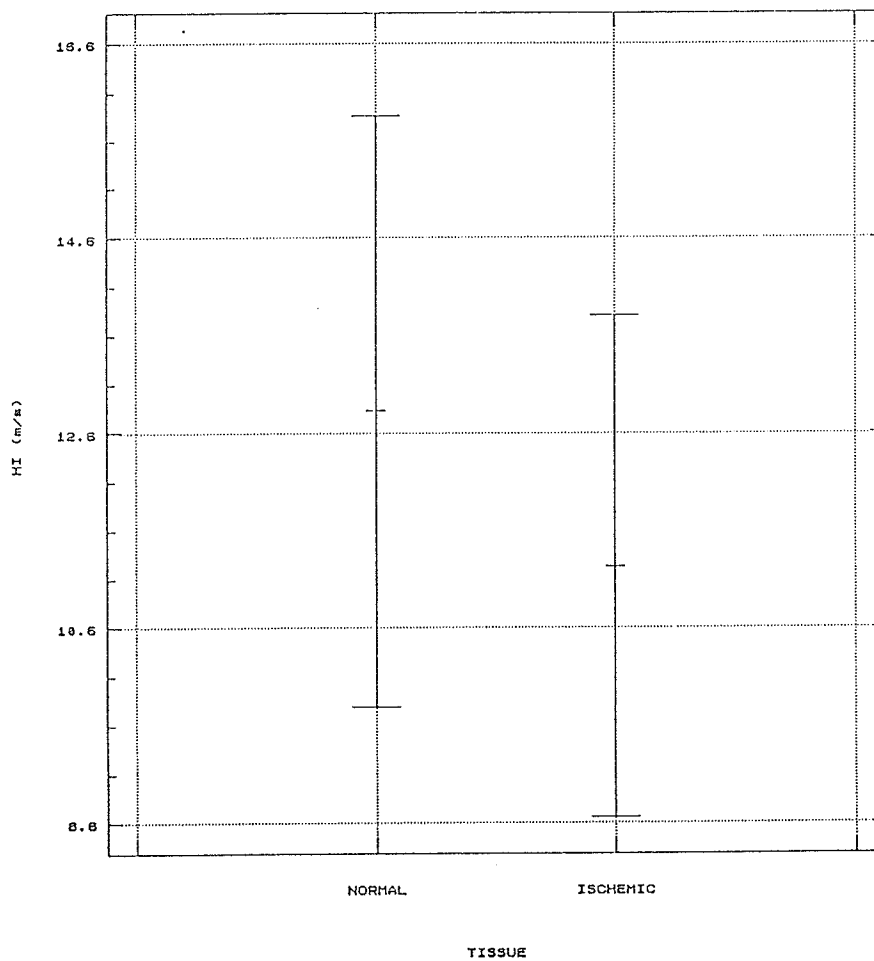


Figure 21. Statgraphics ANOVA: heterogeneity index vs. tissue type excluding 50 μm values.

APPENDIX V: STATGRAPHICS ANALYSIS OF BOVINE ARTICULAR CARTILAGE

Files, tables and graphs generated by Statgraphics while performing the ANOVAs. First, the files of factors and categories needed in the analysis are listed. Next is the table containing the F-ratio and significance level followed by the corresponding graph. The abbreviations used are

TREATMNT	= Treatment 1 = NORMAL (NORML); 2 = CS-DEPLETED (CSDPL); 3 = COLLAGEN ONLY (COLGN); 4 = CROSS-LINKS CLEAVED (XLCLV)
SECTION	= Section 1 = Perpendicular; 2 = Parallel
FIBORIENT	= Fiber orientation 1 = Tangential (TAN); 2 = Transitional (TRA); 3 = Radial (RAD)
ATTENPER	= Attenuation coefficient (dB/mm) Perpendicular section
ATTENPAR	= Attenuation coefficient (dB/mm) Parallel section
SPDTAN	= Speed (m/s) Perpendicular section, Tangential zone
SPDTRA	= Speed (m/s) Perpendicular section, Transitional zone
SPDRAD	= Speed (m/s) Perpendicular section, Radial zone
SPDPAR	= Speed (m/s) Parallel section, Tangential zone
ATTENNOR	= Attenuation coefficient (dB/mm) NORMAL
ATTENCS	= Attenuation coefficient (dB/mm) CS-DEPLETED
ATTENCOLL	= Attenuation coefficient (dB/mm) COLLAGEN ONLY
ATTENXLINK	= Attenuation coefficient (dB/mm) CROSS-LINKS CLEAVED
SPDPER	= Speed (m/s) Perpendicular section
SPDNOR	= Speed (m/s) NORMAL
SPDCS	= Speed (m/s) CS-DEPLETED
SPDCOLL	= Speed (m/s) COLLAGEN ONLY
SPDXLINK	= Speed (m/s) CROSS-LINKS CLEAVED

Table 26. Statgraphics files of factors and categories of bovine articular cartilage.

File ARCART01 7/13/88

row	TREATMNT	ATTENPER	ATTENPAR	SPDTAN	SPDTRA	SPDRAD	SPDPAR
1	1	88	92	1671	1647	1715	1660
2	1	105	147	1635	1617	1720	1690
3	2	108	40	1670	1631	1738	1775
4	2	112	63	1640	1641	1777	1793
5	3	75	77	1648	1620	1704	1744
6	3	85	90		1653	1760	1705
7	4	143	166	1650	1610	1658	
8	4	185	165	1680	1725	1716	1695

Table 26, continued

File ARCART02 7/13/88

row	SECTION	ATTENNOR	ATTENCS	ATTENCOLL	ATTENXLINK	FIBRORIEN1	SPDPER	SPDNOR
1	1	88	108	75	143	1	1671	1671
2	1	105	112	85	185	1	1635	1635
3	2	92	40	77	166	1	1670	1647
4	2	147	63	90	165	1	1640	1617
5						1	1648	1715
6						1		1720
7						1	1650	1660
8						1	1680	1690
9						2	1647	
10						2	1617	
11						2	1631	
12						2	1641	
13						2	1620	
14						2	1653	
15						2	1610	
16						2	1725	
17						3	1715	
18						3	1720	
19						3	1738	
20						3	1777	
21						3	1704	
22						3	1760	
23						3	1658	
24						3	1716	

File ARCART03 7/13/88

row	TREATMNT	SPDPER
1	1	1671
2	1	1635
3	1	1647
4	1	1617
5	1	1715
6	1	1720
7	2	1670
8	2	1640
9	2	1631
10	2	1641
11	2	1738
12	2	1777
13	3	1648
14	3	
15	3	1620
16	3	1653
17	3	1704
18	3	1760
19	4	1650
20	4	1680
21	4	1610
22	4	1725
23	4	1658
24	4	1716

File ARCART02 7/13/88

row	SPDCS	SPDCOLL	SPDXLINK	FIBRORIEN2
1	1670	1648	1650	1
2	1640		1680	1
3	1631	1620	1610	2
4	1641	1653	1725	2
5	1738	1704	1658	3
6	1777	1760	1716	3
7	1775	1744		4
8	1793	1705	1695	4
9				
10				
11				
12				

Table 27. ANOVA results for the effect of treatment on attenuation coefficient perpendicular section.

One-Way Analysis of Variance

Data: ARCART01.ATTENPER

Level codes: ARCART01.TREATMNT

Labels: 4 5 RESHAPE 'NORMLCSDPLCOLGNXLCLV'

Range test: Conf. Int. Confidence level: 95

Analysis of variance

Source of variation	Sum of Squares	d.f.	Mean square	F-ratio	Sig. level
Between groups	7941.3750	3	2647.1250	9.763	.0260
Within groups	1084.5000	4	271.1250		
Total (corrected)	9025.8750	7			

0 missing value(s) have been excluded.

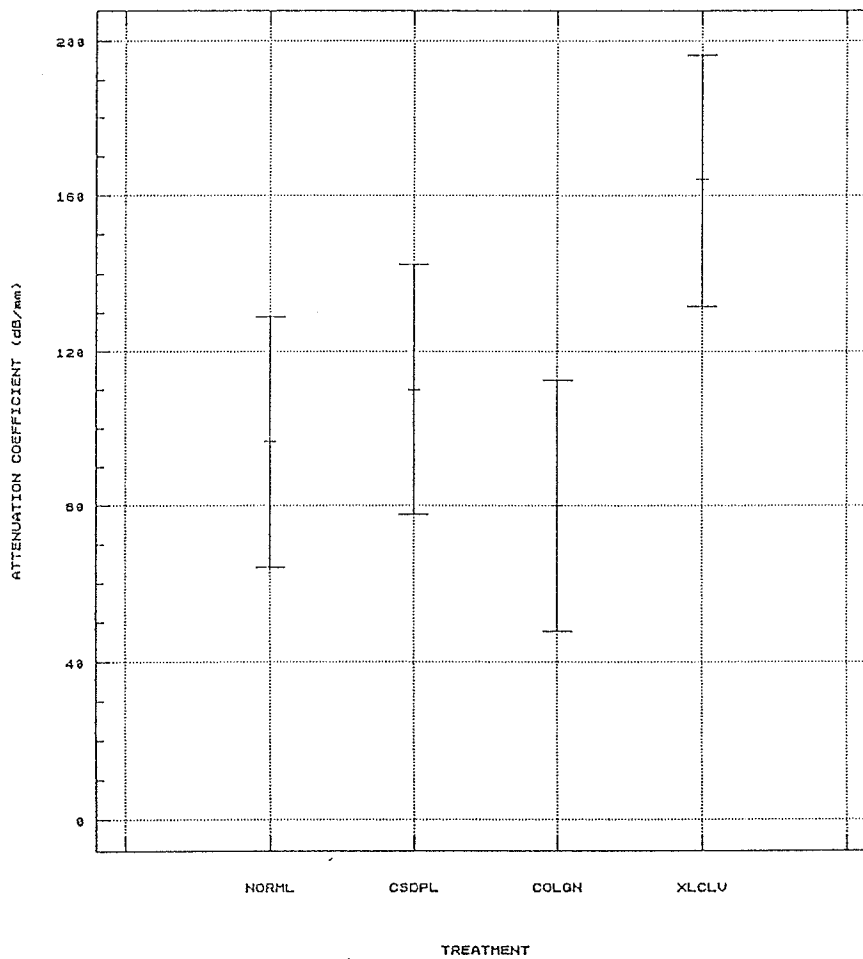


Figure 22. Statgraphics ANOVA: attenuation coefficient perpendicular section vs. treatment.

Table 28. ANOVA results for the effect of treatment on attenuation coefficient parallel section.

One-Way Analysis of Variance

Data: ARCART01.ATTENPAR
 Level codes: ARCART01.TREATMNT
 Labels: 4 5 RESHAPE 'NORMLCSDPLCOLGNXLCLV'
 Range test: Conf. Int. Confidence level: 95

Analysis of variance

Source of variation	Sum of Squares	d.f.	Mean square	F-ratio	Sig. level
Between groups	14390.000	3	4796.6667	10.304	.0237
Within groups	1862.000	4	465.5000		
Total (corrected)	16252.000	7			

0 missing value(s) have been excluded.

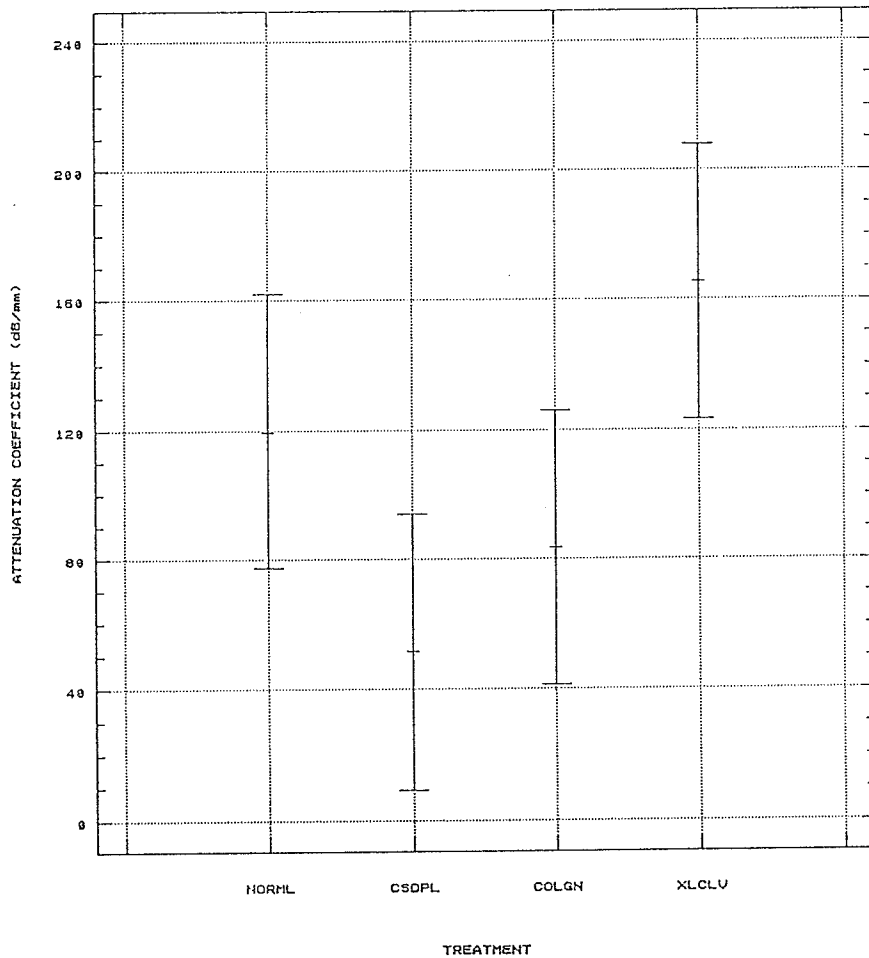


Figure 23. Statgraphics ANOVA: attenuation coefficient parallel section vs. treatment.

Table 29. ANOVA results for the effect of section on attenuation coefficient NORMAL.

One-Way Analysis of Variance

Data: ARCART02.ATTENOR

Level codes: ARCART02.SECTION

Labels: 2 13 RESHAPE 'PERPENDICULARPARALLEL'

Range test: Conf. Int. Confidence level: 95

Analysis of variance

Source of variation	Sum of Squares	d.f.	Mean square	F-ratio	Sig. level
Between groups	529.0000	1	529.00000	.639	.5156
Within groups	1657.0000	2	828.50000		
Total (corrected)	2186.0000	3			

0 missing value(s) have been excluded.

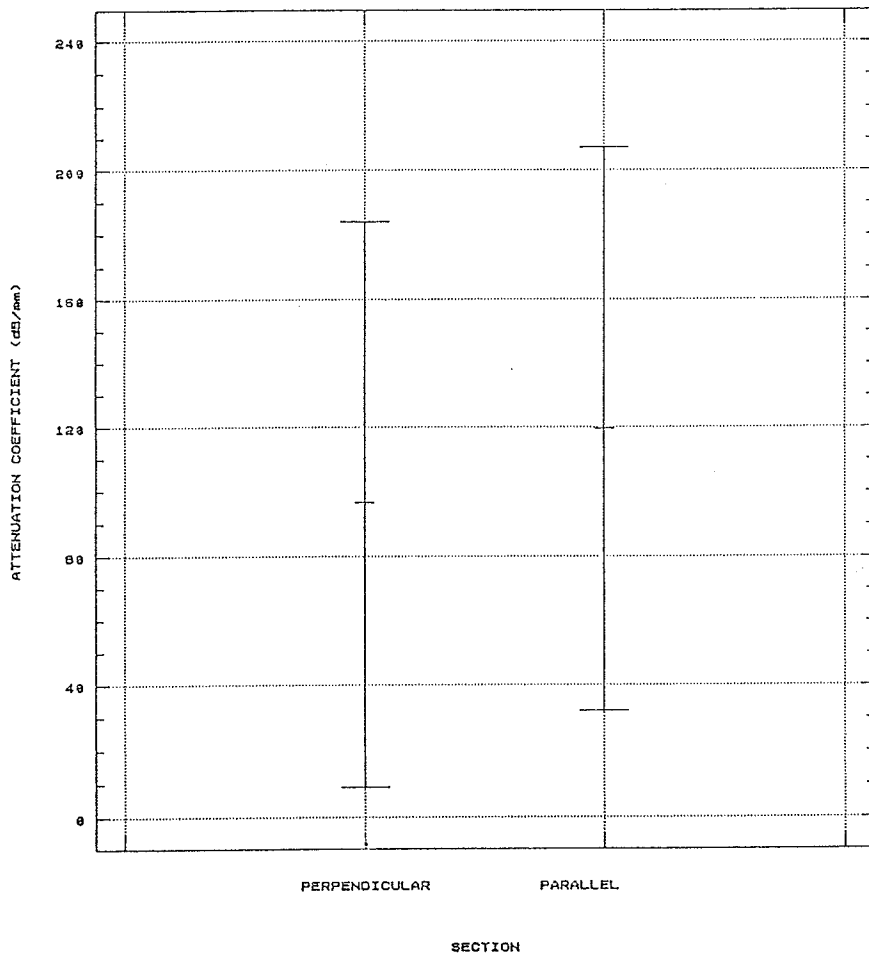


Figure 24. Statgraphics ANOVA: attenuation coefficient NORMAL vs. section.

Table 30. ANOVA results for the effect of section on attenuation coefficient CS-DEPLETED.

One-Way Analysis of Variance

Data: ARCART02.ATTENCS
 Level codes: ARCART02.SECTION
 Labels: 2 13 RES: DE 'PERPENDICULARPARALLEL'
 Range test: Conf. Int. Confidence level: 95

Analysis of variance

Source of variation	Sum of Squares	d.f.	Mean square	F-ratio	Sig. level
Between groups	3422.2500	1	3422.2500	25.117	.0376
Within groups	272.5000	2	136.2500		
Total (corrected)	3694.7500	3			

0 missing value(s) have been excluded.

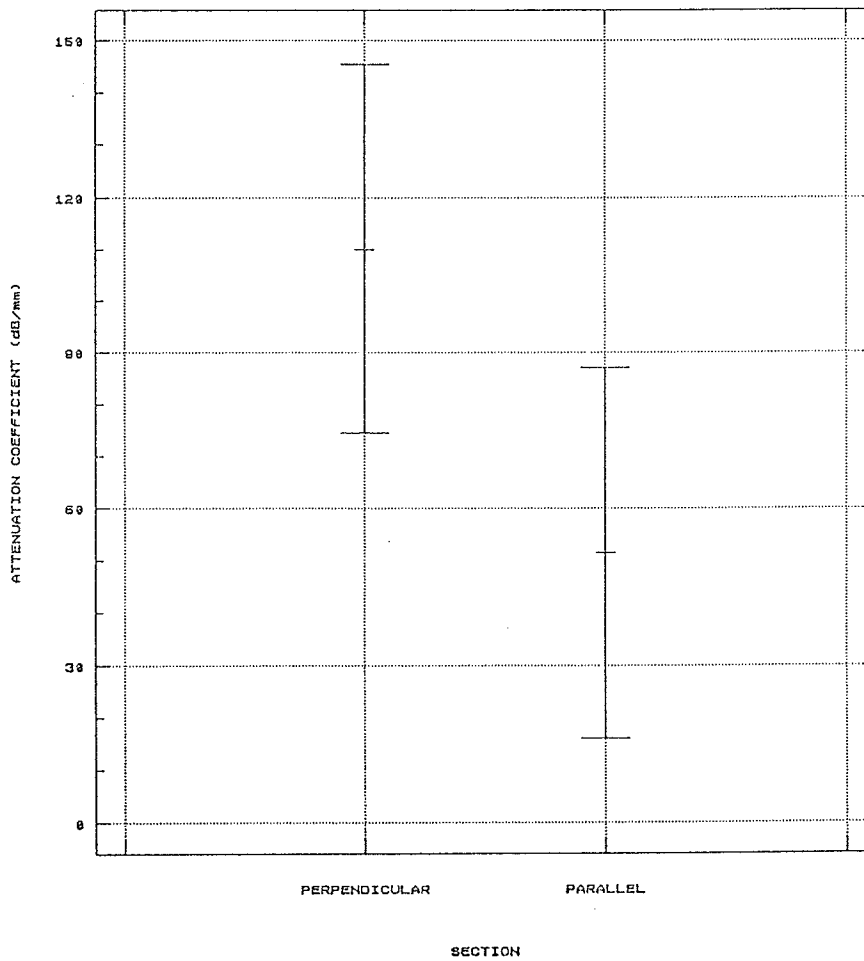


Figure 25. Statgraphics ANOVA: attenuation coefficient CS-DEPLETED vs. section.

Table 31. ANOVA results for the effect of section on attenuation coefficient COLLAGEN ONLY.

One-Way Analysis of Variance

Data: ARCART02.ATTENCOLL
 Level codes: ARCART02.SECTION
 Labels: 2 13 RESHAPE 'PERPENDICULARPARALLEL'
 Range test: Conf. Int. Confidence level: 95

Analysis of variance

Source of variation	Sum of Squares	d.f.	Mean square	F-ratio	Sig. level
Between groups	12.25000	1	12.250000	.182	.7151
Within groups	134.50000	2	67.250000		
Total (corrected)	146.75000	3			

0 missing value(s) have been excluded.

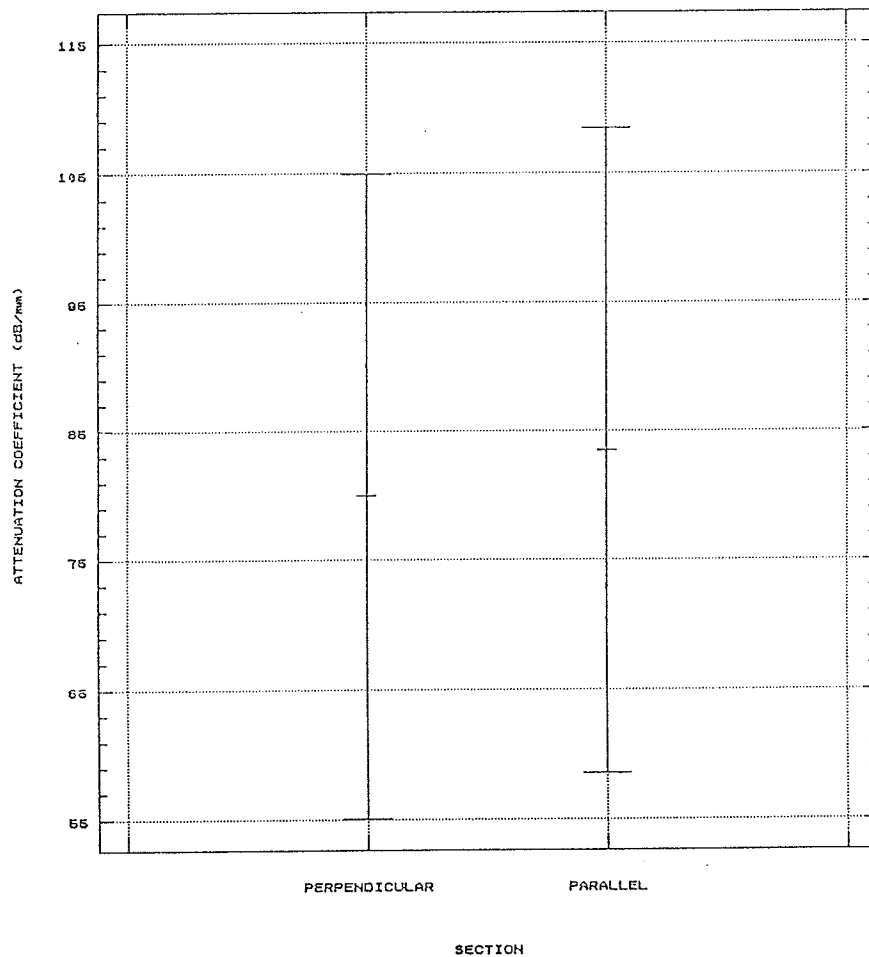


Figure 26. Statgraphics ANOVA: attenuation coefficient COLLAGEN ONLY vs. section.

Table 32. ANOVA results for the effect of section on attenuation coefficient CROSS-LINKS CLEAVED.

One-Way Analysis of Variance

Data: ARCART02.ATTENXLINK
 Level codes: ARCART02.SECTION
 Labels: 2 13 RESHAPE 'PERPENDICULARPARALLEL'
 Range test: Conf. Int. Confidence level: 95

Analysis of variance

Source of variation	Sum of Squares	d.f.	Mean square	F-ratio	Sig. level
Between groups	2.25000	1	2.25000	.005	.9502
Within groups	882.50000	2	441.25000		
Total (corrected)	884.75000	3			

0 missing value(s) have been excluded.

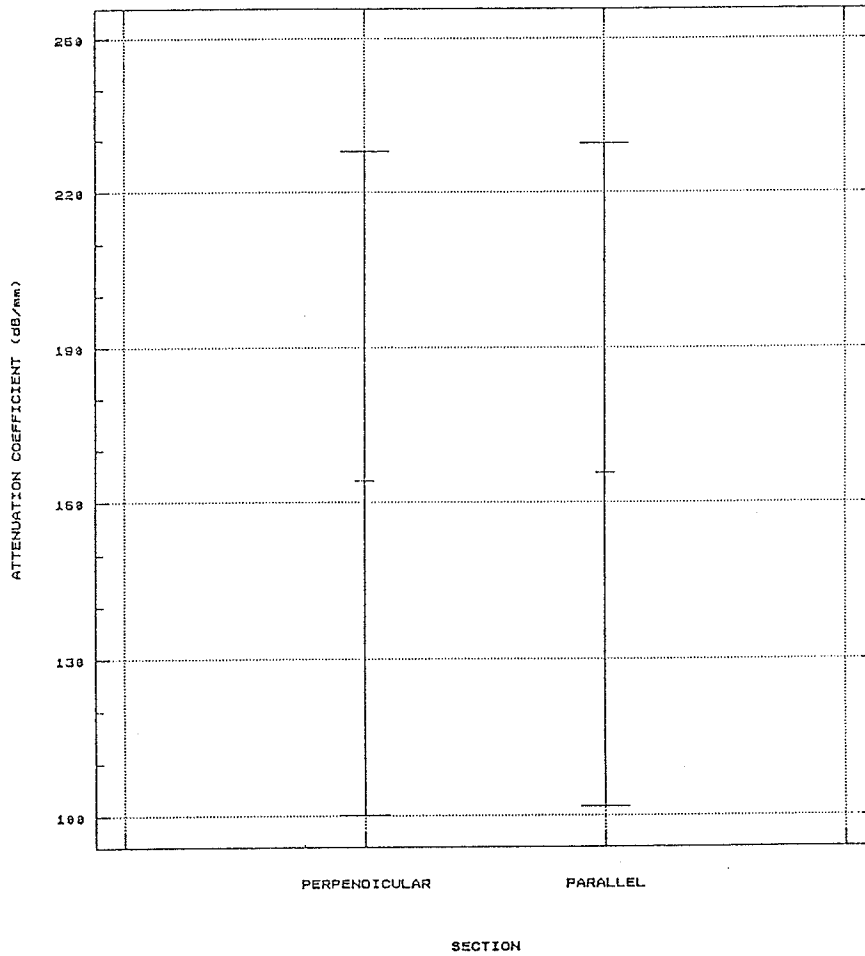


Figure 27. Statgraphics ANOVA: attenuation coefficient CROSS-LINKS CLEAVED vs. section.

Table 33. ANOVA results for the effect of treatment on ultrasonic speed perpendicular section, tangential zone.

One-Way Analysis of Variance

Data: ARCART01.SPDTAN
Level codes: ARCART01.TREATMNT
Labels: 4 5 RESHAPE 'NORMLCSDPLCOLGNXLCLU'
Range test: Conf. Int. Confidence level: 95

Analysis of variance

Source of variation	Sum of Squares	d.f.	Mean square	F-ratio	Sig. level
Between groups	245.4286	3	81.80952	.159	.9177
Within groups	1548.0000	3	516.00000		
Total (corrected)	1793.4286	6			

1 missing value(s) have been excluded.

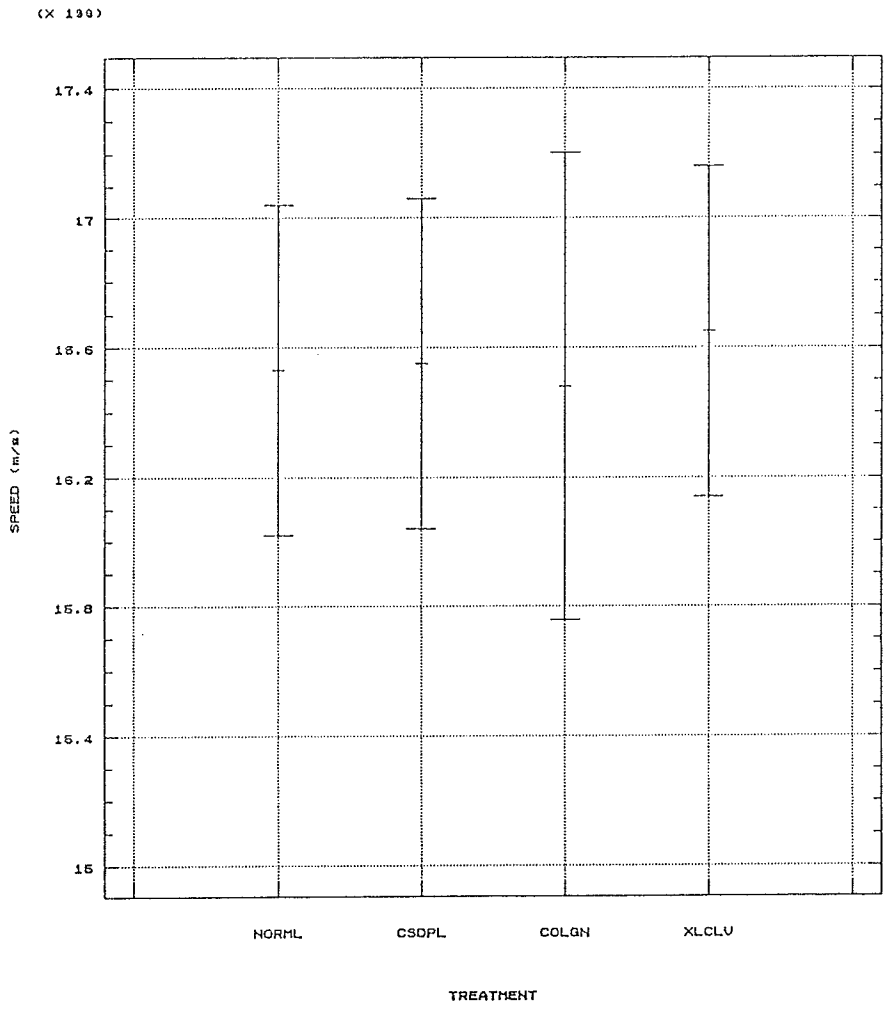


Figure 28. Statgraphics ANOVA: ultrasonic speed perpendicular section, tangential zone vs. treatment.

Table 34. ANOVA results for the effect of treatment on ultrasonic speed perpendicular section, transitional zone.

One-Way Analysis of Variance

Data: ARCART01.SPDTRA
 Level codes: ARCART01.TREATMNT
 Labels: 4 5 RESHAPE 'NORMLCSDPLCOLGNXLCLV'
 Range test: Conf. Int. Confidence level: 95

Analysis of variance

Source of variation	Sum of Squares	d.f.	Mean square	F-ratio	Sig. level
Between groups	1625.0000	3	541.6667	.283	.8361
Within groups	7657.0000	4	1914.2500		
Total (corrected)	9282.0000	7			

0 missing value(s) have been excluded.

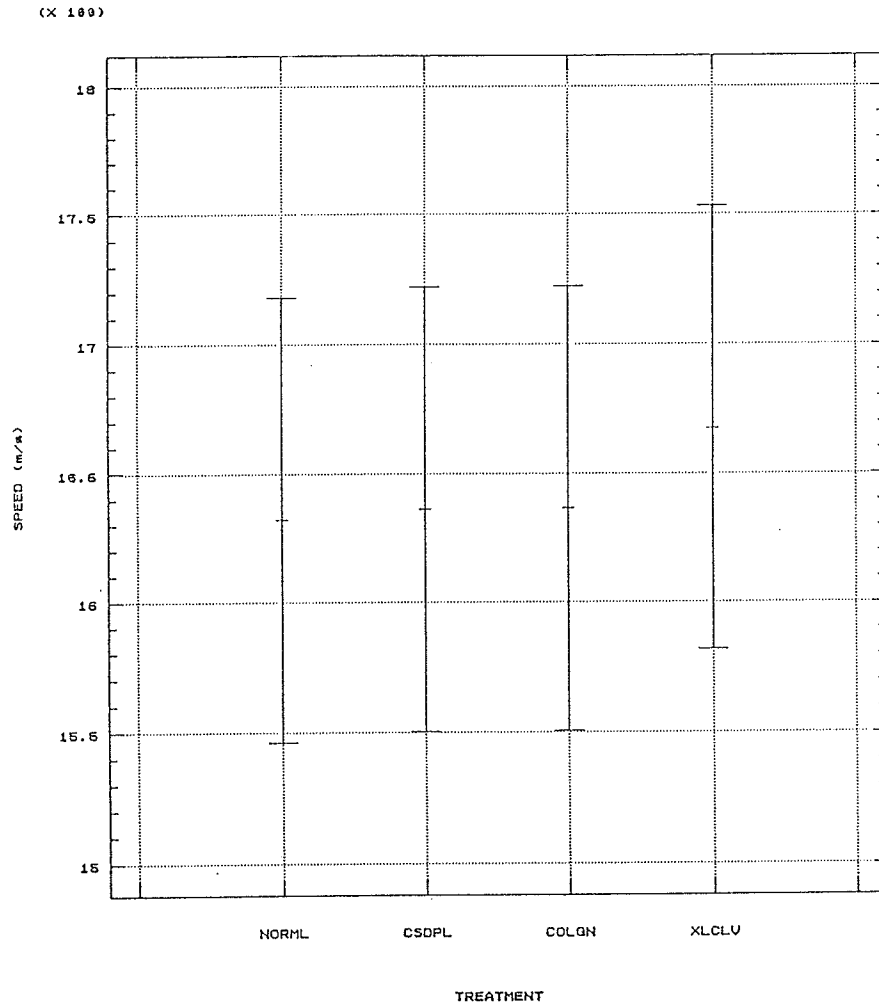


Figure 29. Statgraphics ANOVA: ultrasonic speed perpendicular section, transitional zone vs. treatment.

Table 35. ANOVA results for the effect of treatment on ultrasonic speed perpendicular section, radial zone.

One-Way Analysis of Variance

Data: ARCART01.SPDRAD
 Level codes: ARCART01.TREATMNT
 Labels: 4 5 RESHAPE 'NORMLCSOPLCOLGNXLCLV'
 Range test: Conf. Int. Confidence level: 95

Analysis of variance

Source of variation	Sum of Squares	d.f.	Mean square	F-ratio	Sig. level
Between groups	5193.0000	3	1731.0000	1.721	.3001
Within groups	4023.0000	4	1005.7500		
Total (corrected)	9216.0000	7			

0 missing value(s) have been excluded.

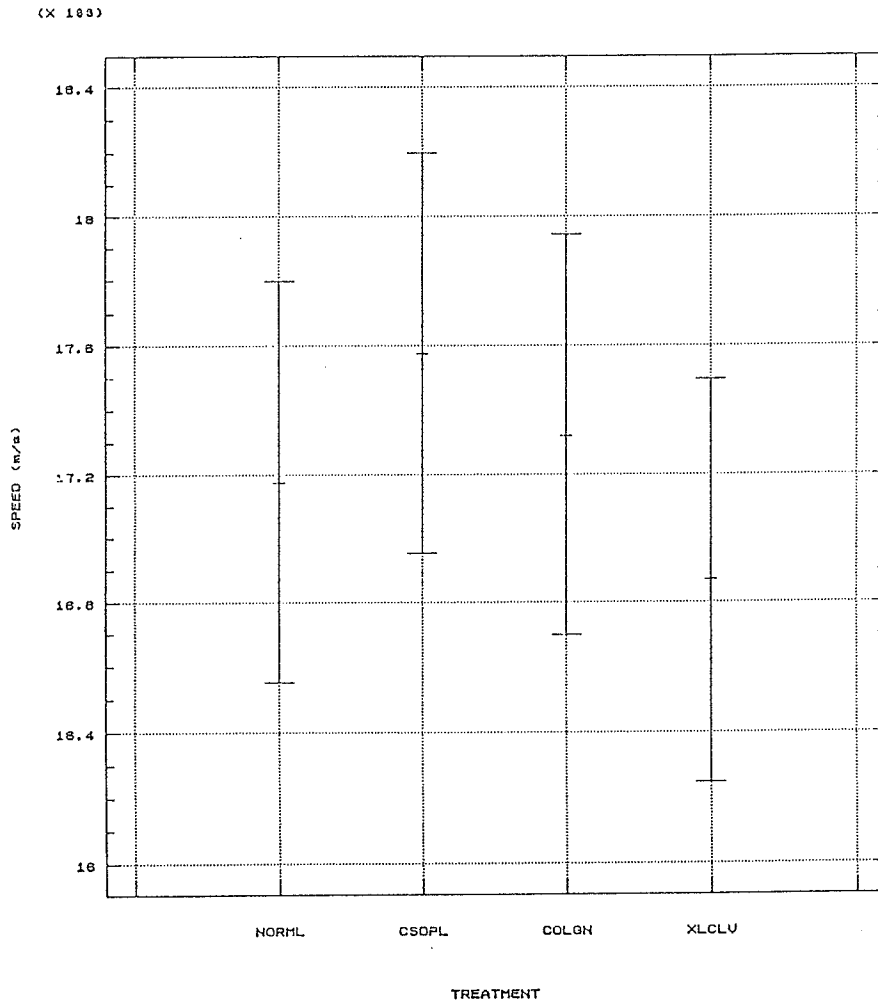


Figure 30. Statgraphics ANOVA: ultrasonic speed perpendicular section, radial zone vs. treatment.

Table 36. ANOVA results for the effect of treatment on ultrasonic speed perpendicular section.

One-Way Analysis of Variance

Data: ARCART03.SPDPER

Level codes: ARCART03.TREATMNT

Labels: 4 5 RESHAPE 'NORMLCSDPLCOLGNXLCLV'

Range test: Conf. Int. Confidence level: 95

Analysis of variance

Source of variation	Sum of Squares	d.f.	Mean square	F-ratio	Sig. level
Between groups	745.790	3	248.5966	.096	.9611
Within groups	49007.167	19	2579.3246		
Total (corrected)	49752.957	22			

1 missing value(s) have been excluded.

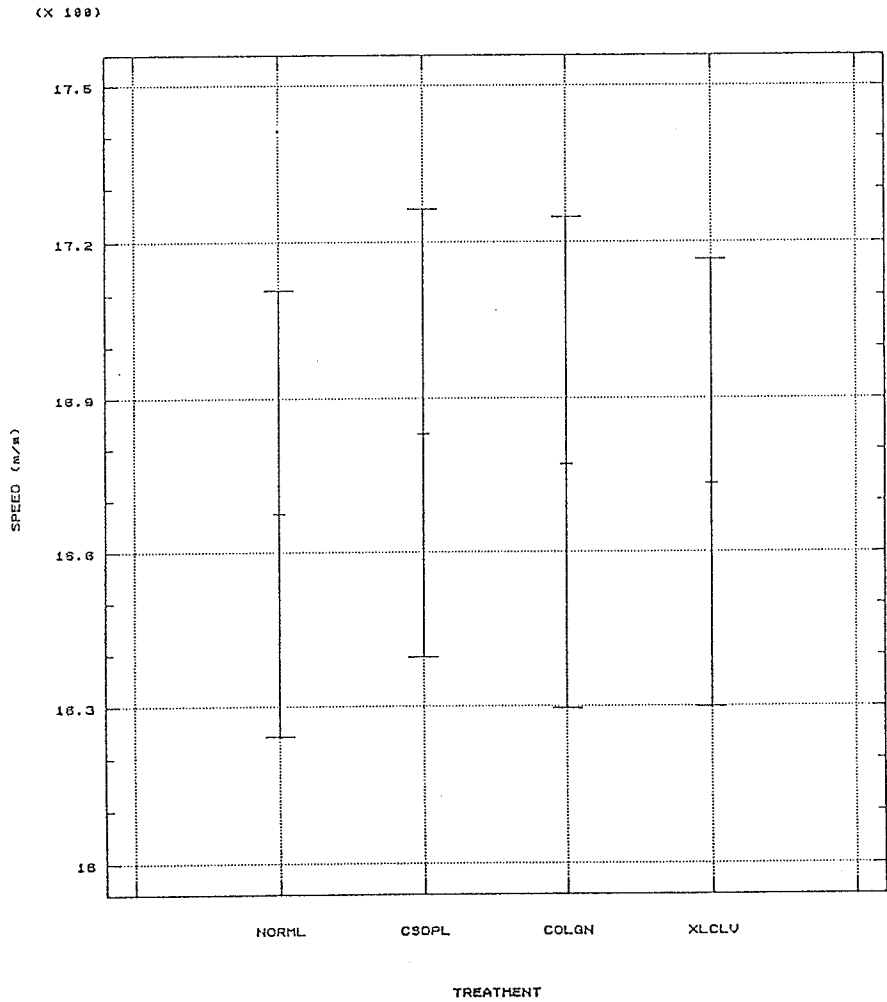


Figure 31. Statgraphics ANOVA: ultrasonic speed perpendicular section vs. treatment.

Table 37. ANOVA results for the effect of treatment on ultrasonic speed parallel section.

One-Way Analysis of Variance

Data: ARCART01.SPDPAR
Level codes: ARCART01.TREATMNT
Labels: 4 5 RESHAPE 'NORMLCSDPLCOLGNXLCLV'
Range test: Conf. Int. Confidence level: 95

Analysis of variance

Source of variation	Sum of Squares	d.f.	Mean square	F-ratio	Sig. level
Between groups	12838.357	3	4279.4524	9.354	.0495
Within groups	1372.500	3	457.5000		
Total (corrected)	14210.857	6			

1 missing value(s) have been excluded.

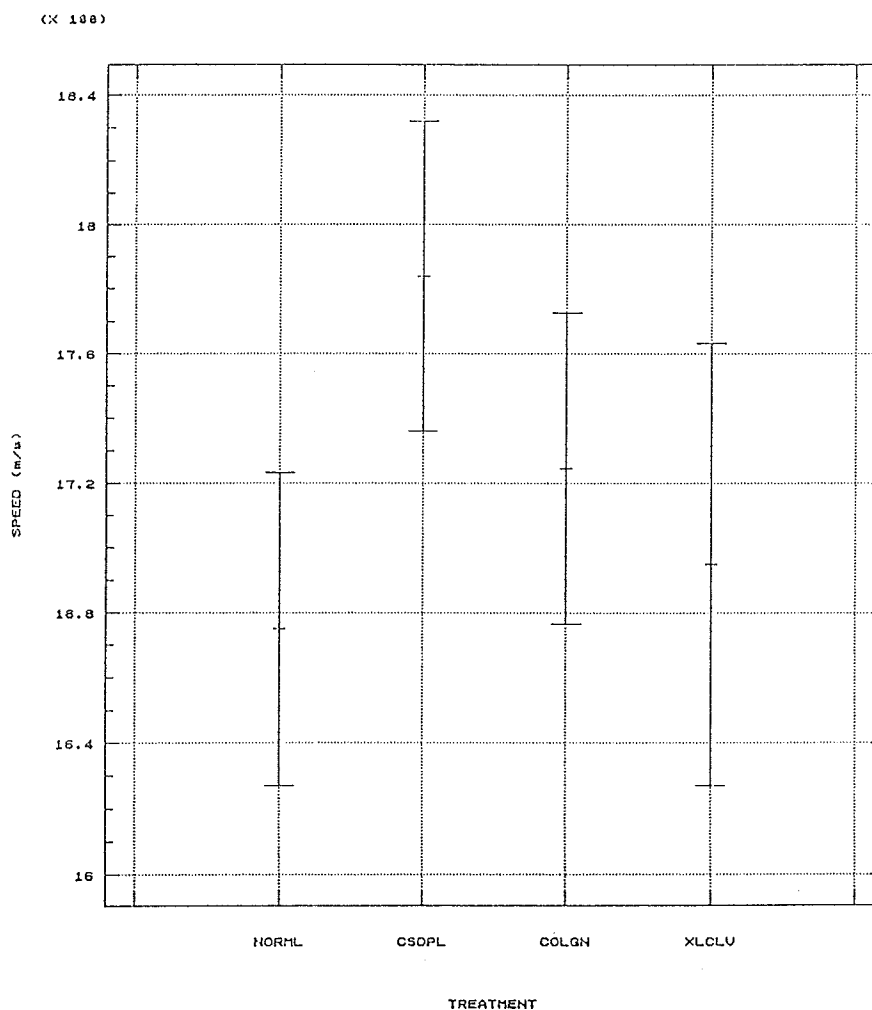


Figure 32. Statgraphics ANOVA: ultrasonic speed parallel section vs. treatment.

Table 38. ANOVA results for the effect of fiber orientation on ultrasonic speed perpendicular section.

One-Way Analysis of Variance

Data: ARCART02.SPDPER
 Level codes: ARCART02.FIBRORIEN1
 Labels: 3 3 RESHAPE 'TANTRARAD'
 Range test: Conf. Int. Confidence level: 95

Analysis of variance

Source of variation	Sum of Squares	d.f.	Mean square	F-ratio	Sig. level
Between groups	29461.528	2	14730.764	14.519	.0001
Within groups	20291.429	20	1014.571		
Total (corrected)	49752.957	22			

1 missing value(s) have been excluded.

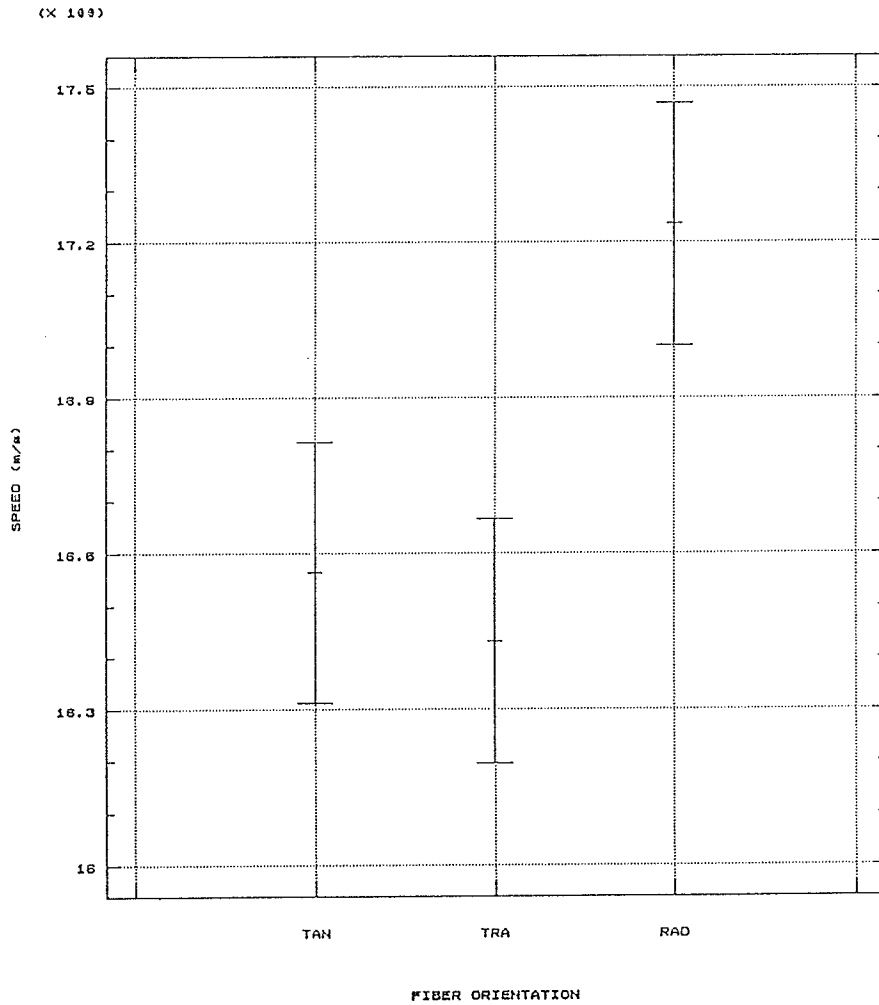


Figure 33. Statgraphics ANOVA: ultrasonic speed perpendicular section vs. fiber orientation.

Table 39. ANOVA results for the effect of fiber orientation on ultrasonic speed NORMAL.

One-Way Analysis of Variance

Data: ARCART02.SPDNOR
 Level codes: ARCART02.FIBRORIEN2
 Labels: 4 3 RESHAPE 'TANTRARADTAN'
 Range test: Conf. Int. Confidence level: 95

Analysis of variance

Source of variation	Sum of Squares	d.f.	Mean square	F-ratio	Sig. level
Between groups	8025.3750	3	2675.1250	6.857	.0469
Within groups	1560.5000	4	390.1250		
Total (corrected)	9585.8750	7			

0 missing value(s) have been excluded.

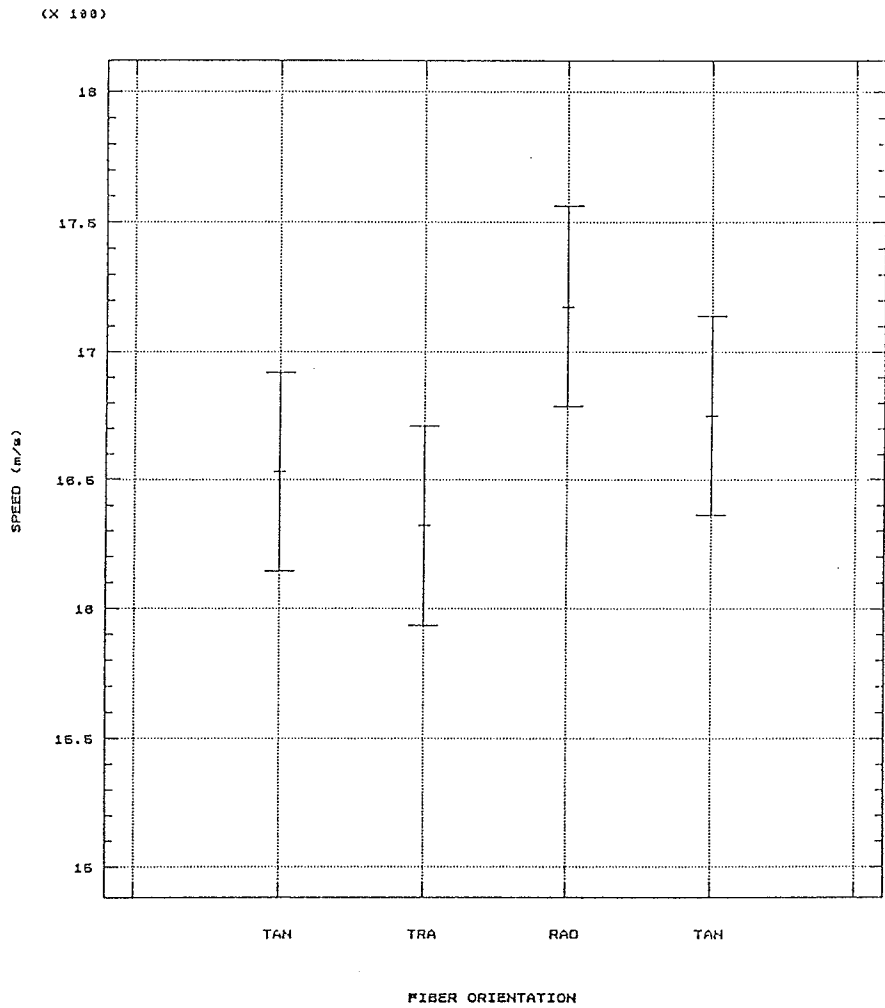


Figure 34. Statgraphics ANOVA: ultrasonic speed NORMAL vs. fiber orientation.

Table 40. ANOVA results for the effect of fiber orientation on ultrasonic speed CS-DEPLETED.

One-Way Analysis of Variance

Data: ARCART02.SPDCS
 Level codes: ARCART02.FIBRORIEN2
 Labels: 4 3 RESHAPE 'TANTRARADTAN'
 Range test: Conf. Int. Confidence level: 95

Analysis of variance

Source of variation	Sum of Squares	d.f.	Mean square	F-ratio	Sig. level
Between groups	32438.375	3	10812.792	30.405	.0033
Within groups	1422.500	4	355.625		
Total (corrected)	33860.875	7			

0 missing value(s) have been excluded.

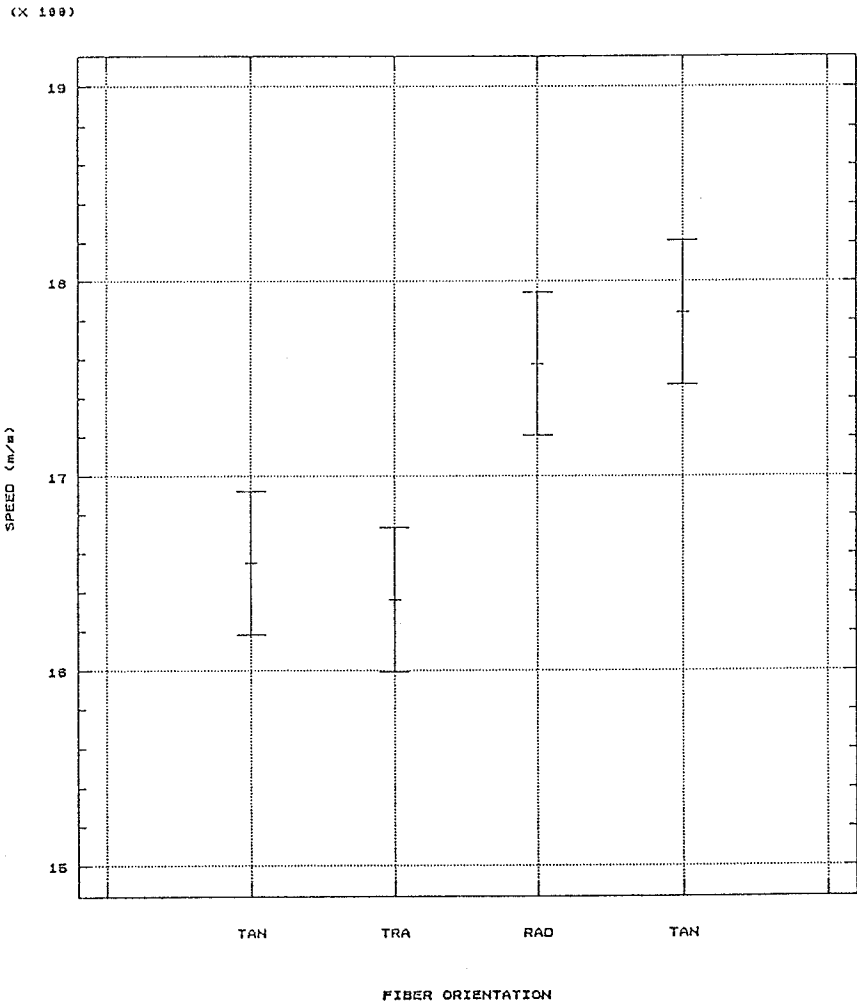


Figure 35. Statgraphics ANOVA: ultrasonic speed CS-DEPLETED vs. fiber orientation.

Table 41. ANOVA results for the effect of fiber orientation on ultrasonic speed COLLAGEN ONLY.

One-Way Analysis of Variance

Data: ARCART02.SPDCOLL
 Level codes: ARCART02.FIBRORIEN2
 Labels: 4 3 RESHAPE 'TANTRARADTAN'
 Range test: Conf. Int. Confidence level: 95

Analysis of variance

Source of variation	Sum of Squares	d.f.	Mean square	F-ratio	Sig. level
Between groups	13394.714	3	4464.9048	4.662	.1191
Within groups	2873.000	3	957.6667		
Total (corrected)	16267.714	6			

1 missing value(s) have been excluded.

(X 189)

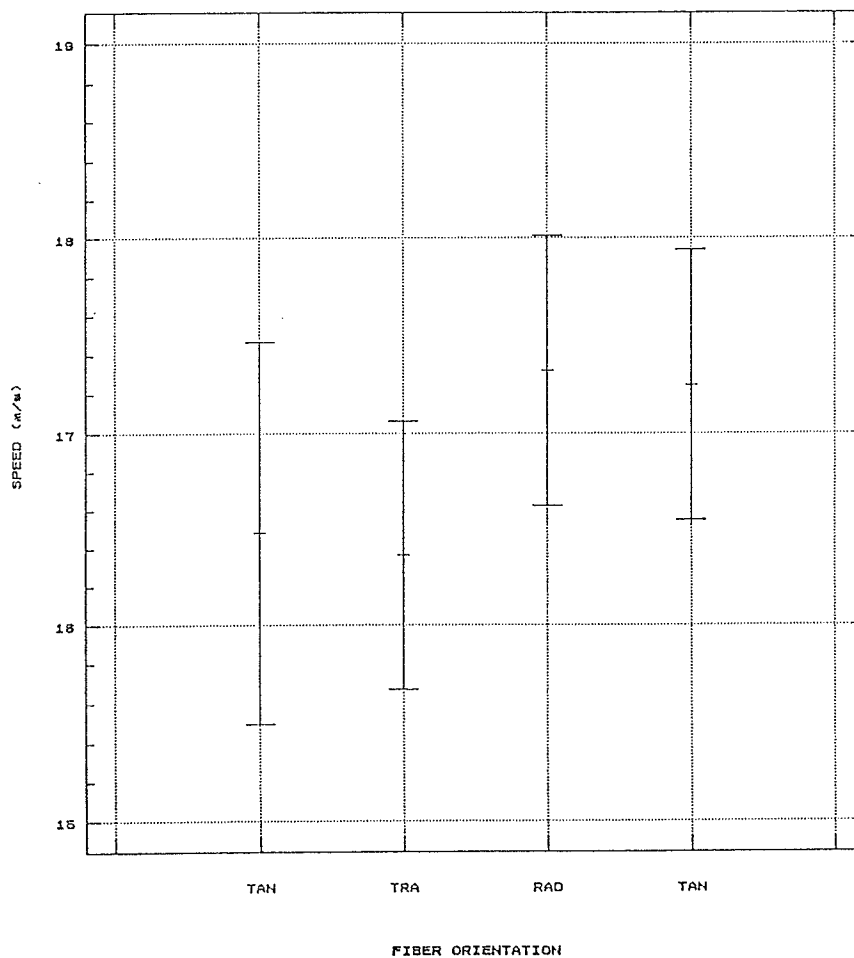


Figure 36. Statgraphics ANOVA: ultrasonic speed COLLAGEN ONLY vs. fiber orientation.

Table 42. ANOVA results for the effect of fiber orientation on ultrasonic speed CROSS-LINKS CLEAVED.

 One-Way Analysis of Variance

 Data: ARCART02.SPDXLINK
 Level codes: ARCART02.FIBRORIEN2
 Labels: 4 3 RESHAPE 'TANTRARADTAN'
 Range test: Conf. Int. Confidence level: 95

 Analysis of variance

Source of variation	Sum of Squares	d.f.	Mean square	F-ratio	Sig. level
Between groups	988.9286	3	329.6429	.113	.9467
Within groups	8744.5000	3	2914.8333		
Total (corrected)	9733.4286	6			

1 missing value(s) have been excluded.

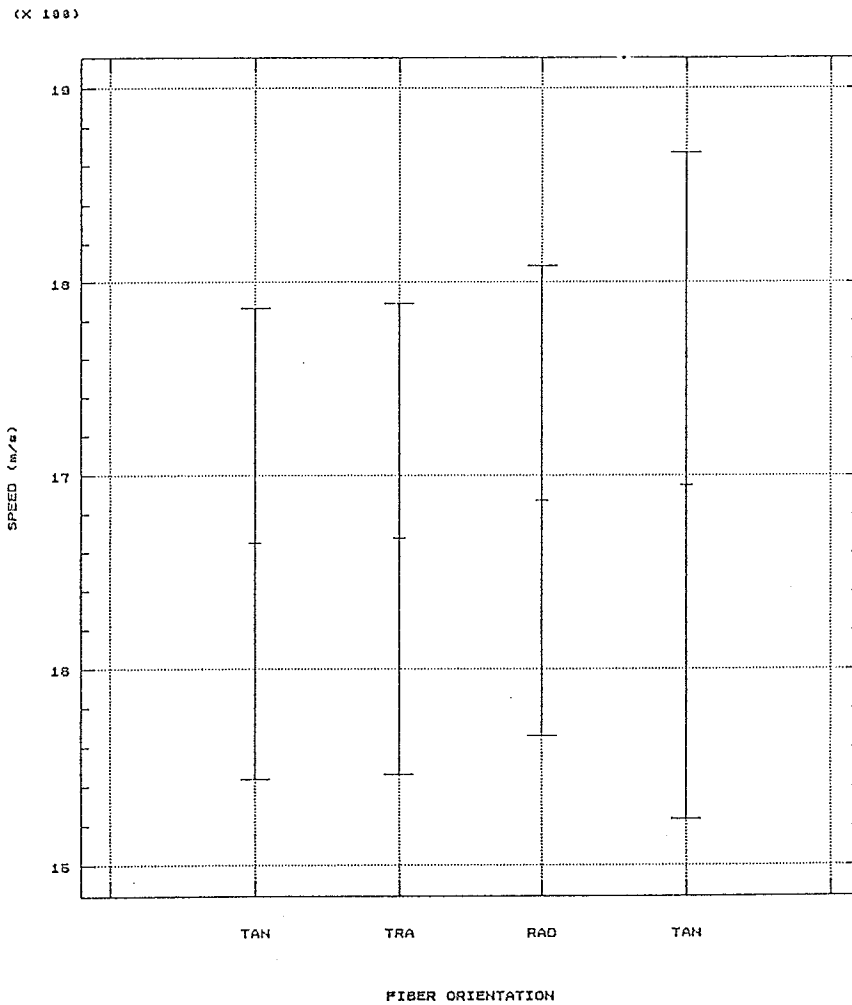


Figure 37. Statgraphics ANOVA: ultrasonic speed CROSS-LINKS CLEAVED vs. fiber orientation.

REFERENCES

- Bamber J.C., Fry J.J., Hill C.R. and Dunn F. Ultrasonic Attenuation and Backscatter by Mammalian Organs as a Function of Time After Excision. *Ultrasound Med. Biol.*, 3, 15, 1977.
- Bamber J.C., Hill C.R. and King J.A. Acoustic Properties of Normal and Cancerous Human Liver-II. Dependence on Tissue Structure. *Ultrasound Med. Biol.*, 7, 135-144, 1981.
- Bhandari A.K. and Nanda N.L. Myocardial Texture Characterization by Two-dimensional Echocardiography. *Am. J. Cardio.*, 51, 817-825, 1983.
- Carstensen E.L., Li K. and Schwan H.P. Determination of the Acoustic Properties of Blood and Its Components. *J. Acoust. Soc. Am.*, 25, 286-289, 1953.
- Carstensen E.L. and Schwan H.P. Acoustic Properties of Hemoglobin Solutions. *J. Acoust. Soc. Am.*, 50, 692-699, 1959.
- Chianamider S.A., Goldman M.A., Zema M.J., Pizzarello R.A. and Goldberg M.H. Real-time Cross-sectional Echocardiographic Diagnosis of Infiltrative Cardiomyopathy Due to Amyloid. *J. Clin. Ultrasound*, 8, 58-62, 1980.
- Chun L.E., Koob T.J. and Eyre D.R. Sequential Enzymic Dissection of the Proteoglycan Complex from Articular Cartilage. *Trans. Orthop. Res. Soc.*, 11, 96 (abstract), 1986.
- Dines K.A., Sheets P.W., Brink J.A., Hanke C.W., Condra K.A., Celendenon J.L., Goss S.A., Smith D.J. and Franklin T.D. High Frequency Ultrasonic Imaging of Skin: Experimental Results. *Ultrason. Imaging*, 6, 408-434, 1984.
- Dunn F. Ultrasonic Properties of Biological Media. In Ultrasound Interactions in Biology and Medicine. R. Millner, E. Rosenfeld and U. Cobet (eds.), Plenum Publishing Corp., pp. 1-6, 1983.
- Dussik K.T., Fritch D.J., Kyriazidou M. and Sear R.S. Measurements of Articular Tissues with Ultrasound. *Am. J. of Phys. Med.*, 37, 160-165, 1958.

- Embree P.M., Forster S.G., Bright G. and O'Brien W.D. Jr. Ultrasonic Velocity Spatial Distribution Analysis of Biological Materials with the Scanning Laser Acoustic Microscope. In Acoustical Imaging, M. Kaveh, R.K. Mueller and J.F. Greenleaf (eds.), 13, Plenum Press, New York, 203-216, 1984.
- Embree P.M. UDAS-Ultrasound Data Acquisition System. Internal Bioacoustics Research Laboratory Report, University of Illinois, Urbana-Champaign, IL, 1985a.
- Embree P.M., Tervola K.M.U., Foster S.G. and O'Brien W.D. Jr. Spatial Distribution of the Speed of Sound in Biological Materials with the Scanning Laser Acoustic Microscope. IEEE Trans. Sonics. Ultrason., SU-32, 341-350, 1985b.
- Eyre D.R., Paz M.A. and Gallop P.M. Cross-linking in Collagen and Elastin. Ann. Rev. Biochem., 53, 717-748, 1984.
- Eyre D.R., Apone S., Wu J.-J., Ericsson L.H. and Walsh K.A. Collagen Type IX: Evidence For Covalence Linkage to Type II Collagen in Cartilage. FEBS Lett., 220, 337-341, 1987.
- Fields S. and Dunn F. Correlation of Echographic Visualizability of Tissue with Biological Compositions and Physiological State. J. Acoust. Soc. Am., 54, 809-812, 1973.
- Forster F.K., Olerud J.E. and Gow E.L. Tissue Characterization of Skin Utilizing High Ultrasonic Frequencies. IEEE Ultrason. Symp. Proc., IEEE Catalog No. 83CH1947-1, 810-5 (appendix item), 1983.
- Foster S. An Image Digitizing System for a Scanning Laser Acoustic Microscope. M.S. Thesis, Department of Electrical and Computer Engineering, University of Illinois, Urbana-Champaign, IL, 1981.
- Geleskie J.V. and Shung K.K. Further Studies on Acoustic Impedance of Major Bovine Blood Vessel Walls. J. Acoust. Soc. Am., 71, 467-470, 1982.
- Goss S.A. and O'Brien W.D. Jr. Direct Ultrasonic Velocity Measurements of Mammalian Collagen Threads. J. Acoust. Soc. Am., 65, 507-511, 1979.

- Goss S.A., Frizzell L.A., Dunn F. and Dines K.A. Dependence of the Ultrasonic Properties of Biological Tissue on Constituent Proteins. *J. Acoust. Soc. Am.*, 67, 1041-1044, 1980.
- Haendchen R.V., Ong K., Fishbein M.C., Zwehl W. Meerbaum S. and Corday E. Early Differentiation of Infarcted and Noninfarcted Reperfused Myocardium in Dogs by Quantitative Analysis of Regional Myocardial Echo Amplitudes. *Circ. Res.*, 57, 718-728, 1985.
- Hukins D.W.L., Aspden R.M. and Yarker Y.E. Fiber Reinforcement and Mechanical Stability in Articular Cartilage. *Engr. Med.*, 13, 153-156, 1984.
- Hukins D.W.L. and Aspden R.M. Composition and Properties of Connective Tissues. *Trends in Biol. Sci.*, 10, 260-264, 1985.
- Johnston R.L., Goss S.A., Maynard V.A., Brady J.K., Frizzell L.A., O'Brien W.D. Jr. and Dunn F. Elements of Tissue Characterization. Part I. Ultrasonic Propagation Properties. In Ultrasonic Tissue Characterization II, M. Linzer (ed.), National Bureau of Standards, Special Publication 525, U.S. Government Printing Office, Washington, D.C., pp. 19-27, 1979.
- Kloner R.A., Rude R.E., Carlson N., Maroko P.R., DeBoer L.W.V. and Braunwald E. Ultrastructural Evidence of Microvascular Damage and Myocardial Cell Injury After Coronary Artery Occlusion: Which Comes First? *Circ. Res.*, 62, 945, 1980.
- Lee S.A., Lindsay S.M., Powell J.W., Weidlick T., Tao N.J. and Lewen G.D. A Brillouin Scattering Study of the Hydration of Li- and Na-DNA Films. *Biopolymers*, 26, XXX-YY, 1987.
- Lele P.P. and Namery J. A Computer-based Ultrasonic System for the Detection and Mapping of Myocardial Infarcts. *Proc. San Diego Biomed. Symp.*, 13, 121-132, 1974.
- Li J.T., Mow V.C., Koob T.J. and Eyre D.R. Effect of Chondroitinase ABC Treatment on the Tensile Behavior of Bovine Articular Cartilage. *Ortho. Trans. Res. Soc.*, 9, 35, 1984.

- Marangoni R.D., Glaser A.A., Must J.S, Brody G.S, Beckwith T.G., Walker G.R. and White W.L. Effect of Storage and Handling Techniques on Skin Tissue Properties. *Ann. N.Y. Acad. Sc.*, 136, 439-454, 1966.
- Martin P.R., Rakowski H., French J. and Popp R.L. Idiopathic Hypertrophic Subaortic Stenosis Viewed by Wide-angle Phased Array Echocardiography. *Circulation*, 59, 1206-1217, 1979.
- Mimbs J.W., Yuhas D.E., Miller J.G., Weiss A.N. and Sobel B.E. Detection of Myocardial Infarction in Vitro Based on Altered Attenuation of Ultrasound. *Circ. Res.*, 41, 192-198, 1977.
- Mimbs J.W., Bauwens D., Cohen R.D., O'Donnell M., Miller J.G. and Sobel B.E. Effects of Myocardial Ischemia on Quantitative Ultrasonic Backscatter and Identification of Responsible Determinants. *Circ. Res.*, 49, 89-96, 1981.
- Muir I.H.M. The Chemistry of the Ground Substance of Joint Cartilage. In The Joints and Synovial Fluid. Volume II, L. Sokoloff (ed.), Academic Press, New York, pp. 27-94, 1980.
- O'Brien W.D. Jr. and Dunn F. Ultrasonic Absorption Mechanisms in Aqueous Solutions of Bovine Hemoglobin. *J. Phys. Chem.*, 76, 523-533, 1972.
- O'Brien W.D. Jr. Ultrasonic Absorption in Aqueous Solutions of Chondroitin Sulfate. *J. Acoust. Soc. Am.*, 57, 956-958, 1975.
- O'Brien W.D. Jr. The Role of Collagen in Determining Ultrasonic Propagation Properties in Tissue. In Acoustical Holography, L.W. Kessler (ed.), 7, Plenum Press, New York, pp. 37-50, 1977a.
- O'Brien W.D. Jr. The Relationship Between Collagen and Ultrasonic Attenuation and Velocity in Tissue. In Ultrasonic International, Guilford, Surrey, UK, IPC Science and Technology Press, pp. 194-205, 1977b.
- O'Brien W.D. Jr., Erdman J.W. and Hebner T.B. Ultrasonic Propagation Properties (@ 100 MHz) in Excessively Fatty Rat Liver. *J. Acoust. Soc. Am.*, 83, 1159-1166, 1988.

- O'Donnell M., Mimbs J.W., Miller J.G. and Sobel B.E. Ultrasonic Attenuation in Normal and Ischemic Myocardium. In Ultrasonic Tissue Characterization II, M. Linzer (ed.), National Bureau of Standards, Special Publication 525, U.S. Government Printing Office, Washington, D.C., pp. 63-71, 1979a.
- O'Donnell M., Bauwnes D., Mimbs J.W. and Miller J.G. Broadband Integrated Backscatter: An Approach to Spatially Localized Tissue Characterization In Vivo. IEEE Ultrason. Symp. Proc., 175-178, 1979b.
- O'Donnell M., Mimbs J.W. and Miller J.G. The Relationship Between Collagen and Ultrasonic Attenuation in Myocardial Tissue. J. Acoust. Soc. Am., 65, 512-517, 1979c.
- Olerud J.E., O'Brien W.D. Jr., Riederer-Henderson M.A., Steiger D., Forster F.K., Daly C., Ketterer D.J. and Odland G.F. Ultrasonic Assessment of Skin and Wounds with the Scanning Laser Acoustic Microscope. J. Invest. Dermatol., 88, 615-623, 1987.
- Olerud J.E., O'Brien W.D. Jr., Riederer-Henderson M.A., Steiger D.L., Debel J. and Odland G.F. Correlation of Tissue Constituents with the Acoustic Properties of Skin and Wound. Submitted to J. Invest. Dermatol.
- Pauly H. and Schwan H.P. Mechanism of Absorption of Ultrasound in Liver Tissue. J. Acoust. Soc. Am., 50, 692-699, 1971.
- Peacock E.E. Jr. and Van Winkle W. Jr. The Biochemistry and the Environment of Wounds and Their Relation to Wound Strength. In Surgery and Biology of Wound Repair, W.B. Saunders Co., Philadelphia, pp. 129-170, 1970a.
- Peacock E.E. Jr. and Van Winkle W. Jr. Structure, Synthesis, and Interaction of Fibrous Protein and Matrix. In Surgery and Biology of Wound Repair, W.B. Saunders Co., Philadelphia, pp. 75-127, 1970b.
- Pohlhammer J. and O'Brien W.D. Jr. The Relationship Between Ultrasonic Attenuation and Speed in Tissues and the Constituents: Water, Collagen, Protein and Fat. In Medical Physics of CT Ultrasound: Tissue Imaging and Characterization, G.D. Fullerton and J.A. Zagzebski (eds.), pp. 409-435, 1980.

- Rasmussen S., Cohya B.C., Feigenbaum H. and Knoebel S.B.
Detection of Myocardial Scar Tissue by M-mode
Echocardiography. *Circulation*, 57, 230-237, 1978.
- Rhyne T.L. Acoustic Instrumentation and Characterization of Lung
Tissue, London, John Wiley and Sons, Research Studies Press,
1977.
- Rhyne T.L., Sagar K.B., Wann L.S. and Haasler G. The
Myocardial Signature: Absolute Backscatter, Cyclic
Variation, Frequency Variation and Statistics. *Ultrason.
Imaging*, 8, 107-120, 1986a.
- Rhyne T.L., Sagar K.B., Wann L.S. and Haasler G. A Myocardial
Backscatter Parameter with Maximal Sensitivity to Cyclic
Variation. *IEEE Ultrason. Symp. Proc.*, IEEE Catalog No.
86H23775-4:909, 1986b.
- Sagar K.B., Rhyne T.L. and Greenfield L.J. Echocardiographic
Tissue Characterization and Range Gated Doppler for
Diagnosis of Pulmonary Embolism. *Circ. Res.*, 67, 365-380,
1983.
- Sagar K.B., Rhyne T.L., Warltier D.C., Pelc L. and Wann L.S.
Intramyocardial Variability in Integrated Backscatter:
Effects of Coronary Occlusion and Reperfusion. *Circ. Res.*,
75, 436-442, 1987.
- Sagar K.B., Pelc L., Rhyne T.L., Wann L.S. and Warltier D.C.
Influence of Heart Rate, Preload, Afterload and Inotropic
State on Integrated Backscatter. *Circ. Res.*, 77, 478-483,
1988.
- Sarvazyan A.P., Lyrchilsov A.G. and Gorelov S.E. Dependence of
Ultrasonic Velocity in Rabbit Liver on Water Content and
Structure of the Tissue. *Ultrasonics*, in press.
- Schmidt M.B., Schoonbeck J.M., Mow V.C., Eyre D.R. and Chun L.E.
Effects of Enzymatic Extraction of Proteoglycans on the
Tensile Properties of Articular Cartilage. *Trans. Orthop.
Res. Soc.*, 12, 134 (abstract), 1987.

- Skorton D.J., Collins S.M., Nichols J., Pandian N.G., Bean J.A. and Kerber R.E. Quantitative Texture Analysis in Two-dimensional Echocardiography: Application to the Diagnosis of Experimental Myocardial Contusion. *Circulation*, 68, 217-223, 1983a.
- Skorton D.J., Melton H.E., Pandian N.G., Nichols J., Koyanagi S., Marcus M.L., Collins S.M. and Kerber R.E. Detection of Acute Myocardial Infarction in Closed Chest Dogs by Analysis of Regional Two-dimensional Echocardiographic Grey-level Distributions. *Circ. Res.*, 52, 36-44, 1983b.
- Steiger D.L. Ultrasonic Assessment of Skin and Wounds with the Scanning Laser Acoustic Microscope. M.S. Thesis, Department of Electrical and Computer Engineering, University of Illinois, Urbana-Champaign, IL, 1986.
- Steiger D.L., O'Brien W.D. Jr., Olerud J.E., Riederer-Henderson M.A. and Odland G.F. Measurement Uncertainty Assessment of the Scanning Laser Acoustic Microscope and Application to Canine Skin and Wound. *IEEE Trans. Ultrason., Ferroelec. and Freq. Con.*, in press.
- Tervola K.M.U., Foster S.G. and O'Brien W.D. Jr. Attenuation Coefficient Measurement Technique at 100 MHz with the Scanning Laser Acoustic Microscope. *IEEE Trans. Sonics. Ultrason.*, SU-32, 259-265, 1985a.
- Tervola K.M.U. and O'Brien W.D. Jr. Spatial Frequency Domain Technique: An Approach for Analyzing the Scanning Laser Acoustic Microscope Interferogram Images. *IEEE Trans. Sonics. Ultrason.*, SU-32, 544-554, 1985b.
- Theroux P., Franklin D., Ross J. and Kemper W.S. Regional Myocardial Function During Acute Coronary Occlusion and Modification by Pharmacologic Agents in Dogs. *Circ. Res.*, 35, 896-902, 1972.
- Viljanto J. Tensile Strength of Healing Wounds. In Biophysical Properties of the Skin, H.R. Elden (ed.), Wiley-Interscience, New York, p. 452, 1971.
- Wear K.A., Shoup T.A. and Popp R.L. Ultrasonic Characterization of Canine Myocardium. *IEEE Trans. Sonics. Ultrason.*, SU-33, 247, 1986.

Wickliffe S.A., Thomas L.J., Miller J.G., Sobel S.E. and Perez J.E. A Relationship Between Ultrasonic Backscatter and Myocardial Contractile Function. J. Clin. Invest., 76, 2151, 1985.

Wild J.J., Crafford M.D. and Reid J.M. Visualization of the Excised Human Heart by Means of Reflected Ultrasound or Echography. Am. Heart J., 54, 903-906, 1957.

Wladimiroff J.W., Craft J.L. and Talbert D.C. In vitro Measurements of Sound Velocity in Human Fetal Brain Tissue. Ultrasound Med. Biol., 1, 377-382, 1977.